A METHOD FOR NUMERICAL RELATIVITY: SIMULATION OF AXISYMMETRIC GRAVITATIONAL COLLAPSE AND GRAVITATIONAL RADIATION GENERATION

by

Charles Ross Evans II, B.A., M.S.

DISSERTATION

Presented to the Faculty of the Graduate School of

The University of Texas at Austin

in Partial Fulfillment

of the Requirements

for the Degree of

DOCTOR OF PHILOSOPHY

THE UNIVERSITY OF TEXAS AT AUSTIN

August 1984

A METHOD FOR NUMERICAL RELATIVITY:
SIMULATION OF AXISYMMETRIC GRAVITATIONAL COLLAPSE
AND GRAVITATIONAL RADIATION GENERATION

APPROVED BY SUPERVISORY COMMITTEE:

Richard A. Matzner

Bryce DeWitt

Thomas A. Deacon

P. Candelas

To my wife, Annetta,
my son, Daniel,
and my
parents,
Charles and Merna

A METHOD FOR NUMERICAL RELATIVITY:
SIMULATION OF AXISYMMETRIC GRAVITATIONAL COLLAPSE
AND GRAVITATIONAL RADIATION GENERATION

by

Charles Ross Evans II, B.A., M.S.

DISSERTATION
Presented to the Faculty of the Graduate School of
The University of Texas at Austin
in Partial Fulfillment
of the Requirements
for the Degree of

DOCTOR OF PHILOSOPHY

THE UNIVERSITY OF TEXAS AT AUSTIN

August 1984

ACKNOWLEDGEMENTS

It is a great pleasure for me to acknowledge the help and encouragement that I have received from many friends and colleagues. Discussions with Richard Matzner, Pieter Dykema, Jim Wilson, Joan Centrella, Larry Smarr, Jim LeBlanc, Jim York, Anil Kulkarni, Richard Isaacson and Bob Rainesberger have been most helpful. I thank John Blunden for cinematic assistance.

I would like to say in particular that I fear it will never be possible for me to fully repay my thesis advisor Richard Matzner for all of the support and help he has given me. I also thank Pieter Dykema for many introductory discussions on this project and the computer code which I "inherited." He showed great patience on many early occasions with my sometimes overly naive eagerness.

I have enjoyed the support of the Center for Relativity at The University of Texas at Austin and the hospitality of the Lawrence Livermore National Laboratory and B-division where most of this research was conducted. I have gratefully received financial support from the Associated Western Universities while at Livermore. I would also like to thank Larry Smarr and the University of Illinois for much patience and for keeping the pot boiling during this last year. Finally let me say that it has been my privilege to have been able to work with Jim Wilson, without whom this work would not have been possible.

A METHOD FOR NUMERICAL RELATIVITY:

SIMULATION OF AXISYMMETRIC GRAVITATIONAL COLLAPSE

AND GRAVITATIONAL RADIATION GENERATION

Publication No._____

Charles Ross Evans II, Ph.D.
The University of Texas at Austin, 1984

Supervising Professor: Richard A. Matzner

A method is presented which allows fully self-consistent numerical simulation of asymptotically flat axisymmetric nonrotating geheral relativistic systems. These techniques have been developed to model and understand resulting relativistic effects in gravitational core collapse and gravitational radiation generation. Both vacuum (Brill) spacetimes and matter-filled configurations can be treated. We use the (3 + 1) decomposition of Arnowitt, Deser and Misner to write general relativity in a dynamical form. The conformal approach, including the transverse-traceless decomposition of extrinsic curvature due to York, is used to solve the initial value problem. In addition, these techniques are extended to provide a fully constrained evolution scheme. Several new boundary conditions, applied at large but finite radius, are derived for the elliptic constraint equations. Our method uses a simplifying three-gauge, placing the metric in quasi-isotropic form. The resulting

three-metric contains only two components for which we must solve. One, the conformal factor, is fixed by the Hamiltonian constraint. The second has nice radiative features and is related in the weak-field limit to the usual transverse-traceless gravitational wave amplitude. The time slicing is determined by implementation of the maximal slicing condition. We show the resulting equations are regular everywhere, including at the symmetry axis, the origin, and across the horizon when a black hole forms. Treatment of the relativistic hydrodynamic equations is described. A computer code has been developed around these techniques. A number of the numerical methods are discussed with particular attention paid the regularization of the finite differencing near the singular points of the spherical polar coordinate system. We show a number of preliminary numerical results from several nonspherical core collapse and bounce calculations. Both the hydrodynamic features, and the balance between gravitational radiation and mass-energy are discussed. We are able to calculate with sufficient accuracy to see the radiation reaction effect of the loss of energy in the system directly in the quasi-local mass indicator. Finally we demonstrate the necessity of making a full relativistic treatment of nonspherical *supernova* core collapse if accurate (better than a factor of 2 -5) results for gravitational radiation emission are to be achieved.

TABLE OF CONTENTS

CHAPTER I

INTRODUCTION

By now most of the analytic fronts in classical general relativity have been well explored. However, it is a testimony to the mathematical difficulty of the theory that the known exact solutions are characterized by high degrees of symmetry. This is true whether one is dealing with spacetime solutions that are asymptotically flat (Schwarzschild, Kerr-Newman geometry, dust collapse, etc.) or those describing the universe as a whole (Friedmann or Bianchi models). We will exclusively concern ourselves here with asymptotically flat spacetimes. Here, nontrivial dynamic solutions (two or three space dimensions) cannot be obtained analytically. It is precisely these dynamic configurations that are necessary for the production of gravitational radiation. If we are to make predictions of the amount of gravitational radiation emission from realistic astrophysical sources, calculational techniques must be extended to at least include dynamic systems exhibiting axisymmetry. It is hoped that in the next decade gravitational radiation detectors will reach sensitivity levels sufficient to observe violent astrophysical sources.[1]

Approximate calculational techniques do exist for general relativity, which do not require special symmetry assumptions. However these techniques are perturbative in nature and apply to systems

in which relativity does not play too large a role. The quadrupole moment formalism for example requires that the source emitting gravitational radiation be moving with slow internal velocities and have a weak gravitational field. While this formalism may be adequate to describe some sources of interest (binary pulsars for example), it loses its applicability for very violent, high speed and strong gravity sources. These sources on dimensional grounds are those likely to be the most efficient emitters of gravitational radiation.

Hence for both these reasons, lack of high degrees of symmetry and inapplicability of perturbative methods, various researchers have turned to what has become known as *numerical relativity* to study these sources. Numerical relativity has as its goal the fully self-consistent calculation of the Einstein equations and relativistic hydrodynamics by typically finite difference techniques. There are no approximations assumed save the finite difference approximation itself. And in this case, this small parameter (ratio of zone size to characteristic physical length) can be made as small as we choose, independently of the physics of the source.

Early work on calculating relativistic systems numerically was undertaken in the sixties by Hahn and Lindquist[2] and May and White.[3] Hahn and Lindquist ambitiously attempted to calculate the axisymmetric (i.e. two-dimensional) collision of two black holes. This attempt was only partially successful and did not yield the desired answer, namely, how much gravitational radiation is produced from the

coalescence. May and White calculated one-dimensional, spherically symmetric spacetimes. While these systems will not emit gravitational radiation, they were nonetheless successful in calculating collapse to neutron stars and to black holes (though in this latter case their calculation terminated very early due to their choice of gauge conditions[4]).

In the seventies the number of numerical relativistic calculations began to grow. Smarr and Eppley[5-8] completed calculations of the head-on black hole collision begun by Hahn and Lindquist and studied by Cadez and DeWitt. Numerical cosmologies with plane symmetry were studied by Centrella[9] and Centrella and Wilson.[10] Piran developed a computer code to study cylindrical collapse and cylindrical spacetimes.[11]

Numerical work was also begun on codes to allow simulation of axisymmetric hydrodynamic systems (to study for example stellar core collapse scenarios). The progenitors of the work reported in this thesis were the efforts by Smarr and Wilson[12] and Dykema and Wilson.[13] Our goals have been to obtain a computer code capable of simulating axisymmetric, nonrotating gravitational collapse and gravitational radiation generation. The desire has been to produce a computer code robust enough to follow either vacuum or matter-filled configurations and to follow collapse through either a deep relativistic hydrodynamic bounce or to the formation of a black hole. We have typically restricted attention to fluids obeying an adiabatic equation of state thus far. Our main concern heretofore has been in obtaining a good

simulation of the gravitational field and gravitational radiation. Thus little emphasis has been placed so far on the detailed microphysics necessary to model a supernova core collapse. In addition, it was felt necessary to restrict the problem to vanishing rotation until one had achieved an understanding of the difficulties in simulating two-dimensional systems containing matter.

This understanding is now largely achieved as it is hoped will be revealed in this thesis. There are questions to be studied with the existing code, but we will no doubt shortly seek to broaden the present technique to include explicit generation mechanisms for producing asphericity and more realistic nuclear equations of state. Parallel efforts, which include rotation, have been undertaken by Nakamura[14] and his coworkers and by Piran and Stark[15] drawing on analytic considerations by Bardeen and Piran.[16] These various efforts are based on very different methods or gauge conditions. Varying amounts of computer power are also available to each group. Ultimately, we believe that if our field is to gain wide spread credibility, several calculations made along different lines of attack must be compared favorably to say with certainty that we have calculated a source's waveform and emitted flux. While each of these methods is becoming further refined, no attempt at comparing test calculations has been made. Hopefully this situation will not long prevail.

Our method of calculating axisymmetric collapse is based on the ADM method[17] of treating general relativity as a dynamical problem. This formalism is reviewed and the necessary equations are

obtained in Chapter II of this thesis. The relativistic hydrodynamic equations are given in the form proposed by Wilson[4,12] as closely as possible. This topic is also discussed in Chapter II.

At nearly the same time that these numerical developments were occurring during the seventies, major advances were being made theoretically on questions relating to the solution of the initial value problem, or constraint equations, of general relativity. These efforts were largely lead through the efforts of York[18] and his co-workers. A number of these methods for obtaining initial data for our numerical evolutions are laid out in Chapter III. Accompanying these advances on the initial value problem were theoretical considerations of dynamical gauge conditions to be used in numerical applications. This topic is also dealt with in Chapter III.

Chapter IV presents the partial differential equations that are obtained for our models of axisymmetric, nonrotating gravitational collapse in the gauge in which we have chosen to work. A number of new considerations are presented there for asymptotic parts of the gravitational field. Our method, which already appears now to be fairly accurate, will probably be further refined using this analysis. Various mass and gravitational radiation flux indicators that have been used to great advantage in our simulations are discussed in Chapters III and IV. Results from the use of these indicators are given in Chapter VI.

Some of the numerical techniques which have recently undergone significant refinement are discussed in Chapter V. These techniques have greatly increased the range of utility of our code and significantly enhanced its accuracy. Several tentative tests of the accuracy of our method are given in Chapter VI. A large scale effort to rigorously test the code and method has not yet been mounted. However, after several additional refinements, which have been discovered during the writing of this thesis, are added to our method, we will undertake this necessary step. Finally, Chapter VI also presents several preliminary results from simulations of oblate core collapse. A sequence of runs to increasing bounce density were carried out. We have obtained gravitational radiation efficiencies for these models and these appear to indicate emission of 0.2 - 0.7% of the mass of the system is possible. These models were *designed* to enhance the amount of gravitational radiation produced. If these numbers stand up under our future scrutiny and if real stellar core collapse can produce asymmetries of this size, then these results applied to supernovae in the Virgo cluster become observationally significant for detectors able to reach $h \approx 10^{-21}$ level strains.

Chapter I References

1. Thorne (1980a).
2. Hahn and Lindquist (1964).
3. May and White (1966); May and White (1967).
4. Smarr, Taubes and Wilson (1980).
5. Smarr (1979).
6. Smarr (1975).
7. Eppley (1975).
8. Smarr, Cadez, DeWitt and Eppley (1976).
9. Centrella (1979); see also Centrella and Matzner (1979).
10. Centrella and Wilson (1983).
11. Piran (1980).
12. Wilson (1979).
13. Dykema (1980).
14. Nakamura (1981).
15. Stark and Piran (1984).
16. Bardeen and Piran (1983).
17. Arnowitt, Deser, and Misner (1962).
18. York (1979).

CHAPTER II

a) Formalism and Gravitational Field

In order to uncover the dynamical structure of general relativity, it is necessary to break the four-dimensional, covariant form of the theory and isolate the special nature of time. This is the aim of the (3 + 1) formalism of Arnowitt, Deser, and Misner (ADM).[1] Part of the splitting will involve considering a spacelike foliation $\{\Sigma\}$, a set or family of non-intersecting spacelike three surfaces $\Sigma(t)$, defined locally as level surfaces of a scalar function t. In a dynamical context, t will amount to the coordinate time for the calculation and the data (gravitational field and matter fields) will be represented by three-dimensional constructs on the simultaneities $\Sigma(t)$.

In terms of the foliation, Einstein's equations can be described as a Cauchy initial value problem. For the moment we keep the discussion in terms of the four-dimensional metric g_{ab}.[2] A Cauchy description then requires knowledge of g_{ab} and $\partial_t g_{ab} = \partial_0 g_{ab}$ throughout an initial three-surface $\Sigma(t_0) = \Sigma_0$.[3] The field equations,[4] $G^{ab} = T^{ab}$, then will contain terms with second time derivatives $\partial_t^2 g_{ab}$ and these can be used with the initial data set to produce new values on a slice $\Sigma(t_0 + \Delta t)$. The problem is not quite this simple, however. General relativity is a gauge theory (general covariance under four-dimensional coordinate transformations) and a direct consequence is the existence

of four constraint relations on the initial values of g_{ab} and $\partial_t g_{ab}$ on Σ_o. The constraints can be revealed by examining the contracted Bianchi identities:

$$\nabla_o G^{oa} = -\nabla_i G^{ia} \quad . \tag{1}$$

The right-hand-side can contain at most second time derivatives and therefore G^{oa} at most first time derivatives. The four equations

$$G^{oa} = T^{oa} \quad , \tag{2}$$

are the constraints and the remaining equations

$$G^{ij} = T^{ij} \quad , \tag{3}$$

are dynamical (contain $\partial_t^2 g_{ab}$). The latter are however only six such second order equations and the system is four-fold underspecified. This ambiguity is due to the general covariance and is removed by the imposition of four coordinate conditions which fix the coordinates in the future of Σ_o.

The final aspect of the Cauchy problem, which makes it well posed, is that the Bianchi identities guarantee that the evolution of properly constrained initial data continues to satisfy the constraints. Using the Bianchi identities (1) and the equations of motion for the matter, $\nabla_a T^{ab} = 0$, gives

$$\nabla_o (G^{oa} - T^{oa}) = -\nabla_i (G^{ia} - T^{ia}) \quad . \tag{4}$$

Since the Einstein equations (2) - (3) cause the right-hand-side to vanish on Σ_o, data satisfying (2) initially are maintained in time. While this is true analytically (here defined as non-numerically), it is important to note that this will not exactly hold during a numerical evolution. Such a calculation will shortly be advancing *non-Einstein data* in time and there is, understandably, little known about the stability of such a procedure (see however Moncrief[5] for a method of describing real, gauge, *and* constraint perturbations). How we have chosen to deal with this difficulty will form a central part of this thesis.

The ADM formalism has several compelling features from a computational point of view. First, because it derives from a Hamiltonian, or canonical approach, the equations for the evolution of the gravitational field naturally appear in first-order form (i.e., in terms of conjugate configuration and momentum fields with first time derivatives only). This form is better suited for a numerical calculation. Also, as will be shown, our algorithm reduces the evolution of the gravitational field to a minimum number of canonical pairs corresponding precisely to the number of operative degrees of freedom.[6] This has advantages for the calculation of gravitational radiation.

Finally, the ADM formalism provides a very intuitive approach to coordinate conditions. Once proper initial data have been posed, gauge conditions are given which determine, as the calculation unfolds, the set of surfaces $\Sigma(t)$ in the future of Σ_o and, in effect, a

congruence of curves which thread $\{\Sigma\}$ and carry the initial spatial coordinates x^i on Σ_o from slice to slice.

We associate with the surfaces $\{\Sigma\}$ a closed one-form ω. Since $d\omega = 0$, this will locally give

$$\omega = dt \quad , \tag{5}$$

with t the scalar time function. Assume a dual basis of forms E^a and vectors E_a so $\langle E^a, E_b \rangle = \delta^a{}_b$. In terms of the basis,

$$\omega_a = \nabla_a t = \partial_a t \quad . \tag{6}$$

This one-form will have a norm which is defined by the four-metric g_{ab}:

$$g^{ab}\omega_a\omega_b = -\alpha^{-2} \quad . \tag{7}$$

Here, α, called the lapse function, is defined to be strictly positive and the minus sign indicates ω is timelike and the slices $\{\Sigma\}$ are spacelike. A normalized form can now be defined

$$\Omega_a = \alpha\omega_a \quad , \tag{8}$$

so that $g^{ab}\Omega_a\Omega_b = -1$. Because ω is closed, $d\omega = 0$, Ω_a is irrotational as can be seen by $\Omega \wedge d\Omega = 0$ which implies

$$\Omega_{[a}\nabla_b\Omega_{c]} = 0 \quad . \tag{9}$$

With Ω, a unit vector normal to the slices can be defined (with respect to $\{E_a\}$) as

$$n^a = -g^{ab}\Omega_b \quad . \tag{10}$$

The sign is chosen to make n^a future pointing with respect to t, since from (8) and (7)

$$\langle \Omega, n \rangle = 1 \quad , \tag{11}$$

and n^a is obviously timelike, $n_a n^a = -1$.

The metric induced on the slices by g_{ab}, called the first fundamental form by differential geometers, is

$$\gamma_{ab} = g_{ab} + n_a n_b \quad . \tag{12}$$

This is the first example of a tensor which is *spatial*, since $n^a\gamma_{ab} = 0$. The contravariant form, defined by $\gamma^{ab} = g^{ac}g^{bd}\gamma_{cd}$, is

$$\gamma^{ab} = g^{ab} + n^a n^b \quad . \tag{13}$$

The mixed form has the properties of a projection operator since

$$\gamma^a{}_b = \delta^a{}_b + n^a n_b \tag{14}$$

satisfies $n_a\gamma^a{}_b = 0$ and $\gamma^a{}_b\gamma^b{}_c = \gamma^a{}_c$ (and note that $\gamma^a{}_a = 3$). The former property indicates that $\gamma^a{}_b$ projects free indices "into" the slice; that is if $T^{b\cdots d}_{e\cdots g}$ is a general spacetime tensor then $\gamma^a{}_b T^{b\cdots d}_{e\cdots g}$ has been spatially projected on the "a" index since $n_a\gamma^a{}_b T^{b\cdots d}_{e\cdots g} = 0$.

Conversely, a normal projection operator $N^a{}_b$ can be defined by reversing (14):

$$N^a{}_b = -n^a n_b = \delta^a{}_b - \gamma^a{}_b \quad . \tag{15}$$

If V^a is an arbitrary vector then it can be decomposed into a tangential and orthogonal part:

$$V^a = \delta^a{}_b V^b = (\gamma^a{}_b + N^a{}_b)V^b = S^a + T^a \quad , \tag{16}$$

where $S^a \equiv \gamma^a{}_b V^b$ is a spatial vector (i.e., $S_a n^a = 0$) and $T^a \equiv N^a{}_b V^b = -n^a n_b V^b$ lies in the normal direction. Each index of an arbitrary tensor of rank-n can be projected either tangentially (spatially) or orthogonally yielding 2^n pieces.

Since γ_{ab} is the metric for the slices, we can define a corresponding three-dimensional covariant derivative. Such an operator should produce a spatial tensor when acting on spatial objects and should be compatible with γ_{ab}. This operator, D_a, is defined by projecting into the slice all free indices of the object formed by action of the four-covariant derivative, ∇_a. Thus

$$\begin{aligned} D_a f &= \gamma^b{}_a \nabla_b f \quad , \\ D_a S^b &= \gamma^c{}_a \gamma^b{}_d \nabla_c S^d \quad , \\ D_a T^b{}_c &= \gamma^d{}_a \gamma^b{}_e \gamma^f{}_c \nabla_d T^e{}_f \quad , \end{aligned} \tag{17}$$

are its actions on scalars, vectors, and two-tensors respectively (with obvious extension). To check compatibility, use (12) to see

$$D_a \gamma_{bc} = \gamma^d{}_a \gamma^e{}_b \gamma^f{}_c \nabla_d (g_{ef} + n_e n_f) = 0 \quad , \tag{18}$$

since $\nabla_a g_{bc} = 0$ and $n_a \gamma^a{}_b = 0$. D_a must be applied only to spatial tensors; its action on arbitrary objects violates the Leibnitz rule, as is evident by

$$\begin{aligned} D_a(V_b W^b) &= V_b D_a W^b + W^b D_a V_b \\ &\quad + \gamma^c{}_a V_b N^b{}_d \nabla_c W^d + \gamma^c{}_a W^b N^d{}_b \nabla_c V_d \quad . \end{aligned} \tag{19}$$

The curvature tensor for the slice $R^c{}_{dab}$ is defined by requiring

$$D_{[a} D_{b]} V^c = \tfrac{1}{2} R^c{}_{dab} V^d \quad , \tag{20}$$

and

$$n^d R^c{}_{dab} = 0 \quad , \tag{21}$$

for every spatial vector V^c. Equation (21) insures $R^c{}_{dab}$ is totally spatial. The Ricci tensor is defined as expected by

$$R_{ab} = R^c{}_{acb} \quad , \tag{22}$$

and the scalar curvature by

$$R = g^{ab} R_{ab} = \gamma^{ab} R_{ab} \quad . \tag{23}$$

It is clear that the relationship between $R^c{}_{dab}$ and the four-dimensional curvature tensor ${}^4R^c{}_{dab}$ will be important. ${}^4R^c{}_{dab}$ will however involve the "time" derivatives of (1) and (4). We have thus far only dealt with the notion (17) of a spatial projection of ∇_a.

What is now required is to use ∇_a to produce a generalized notion of a normal derivative. To this end we use the Lie derivative whose effect along a vector field V^a is

$$\pounds_V f = V^a \nabla_a f \quad ,$$

$$\pounds_V S^a = V^b \nabla_b S^a - S^b \nabla_b V^a \quad ,$$

$$\pounds_V S_a = V^b \nabla_b S_a + S_b \nabla_a V^b \quad ,$$

$$\pounds_V T^a{}_b = V^c \nabla_c T^a{}_b + T^a{}_c \nabla_b V^c - T^c{}_b \nabla_c V^a \quad , \tag{24}$$

with obvious extension. Note that the covariant derivative ∇_a has been employed; not the partial derivatives ∂_a which would be valid only in a holonomic (coordinate) basis, $\{E_a\} = \{\partial_a\}$.[7,8]

The Lie derivative may be used immediately to construct the extrinsic curvature tensor (also called the second fundamental form):

$$K_{ab} = -\tfrac{1}{2} \pounds_n \gamma_{ab} \quad . \tag{25}$$

This represents in essence a velocity of the three-metric and is a quantity of fundamental importance in the ADM scheme. Using (24) and the fact that n^a is a unit normal, K_{ab} can be shown to satisfy

$$K_{ab} = -\gamma^c{}_a \gamma^d{}_b \nabla_{(c} n_{d)} \quad , \tag{26}$$

as well. Thus K_{ab} is also interpreted as the projected *shear* of the unit timelike normal of the slices. It is obviously spatial, $n^a K_{ab} = 0$, and symmetric. The acceleration of the unit normal is

defined by

$$a_c = n^a \nabla_a n_c \quad , \tag{27}$$

and is also spatial, $n^c a_c = 0$. Given (26) and (27) the following form can be obtained:

$$K_{ab} = -\nabla_{(a} n_{b)} - n_{(a} a_{b)} \quad . \tag{28}$$

The irrotational condition (9) can now be written equivalently as

$$n_{[a} \nabla_b n_{c]} = 0 \quad , \tag{29}$$

and projecting on n^a and spatially projecting we obtain

$$\gamma^c{}_a \gamma^d{}_b \nabla_{[c} n_{d]} = 0 \quad . \tag{30}$$

With (26) this implies

$$K_{ab} = -\gamma^c{}_a \gamma^d{}_b \nabla_c n_d \quad . \tag{31}$$

Then finally, using the identity $\nabla_a n_b = (\gamma^c{}_a - n^c n_a)(\gamma^d{}_b - n^d n_b) \nabla_c n_d$, the useful expression

$$\nabla_a n_b = -K_{ab} - n_a a_b \quad , \tag{32}$$

is obtained.

The acceleration a_c (27) can be simplified by use of $n_a = -\alpha \omega_a$, (8) and (10), and the closure of ω (5), $d\omega = 0 \Leftrightarrow \nabla_{[a} \omega_{b]} = 0$ to find

$$a_c = D_c \ln \alpha \quad . \tag{33}$$

The vector field n^a can be regarded as unit tangent vectors to a congruence of observer worldlines. These observers can be considered at rest in the foliation and are termed "Eulerian" observers. The acceleration of these observers is thus (33) determined by spatial gradients in the lapse. We have already mentioned the spatial coordinate congruence along which x^i = constant. These will in general be different.

We are now in a position to obtain some of the projections of ${}^4R^c{}_{dab}$. Starting with (20), the commutator of D_a acting on an arbitrary spatial vector V^b is rewritten in terms of ∇_a. Using (17) and (32) the spatial gradient is expanded to:

$$D_b V^c = \gamma^d{}_b \nabla_d V^c + K_{bd} V^d n^c \quad . \tag{34}$$

Since this is spatial we may compute $D_a D_b V^c = \gamma^d{}_a \gamma^e{}_b \gamma^c{}_f \nabla_d (D_e V^f)$ by substituting (34) to obtain

$$D_a D_b V^c = \gamma^d{}_a \gamma^e{}_b \gamma^c{}_f \nabla_d \nabla_e V^f - K_{ab} n^d \gamma^c{}_f \nabla_d V^f - K_a{}^c K_{bd} V^d \quad . \tag{35}$$

Antisymmetrizing, using (20), the four-dimensional form $\nabla_{[a} \nabla_{b]} V^c = \frac{1}{2} {}^4R^c{}_{dab} V^d$, and noting that V^c is arbitrary (aside from being spatial), yields

$$\gamma^e{}_a \gamma^f{}_b \gamma^g{}_c \gamma^h{}_d \, {}^4R_{efgh} = R_{abcd} + K_{ac} K_{bd} - K_{ad} K_{bc} \quad . \tag{36}$$

This is Gauss' equation.[8] The projection of ${}^4R^c{}_{dab}$ with one index

contracted on n^a can also be obtained. Starting with the spatial covariant derivative of K_{bc}:

$$D_a K_{bc} = -\gamma^d{}_a \gamma^e{}_b \gamma^f{}_c \nabla_d \nabla_f n_e + K_{ac} a_b \quad , \tag{37}$$

this is antisymmetrized on indices a and b to yield the Codazzi equation

$$\gamma^e{}_b \gamma^f{}_a \gamma^g{}_c n^d \, {}^4R_{efgd} = D_a K_{bc} - D_b K_{ac} \quad . \tag{38}$$

Several contracted results will be important. From (36) we obtain

$$\gamma^{eg} \gamma^f{}_b \gamma^h{}_d \, {}^4R_{efgh} = R_{bd} + K K_{bd} - K_{bc} K^c{}_d \quad , \tag{39}$$

and

$$\gamma^{eg} \gamma^{fh} \, {}^4R_{efgh} = R + K^2 - K_{ab} K^{ab} \quad , \tag{40}$$

where $K = \mathrm{tr}(K) = K_a{}^a$. Contracting (38) yields

$$\gamma^{eg} \gamma^f{}_b n^d \, {}^4R_{efgd} = D_b K - D_a K^a{}_b \quad . \tag{41}$$

Thus far the relations that have been derived refer only to conditions within a given slice. Even the extrinsic curvature K_{ab}, which was formed (25) by Lie transporting γ_{ab} along n^a, is *independent* of the extension of n^a away from a given slice. This can be seen from (26) since the projections restrict the covariant derivative to directions tangent to the slice. Equations (36) and (38) must be

regarded as necessary and sufficient integrability conditions to enable imbedding of a slice with data (γ_{ab}, K_{ab}) in the four-dimensional manifold with g_{ab}.[7] As these conditions relate the data only within a given slice, it can be anticipated that they produce the initial value constraints (2). This is the case as we proceed to show.

The left-hand-side of (40) can be rewritten:

$$\gamma^{eg}\gamma^{fh}\,{}^4R_{efgh} = (g^{eg} + n^e n^g)(g^{fh} + n^f n^h)\,{}^4R_{efgh}$$

$$= {}^4R + 2n^c n^d\,{}^4R_{cd} \quad . \tag{42}$$

Using the Einstein tensor, $G_{ab} = {}^4R_{ab} - \tfrac{1}{2}g_{ab}\,{}^4R$, (42) can be shown to equal $2n^c n^d G_{cd}$ as well. Thus,

$$2n^c n^d G_{cd} = R + K^2 - K_{cd}K^{cd} \quad . \tag{43}$$

The left-hand-side of (41) can be recast as $\gamma^f{}_b n^d\,{}^4R_{fd}$ and in turn give

$$\gamma^f{}_b n^d G_{fd} = D_b K - D_a K^a{}_b \quad . \tag{44}$$

Connection is now made with the matter by defining the following projections of the stress-energy tensor T_{cd}:

$$\rho_H = n^c n^d T_{cd} \quad ,$$

$$S_a = -\gamma^c{}_a n^d T_{cd} \quad ,$$

$$S_{ab} = \gamma^c{}_a \gamma^d{}_b T_{cd} \quad . \tag{45}$$

Here ρ_H, S_a, S_{ab} are the energy density, momentum density, and spatial stresses, respectively, defined in the frame at rest in the slice. They are spatial i.e., $S_a n^a = 0$ and $S_{ab} n^b = 0$. These quantities, it should be noted, are less useful in a physical calculation than the corresponding projections obtained in the fluid rest frame. This will be discussed more completely later as the hydrodynamics is considered. Results (43) and (44) can be rewritten as

$$R + K^2 - K_{cd}K^{cd} = 2\rho_H \quad , \tag{46}$$

$$D_a K^a{}_b - D_b K = S_b \quad . \tag{47}$$

These are the initial value equations. Equation (46) is called the Hamiltonian constraint and (47) the momentum constraint.

The remaining Einstein equations refer to the development of the data and the foliation and not just to the individual slices. The final projected components of the curvature tensor are $\gamma^c{}_a \gamma^d{}_b n^e n^f\,{}^4R_{cedf}$. These contain the second derivatives of the metric in the normal direction. Before proceeding to reduce these components, it is important to quantify the notion of the spatial coordinate congruence given before. We first note, $\pounds_n$ is *not* the natural (orthogonal) time derivative along which γ_{ab} and K_{ab} are propagated through the foliation. A vector field t^a is required which will satisfy the duality condition

$$\langle \omega, t \rangle = \langle dt, t \rangle = 1 \quad . \tag{48}$$

One such vector is αn^a as can be seen from (8) and (11). However this is not unique as any vector of the form

$$t^a = \alpha n^a + \beta^a \quad , \tag{49}$$

will satisfy (48) as long as $\langle dt,\beta \rangle = 0$ or

$$\beta_a n^a = 0 \quad . \tag{50}$$

This spatial vector β^a is termed the shift vector; it introduces a tilt between the congruence associated with t^a and the surface normals. The four functions, α and β^a (given (50)), represent the kinematical freedom, guaranteed by general covariance, to choose coordinates in the future of the initial slice, Σ_0. We leave open for the moment the connection between t^a and any spatial coordinates. But note that if (5) holds, this congruence with tangent vectors t^a is parametrized by the time function t and we may write

$$t^a E_a = \frac{\partial}{\partial t} = \partial_t \quad , \tag{51}$$

and so (48) is $\langle dt,\partial_t \rangle = 1$.

The Lie derivative $\pounds_n$ is now supplanted by

$$\pounds_t = \pounds_{(\alpha n+\beta)} = \pounds_{\alpha n} + \pounds_\beta \quad . \tag{52}$$

The derivative $\pounds_{\alpha n}$ has an important property; it always produces spatial tensors when applied to spatial tensors since

$$\pounds_{\alpha n} \gamma^a{}_b = 0 \quad . \tag{53}$$

Calculation of $\pounds_{\alpha n} K_{ab}$ leads to the result

$$\frac{1}{\alpha}\pounds_{\alpha n} K_{ab} = -\frac{1}{\alpha} D_a D_b \alpha - K_{ac}K^c{}_b + \gamma^e{}_a \gamma^f{}_b n^c n^d \, {}^4R_{ecfd} \quad . \tag{54}$$

The last term can be evaluated by noting,

$$\gamma^e{}_a \gamma^f{}_b n^c n^d \, {}^4R_{ecfd} = \gamma^{cd}\gamma^e{}_a \gamma^f{}_b \, {}^4R_{ecfd} - \gamma^e{}_a \gamma^f{}_b \, {}^4R_{ef} \quad . \tag{55}$$

The first term on the right-hand-side is (39), and using (45), ${}^4R_{ab} = G_{ab} - \frac{1}{2} g_{ab} G$ (with $G = g^{ab}G_{ab}$), and (52) we obtain

$$\pounds_t K_{ab} = -D_a D_b \alpha + \alpha[R_{ab} - 2K_{ac}K^c{}_b + KK_{ab} - S_{ab} - \frac{1}{2}\gamma_{ab}(\rho_H - S)] + \pounds_\beta K_{ab} \quad . \tag{56}$$

Here S is the trace $\gamma^{ab}S_{ab}$ of the spatial stresses. When we deal with application of the formalism (Chapter IV) it is convenient to use the mixed form $K^a{}_b$. Using the fact $\pounds_{\alpha n}\gamma_{ab} = \alpha \pounds_n \gamma_{ab}$, (25), and (53) give

$$\gamma^{ac}\pounds_{\alpha n} K_{cb} = \pounds_{\alpha n} K^a{}_b - 2\alpha K^{ac}K_{cb} \quad , \tag{57}$$

and

$$\pounds_t K^a{}_b = -D^a D_b \alpha + \alpha[R^a{}_b + KK^a{}_b - S^a{}_b - \frac{1}{2}\gamma^a{}_b(\rho_H - S)] + \pounds_\beta K^a{}_b \quad . \tag{58}$$

Note the term $-2K_{ac}K^c{}_b$ is removed. Finally, t^a is used to rewrite (25) to obtain

$$\pounds_t \gamma_{ab} = -2\alpha K_{ab} + \pounds_\beta \gamma_{ab} \quad . \tag{59}$$

Equations (46), (47), (56) or (58) and (59) are the first order formulation of the theory for the gravitational field. It is also possible to decompose the equations of motion $\nabla_a T^{ab} = 0$ in a similar fashion and obtain evolution equations for ρ_H and S_a. These are given for completeness:

$$\pounds_t \rho_H + \alpha D_a S^a = \alpha(S_{ab}K^{ab} + K\rho_H) - 2S^a D_a \alpha + \pounds_\beta \rho_H \quad , \tag{60}$$

and

$$\pounds_t S^a + \alpha D_b S^{ab} = \alpha(2K^{ab}S_b + KS^a) - S^{ab}D_b\alpha - \rho_H D^a\alpha + \pounds_\beta S^a \quad , \tag{61}$$

where (60) is found from $n_b \nabla_a T^{ab} = 0$ and (61) from $\gamma^a{}_c \nabla_b T^{bc} = 0$. The spatial stresses S_{ab} are obtained from a constitutive relation, an equation of state, dependent upon ρ_H, S_a and other fluid attributes. However, we have already stated this is not the best approach computationally and it will not be pursued further.

The bases $\{E_a\}$ and $\{E^a\}$ are thus far completely general; they have no special relationship to the one-form ω_a or the congruence described by t^a. We proceed to specialize to a degree. A basis of vectors $\{e_i\}$ $(i = 1,2,3)$ is introduced with each vector tangent to every slice Σ. This requires

$$\langle \omega, e_i \rangle = 0 \quad . \tag{62}$$

We also require that for each vector e_i,

$$\pounds_t e_i = 0 \quad ; \tag{63}$$

i.e., the basis is dragged along t^a. Of course it must be verified that (62) and (63) are compatible; that the transported basis remains spatial. To be true this necessitates $\pounds_t \omega_a = 0$, which can be shown by use of (48):

$$\pounds_t \omega = \pounds_t d\tilde{t} = d(\pounds_t \tilde{t}) = d(t^a \omega_a) = 0 \quad , \tag{64}$$

where to avoid confusion the time function $\tilde{t}$ is here distinguished from the vector t^a.

We take as the fourth basis vector: $e_o{}^a = t^a$. This implies t^a has components, using (48) and (62),

$$t^a = (1,0,0,0) \quad , \tag{65}$$

and t^a commutes with the entire basis: $\pounds_t e_\mu = 0$ $(\mu = 0,1,2,3)$. So by enforcement of (63) the congruence with which t^a is associated is the spatial coordinate congruence alluded to earlier. The condition (65) implies t^a is *a* coordinate basis vector. Its action on a scalar function f, $\underline{t}f = \underline{e}_o f = \partial_t f$ is partial differentiation. Using (63), the effect of $\pounds_t$ on any *tensor* is also partial differentiation:

$$\pounds_t \to \partial_t \quad . \tag{66}$$

With (62), (8), and (10) we obtain

$$n_i = 0 \quad , \tag{67}$$

and so any zeroth contravariant component of a spatial tensor vanishes. Thus $\beta^a = (0,\beta^i)$ and with (49) and (65) this yields

$$n^a = (\alpha^{-1}, -\alpha^{-1}\beta^i) \quad , \tag{68}$$

and

$$n_a = (-\alpha, 0, 0, 0) \quad , \tag{69}$$

since $n_a n^a = -1$. We obtain the immediate consequences,

$$\gamma_{ij} = g_{ij} \quad , \tag{70}$$

from (69) and (12) and also,

$$\gamma^{ab} = \begin{pmatrix} 0 & 0 \\ 0 & \gamma^{ij} \end{pmatrix} \quad . \tag{71}$$

These in turn imply $\gamma^{ij}\gamma_{jk} = \delta^i{}_k$ are three-dimensional inverses and therefore $\beta_i = \gamma_{ij}\beta^j$. This is true in general; spatial indices on spatial tensors are raised and lowered with γ^{ij} and γ_{ij}.

The components of the full four-dimensional metric g_{ab} are now expressible:

$$g_{ab} = \begin{pmatrix} -\alpha^2 + \beta_i\beta^i & \beta_k \\ \beta_\ell & \gamma_{k\ell} \end{pmatrix} \quad , \tag{72}$$

giving the line element

$$ds^2 = (-\alpha^2 + \beta_i\beta^i)dt^2 + 2\beta_i\, dx^i dt + \gamma_{ij}\, dx^i dx^j \quad . \tag{73}$$

Since $V^0 = 0$ for contravariant spatial vectors and V_0 can be obtained by solving $n^a V_a = 0$ in the case of covariant vectors (the argument extends to arbitrary rank tensors), the entire content of equations (46), (47), (56), and (59) is available in their restriction to spatial components. Using (66), the fundamental equations (for the gravitational field) of the ADM method are

Hamiltonian constraint:
$$R + K^2 - K_{ij}K^{ij} = 2\rho_H \quad , \tag{74}$$

Momentum constraint:
$$D_j(K^{ij} - \gamma^{ij}K) = S^i \quad , \tag{75}$$

$$\begin{aligned} \partial_t K_{ij} = {} & -D_i D_j \alpha + \alpha[R_{ij} - 2K_{i\ell}K^\ell{}_j + KK_{ij} \\ & - S_{ij} - \tfrac{1}{2}\gamma_{ij}(\rho_H - S)] + \beta^\ell D_\ell K_{ij} \\ & + K_{i\ell}D_j\beta^\ell + K_{\ell j}D_i\beta^\ell \quad , \end{aligned} \tag{76}$$

and

$$\partial_t \gamma_{ij} = -2\alpha K_{ij} + D_i\beta_j + D_j\beta_i \quad . \tag{77}$$

Here the Lie derivative terms have been expanded by (24) and the mixed index result (58) can be found easily,

$$\begin{aligned} \partial_t K^i{}_j = {} & -D^i D_j \alpha + \alpha[R^i{}_j + KK^i{}_j - S^i{}_j \\ & - \tfrac{1}{2}\delta^i{}_j(\rho_H - S)] + \beta^\ell D_\ell K^i{}_j \\ & + K^i{}_\ell D_j\beta^\ell - K^\ell{}_j D_\ell \beta^i \quad . \end{aligned} \tag{78}$$

The equations have now been written solely in terms of three-dimensional spatial tensors and the (3 + 1) splitting has been achieved.

Finally we note that (74) -(78) embody a great deal of generality in that we have made no restriction on the spatial basis $\{e_i\}$ and its one-form dual $\{e^i\}$.[7] These basis vectors need not commute $[e_i,e_j] = e_k C^k{}_{ij} \neq 0$ (a non-coordinate basis) and in these cases preservation of the spatial covariant derivatives in the Lie derivative expansions in (76) -(78) is essential. In most applications, the simplifications attendant to coordinate bases will be desirable and, with the vanishing of the structure constants $C^k{}_{ij} = 0$, we may replace D_i with ∂_i in these terms.

b) Hydrodynamics

We now turn our attention to the formulation, due to Wilson,[9,10] of the relativistic hydrodynamic equations. Using (45), the stress-energy tensor can be reconstructed in terms of ADM quantities:

$$T^{ab} = \rho_H n^a n^b + S^a n^b + S^b n^a + S^{ab} \quad . \tag{79}$$

In the frame of the Eulerian observers, the fluid *appears* imperfect since there will be a momentum flux (S^a) and anisotropic stresses (S^{ab}) in general. To describe a perfect fluid we work instead in the fluid rest frame. There the stress-energy tensor has the form

$$T^{ab} = \rho h U^a U^b + p g^{ab} \quad , \tag{80}$$

where the relativistic specific enthalpy is

$$h = 1 + \varepsilon + p/\rho \quad . \tag{81}$$

Here ρ, ε, and p are the rest energy density, specific internal energy density and the isotropic pressure respectively. The fluid four-velocity satisfies, of course,

$$U_a U^a = -1 \quad . \tag{82}$$

These two forms of the stress-energy tensor can be related. The scalar quantity

$$U = -n_a U^a = \alpha U^t \quad , \tag{83}$$

evaluated using (69), is of primary importance. Since this is the inner product of the two timelike unit vectors, it represents the local boost factor (analogous to the special relativistic γ) between the Eulerian observers (n^a) and Lagrangian observers (U^a). Projecting (80) with n_a and $\gamma^b{}_a$ we obtain the connections

$$\rho_H = \rho h U^2 - p \quad , \tag{84}$$

$$S_i = \rho h U U_i \quad , \tag{85}$$

$$S_{ij} = p\gamma_{ij} + \rho h U_i U_j = p\gamma_{ij} + \frac{S_i S_j}{\rho h U^2} \quad , \tag{86}$$

with the ADM quantities. Using (82) a more useful form for U is

derived by noting

$$U_t = \beta^i U_i - \alpha(1 + \gamma^{ij}U_iU_j)^{\frac{1}{2}} \quad , \tag{87}$$

$$U^t = \frac{1}{\alpha}(1 + \gamma^{ij}U_iU_j)^{\frac{1}{2}} \quad , \tag{88}$$

and so

$$U = (1 + \gamma^{ij}U_iU_j)^{\frac{1}{2}} \quad . \tag{89}$$

With this latter result, the trace $S = S^a{}_a$, used in (76) and (78), is shown to be:

$$S = 3p + \rho h(U^2 - 1) \quad . \tag{90}$$

We employ fluid rest frame quantities (84) -(86) in the hydrodynamic description and the decomposition is performed relative to U^a and not n^a.

The matter may be taken to have a number of conserved scalar attributes (e.g., baryon number, lepton number, charge, etc.) each satisfying equations of the form

$$\nabla_a(\rho_{(i)}U^a) = 0 \quad . \tag{91}$$

We will assume of our fluid at minimum that baryon number, proportional to ρ, is conserved:

$$\nabla_a(\rho U^a) = 0 \quad , \tag{92}$$

or equivalently, where $g \equiv \det(g_{ab})$,

$$\frac{1}{\sqrt{-g}}\partial_a(\sqrt{-g}\,\rho U^a) = 0 \quad . \tag{93}$$

The equations of motion

$$\nabla_a T^{ab} = 0 \quad , \tag{94}$$

give an equation for internal energy by evaluating $U_b\nabla_a T^{ab} = 0$:

$$\nabla_a(\rho\varepsilon U^a) = -p\nabla_a U^a \quad , \tag{95}$$

and (92) has been used to subtract the rest energy density. This can be rewritten as

$$\frac{1}{\sqrt{-g}}\partial_a(\sqrt{-g}\,\rho\varepsilon U^a) = -\frac{p}{\sqrt{-g}}\partial_a(\sqrt{-g}\,U^a) \quad . \tag{96}$$

Finally, the momentum equation is determined from the $(\delta^a{}_c - U^aU_c)$ projection of

$$\nabla_b T^b{}_a = \nabla_b(\rho h\, U^bU_a) + \nabla_a p = 0 \quad , \tag{97}$$

which can be put in the form

$$\frac{1}{\sqrt{-g}}\partial_b(\sqrt{-g}\,\rho h\, U_aU^b) + \partial_a p + \frac{1}{2}\rho h\, U_bU_c\partial_a g^{bc} = 0 \quad . \tag{98}$$

Wilson's method involves writing these equations in a form which most closely resembles Newtonian hydrodynamics. In this way the vast body of knowledge on how to treat numerically ordinary hydrodynamics can be brought to bear on the relativistic version. To this

end, we define the following quantities:

$$V^i = U^i/U^t \quad ,$$

$$D = \rho U \quad ,$$

$$E = \rho\varepsilon U \quad , \tag{99}$$

and, in terms of these, (85) becomes

$$S_i = \rho h\, UU_i = (D + E + pU)U_i \quad . \tag{100}$$

Then, using $\sqrt{-g} = \alpha\gamma^{1/2}$ where $\gamma = \det(\gamma_{ij})$, the fluid equations become

$$\partial_t(\gamma^{1/2}D) + \partial_i(\gamma^{1/2}DV^i) = 0 \quad , \tag{101}$$

$$\partial_t(\gamma^{1/2}E) + \partial_i(\gamma^{1/2}EV^i) = -p[\partial_t(\gamma^{1/2}U) + \partial_i(\gamma^{1/2}UV^i)] \quad , \tag{102}$$

$$\partial_t(\gamma^{1/2}S_j) + \partial_i(\gamma^{1/2}S_jV^i) = -\alpha\gamma^{1/2}[\partial_j p + \tfrac{1}{2}\rho h U_a U_b \partial_j g^{ab}] \quad . \tag{103}$$

Part of the analogy with Newtonian hydrodynamics comes from the divergence form of the transport terms. Later this fact will be very important (Chapter V) as we will employ a conservative differencing algorithm for the transport. Equation (102) represents our general relativistic version of the first law of thermodynamics. The right-hand-side of (102) is the "pdV" work term. The source for the momentum density (103) contains the pressure gradient and the term $U_aU_b\partial_j(g^{ab})$, which remains to be simplified in a particular gauge. The latter term supplies the gravitational and coordinate accelerations.

The ρh in this term plays the role of an effective inertial energy density.[11]

We have already noted that the factor U, appearing in the equations (101) -(103) and in the definitions (99) and (100), is a local boost; it reduces to the usual special relativistic Lorentz factor in flat space. There are also additional relativistic effects in (101) -(103) due to the appearance of $\gamma^{1/2}$.

It is also useful to be able to obtain U from the fluid state variables and ADM quantities. Using (89) and (100) the following *implicit* equation results:

$$U = \left[1 + \frac{\gamma^{ij}S_iS_j}{(D + E + pU)^2}\right]^{1/2} \quad . \tag{104}$$

As was mentioned earlier, an equation of state must be specified to determine the pressure. The matter could be quite complex, requiring several equations of state to relate, say, pressure, temperature, chemical potentials $\mu_{(i)}$ to the density ρ, energy density $\rho\varepsilon$, and abundances.[12] We will for the most part want to consider simple (one component) fluids and, in particular, consider a *barotropic* equation of state (EOS). Such an EOS relates the pressure to only *one* other thermodynamic variable, e.g., $p = p(\rho)$.

The EOS that we use is the *adiabatic* law

$$p = (\Gamma - 1)\rho\varepsilon \quad , \tag{105}$$

with adiabatic index Γ. Note, Γ cannot be referred to as the ratio of specific heats since the second equation of state relating p and $\rho\varepsilon$ to temperature, T, is ignored (a specification of specific heats is required). Substituting (105) in (92) and (95) results in the usual adiabatic relation

$$U^a\nabla_a(p/\rho^\Gamma) = 0 \quad , \tag{106}$$

i.e., that $p/\rho^\Gamma = \kappa$ is constant along fluid flow lines. The equation

$$p = \kappa\rho^\Gamma \quad , \tag{107}$$

is a *polytropic* law and the polytropic index is $n = (\Gamma - 1)^{-1}$.

A consequence of the perfect fluid assumption (80) and conservation of baryon number (92) is that the entropy of the fluid is conserved along flow lines. This can be seen by writing the first law in the form

$$Tds = dh - \rho^{-1}\, dp \quad , \tag{108}$$

where s is the specific entropy. This can be rewritten as

$$TU^a\nabla_a s = -U_b U^a\nabla_a(hU^b) - \rho^{-1}\, U^a\nabla_a p \quad , \tag{109}$$

which combined with (92) and (95) gives

$$U^a\nabla_a s = 0 \quad . \tag{110}$$

A perfect fluid is said to be *locally adiabatic*. Note, however, the fluid need not be *isentropic* i.e., $\nabla_a s = 0$.

The fluids encountered in real situations will in general not only be anisentropic but also imperfect. If for no other reason, this is due to the fact that fluids *shock*. Even if viscous effects are small enough to be ignored in the smooth regions of a flow, they are always important in the shock fronts.

If viscous effects in the smooth regions of the flow need to be included, then the standard theories[13,14,20] of relativistic imperfect fluids can be applied to modify the stress-energy tensor (80) and account for entropy transport (cf. equation (110)). Shocks, however, will not be modeled in detail in general, unless this result is the main reason for the calculation. The problem here is that shock fronts are no more than several mean-free-paths wide, whereas the smooth flow may have a characteristic length, particularly true of astrophysical problems, many orders of magnitude larger. In a numerical calculation the effects of the shock must be spread over a region several zones wide. What is important is the satisfaction of the Rankine-Hugoniot jump conditions[13,15] across this region (the relativistic version of these conditions is given in the Appendix). This is accomplished by the introduction of a mathematical artifice,[16] called an artificial viscosity or pseudo-viscosity, into the numerical algorithm. It is equivalent to adding a term to the stress-energy tensor (80), which makes the fluid imperfect (viscous) in localized regions that are shocking, and which guarantees the fluid equations reproduce the jump conditions. The adiabatic condition (110) is then violated and heat is generated. We return to this topic in Chapter V.

A second effect due to shocks, the generation of vortices, is also important and very evident in our calculations. To describe vortices in our calculational framework, a relativistic definition of circulation and a generalization of the Helmholtz theorem is required. Such a generalization, discussed by Smarr, Taubes, and Wilson,[11] has been developed by Taub[17] drawing on earlier work of Synge[18] and Lichnerowicz.[15,19]

To this end, the *enthalpy current* defined by

$$\mu_a = hU_a \quad , \tag{111}$$

is a fundamental quantity. We consider a closed curve, with path parameter σ, and corresponding spacelike tangent vector λ^a. The relativistic circulation is defined by

$$C = \oint \mu_a \alpha^a \, d\sigma = \oint hU_a \lambda^a \, d\sigma \quad . \tag{112}$$

Note that the non-relativistic definition[13] is recovered in the limits $h \to 1$ and $U_a \to V_i$. By use of Stoke's theorem it can be shown that the initial circulation vanishes only if the initial flow is both irrotational *and* isentropic. This result is proved in the Appendix of this chapter.

The circulation theorem (Helmholtz theorem) is a statement on the conditions for growth (or decay) of C. If we consider the contour of (112) as carried forward in time along the fluid flow lines, the rate of change of C with proper time is

$$\frac{dC}{d\tau} = \oint T(\nabla_a s)\lambda^a \, d\sigma \tag{113}$$

where T and s are the temperature and specific entropy, respectively, from (108). Obviously entropy gradients are necessary to drive changes in the circulation. Not so obvious is the result that, with Stoke's theorem and (113), the circulation is conserved, i.e., $\frac{dC}{d\tau} = 0$, only if the EOS is barotropic. This is also shown in the Appendix.

Despite the assumption of an EOS of the form (105), the barotropic condition necessarily is violated in shocks. A shock will leave entropy gradients in its wake (even if none were present initially) and thus drive circulation. At the risk of racing ahead in the discussion, this can be graphically illustrated by a collapse and bounce calculation made with the code. Figures 1a, b show the hydrodynamical motion, density contours and velocity field, at two times in the collapse. Figure 1a represents the situation at t = 0. The material was assumed isentropic initially and is very nearly irrotational. A strong shock wave is apparent in figure 1b at cycle = 2500 in the calculation and after the core has bounced. A vortex is clearly evident in the wake of the shock. Note that the circulation appears largest in the region where the shock has descended density contours *obliquely*. It is here that the contour integral of $T\nabla_a s$ is maximized.

Figures 1a,b. Hydrodynamic snapshots showing rest energy density contours and velocity field vectors. The symmetry axis is the vertical axis; the equatorial plane is represented by the horizontal axis. Figure 1a indicates the start of the calculation. The material is assumed initially isentropic and nearly irrotational. Figure 1b shows the motion at 2500 cycles into the calculation after the core has bounced. A vortex is evident in the wake of the primary shock.

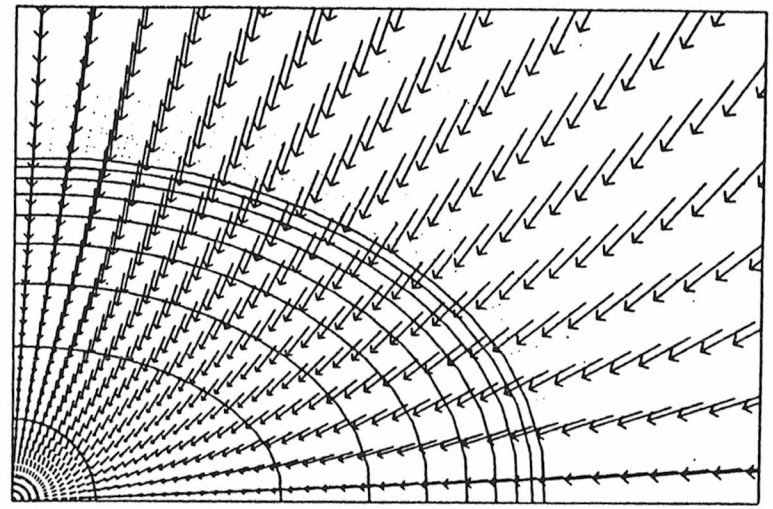

Figure 1a

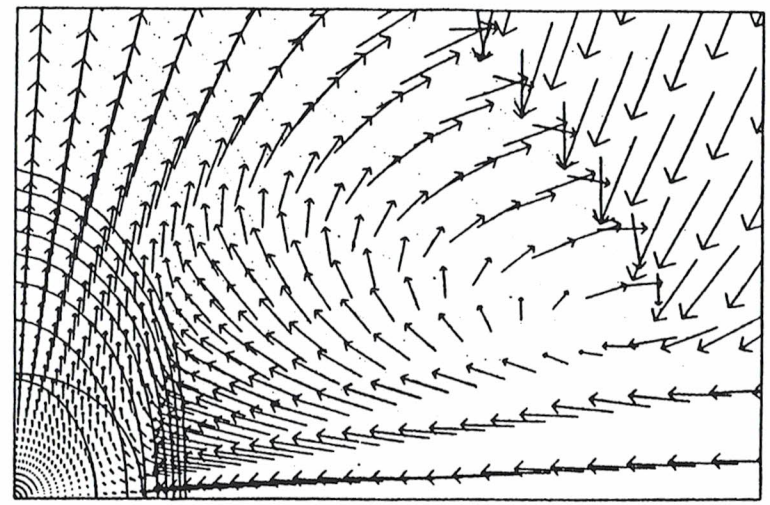

Figure 1b

Chapter II References

1. Arnowitt, Deser, and Misner (ADM) (1962).
2. Small Latin indices from a to h run over 0,1,2,3. Indices from i to n range from 1,2,3, i.e., are spatial indices.
3. Weinberg (1972).
4. We adopt geometrized units by setting $8\pi G = 1$ and $c = 1$.
5. Moncrief (1975).
6. Evans (1984).
7. York (1979).
8. Hawking and Ellis (1973).
9. Wilson (1979).
10. Dykema (1980).
11. Smarr, Taubes, and Wilson (1980).
12. Callen (1960).
13. Landau and Lifshitz (1959).
14. Eckart (1940).
15. Lichnerowicz (1967).
16. von Neumann and Richtmyer (1950).
17. Taub (1959).
18. Synge (1937).
19. Lichnerowicz (1955).
20. May and White (1967); May and White (1966).
21. Crowley (1975).

APPENDIX

To verify the claims on relativistic circulation, the closed contours with path parameter σ and spacelike tangent vector, λ^a, are used to produce *tubes* through spacetime. These tubes have topology $S^1 \times R$ and are derived from transporting the contours along fluid flow lines (along integral curves of the four-velocity U^a). If X^a represent locations on the tube, these points are parametrized by the two coordinates σ and the proper time τ; i.e., $X^a(\sigma,\tau)$. This implies the basis vectors $\lambda^a = \frac{\partial X^a}{\partial \sigma}$ and $U^a = \frac{\partial X^a}{\partial \tau}$ on the tube form a coordinate basis and thus commute:

$$\frac{\partial U^a}{\partial \sigma} = \frac{\partial}{\partial \sigma}\frac{\partial X^a}{\partial \tau} = \frac{\partial}{\partial \tau}\frac{\partial X^a}{\partial \sigma} = \frac{\partial \lambda^a}{\partial \tau} \quad . \tag{A1}$$

The relativistic enthalpy h, as we have defined it, has also been called the *index function*[18] and the *index of the fluid*.[15] The enthalpy current (111), defined with h, can be used to form what will be called here the *enthalpy vorticity tensor*:

$$\Lambda_{ab} = \nabla_b \mu_a - \nabla_a \mu_b \quad . \tag{A2}$$

This is related to the velocity vorticity tensor,

$$\omega_{ab} = \nabla_b U_a - \nabla_a U_b \quad , \tag{A3}$$

by

$$\Lambda_{ab} = h\omega_{ab} + U_a\nabla_b h - U_b\nabla_a h \quad . \tag{A4}$$

We additionally have use for the vorticity vector ξ^a defined with ω_{cd} by

$$\xi^a = \frac{1}{2}\eta^{abcd}\omega_{cd}U_b \quad , \tag{A5}$$

where η^{abcd} is the four-dimensional Levi-Civita tensor. Equation (A5) can be inverted to give

$$\omega_{ab} = \xi^c U^d \eta_{cdab} - U_a(\nabla_d U_b)U^d + U_b(\nabla_d U_a)U^d \quad . \tag{A6}$$

To proceed further, we take the spatial projection of (97)

$$(\delta^a{}_c - U^a U_c)[\nabla_b(\rho h U^b U_a) + \nabla_a p] = 0 \quad , \tag{A7}$$

which can be rewritten as

$$\rho h U^b \nabla_b U_c + (\delta^a{}_c - U^a U_c)\nabla_a p = 0 \quad . \tag{A8}$$

A second intermediate result comes from putting (108) in the form

$$T\nabla_a s = \nabla_a h - \frac{1}{\rho}\nabla_a p \quad . \tag{A9}$$

Combining (A8), (A9) with (A6) and (A4) yields a fundamental result:

$$\Lambda_{ab} = h\xi^c U^d \eta_{cdab} + T(\nabla_b s)U_a - T(\nabla_a s)U_b \quad . \tag{A10}$$

Before discussing the significance of (A10), we recast the definition (112) of the relativistic circulation. The integrand $\mu_a\lambda^a d\sigma$ can be written as the differential 1-form $\mu = \mu_a dx^a$, where $x^a = X^a(\sigma,\tau)$, and the path forms the closed boundary of a 2-surface, A. Stoke's theorem may then be used with (A2) to obtain

$$C = \int_{\partial A}\mu = \int_A d\mu = \frac{1}{2}\int_A \Lambda_{ab}\, dx^b \wedge dx^a \quad . \tag{A11}$$

It can be seen that if Λ_{ab} vanishes on a surface bounded by the initial closed curve then the circulation also vanishes. From (A10) it is clear that $\xi^a = 0$ and $\nabla_a s = 0$ imply $\Lambda_{ab} = 0$. The converse can also be demonstrated. Contracting (A10) with U^b and using the perfect fluid assumption through (110) gives

$$\Lambda_{ab}U^b = T\nabla_a s \quad , \tag{A12}$$

and thus if $\Lambda_{ab} = 0$ then $\nabla_a s = 0$ follows. In this case using (A10) we obtain

$$\xi^c U^d \eta_{cdab} = 0 \quad , \tag{A13}$$

as well. If ξ^c is to be nonvanishing, (A13) is possible only if ξ^c is proportional to U^c. From (A5) however we have $\xi_a U^a = 0$ and since U^a is timelike (nonnull) this leads to the conclusion $\xi^a = 0$. Thus the vanishing of Λ_{ab} has the necessary and sufficient conditions that the fluid be irrotational ($\xi^a = 0$) and isentropic ($\nabla_a s = 0$), locally.

The vanishing of the circulation on a contour or tube is a nonlocal result; it requires that the flow satisfy the above conditions throughout a 2-surface bounded by the contour.

We digress momentarily to obtain an interesting result. So far the bounded 2-surface A has been quite general except that the tangent vectors to the bounding contour must be spacelike. If this 2-surface is restricted to lie (as well as the contour) in the hypersurfaces $\Sigma(t)$, connection with the ADM approach can be made. Positions in A can be represented as $Z^a(u,v)$ where u and v are coordinates parametrizing the surface. These generate tangent vectors: $\zeta^a_{(u)} = \frac{\partial Z^a}{\partial u}$ and $\zeta^a_{(v)} = \frac{\partial Z^a}{\partial v}$ spanning the tangent plane. The restriction of A to $\Sigma(t)$ implies $\zeta^a_{(u)}$ and $\zeta^a_{(v)}$ are spatial, i.e.,

$$\zeta^a_{(u)} n_a = \zeta^a_{(v)} n_a = 0 \quad . \tag{A14}$$

The result for the circulation can be written out as

$$C = \int_A \nabla_{[b}\mu_{a]}\, dx^b \wedge dx^a \quad . \tag{A15}$$

Using the tangent vectors $\zeta^a_{(u)}$ and $\zeta^a_{(v)}$, this can be reduced to

$$C = \int \nabla_{[b}\mu_{a]}(\zeta^b_{(u)}\zeta^a_{(v)} - \zeta^a_{(u)}\zeta^b_{(v)})du \wedge dv \quad . \tag{A16}$$

Then since the tangent vectors are spatial, (A14), we obtain

$$C = \int \gamma^d{}_b \gamma^c{}_a \nabla_{[d}\mu_{c]}(\zeta^b_{(u)}\zeta^a_{(v)} - \zeta^a_{(u)}\zeta^b_{(v)})du \wedge dv \quad . \tag{A17}$$

The enthalpy current μ_c is timelike (111) but may be decomposed to

$$\mu_c = \tilde{\mu}_c + hUn_c \quad , \tag{A18}$$

where $\tilde{\mu}_c = \gamma^d{}_c \mu_d$ is the spatial projection. Using this decomposition we obtain

$$\gamma^d{}_b \gamma^c{}_a \nabla_{[d}\mu_{c]} = D_{[b}\tilde{\mu}_{a]} \quad , \tag{A19}$$

using (30). This result is totally spatial; with its substitution in (A17) the summations can be restricted to spatial indices. Thus,

$$C = \int D_{[i}\tilde{\mu}_{j]}(\zeta^i_{(u)}\zeta^j_{(v)} - \zeta^j_{(u)}\zeta^i_{(v)})du \wedge dv \quad . \tag{A20}$$

To proceed further a normal unit vector m_k is introduced by $Am_k \equiv \epsilon_{k\ell m}\zeta^\ell_{(u)}\zeta^m_{(v)}$ where $m_k m^k = 1$ and $\zeta^i_{(u)}\zeta^j_{(v)} - \zeta^j_{(u)}\zeta^i_{(v)} = \epsilon^{ijk}Am_k$. Using the definition $\epsilon^{ijk}D_{[i}\tilde{\mu}_{j]} \equiv (\text{curl}\ \tilde{\mu})^k$ and choosing the surface tangent vectors to be right-handed with respect to the boundary tangent, λ^i, allows the circulation to be expressed as

$$C = \int (\text{curl}\ \tilde{\mu})^k\, m_k A\, du dv \quad . \tag{A21}$$

The normalizing factor A can be determined from the above definition, which gives

$$A^2 = |\zeta_{(u)}|^2|\zeta_{(v)}|^2 - (\zeta_{(u)}\cdot\zeta_{(v)})^2 \quad , \tag{A22}$$

where $|\xi_{(u)}|^2 = \zeta^i_{(u)}\zeta_{(u)i}$ and $\zeta_{(u)}\cdot\zeta_{(v)} = \zeta^i_{(u)}\zeta_{(v)i}$. To interpret this

factor, we calculate the induced metric on the 2-surface. We have

$$ds^2 = \gamma_{ij}\, dx^i dx^j = \gamma_{ij}\zeta^i{}_A \zeta^j{}_B\, du^A du^B \quad , \tag{A23}$$

where capital indices A, B are restricted to A = 1,2 and $du^A = (du, dv)$. The two-dimensional metric is therefore ${}^2\gamma_{AB} = \gamma_{ij}\zeta^i{}_A\zeta^j{}_B$. Its determinant, ${}^2\gamma \equiv \det({}^2\gamma_{AB})$, is shown easily to be just (A22) A^2. Thus the result (A21) can be rewritten in the particularly simple covariant three-dimensional form

$$C = \int (\mathrm{curl}\ \tilde{\mu})^k\, m_k\, ({}^2\gamma)^{\frac{1}{2}}\, du dv \quad , \tag{A24}$$

despite that this derives originally from four-dimensional quantities.

The result (113) for the rate of change of the circulation along the tube with respect to proper time is now derived. Taking the derivative (112) gives[17]

$$\frac{dC}{d\tau} = \oint \left\{ (\nabla_b \mu_a) U^b \lambda^a + \mu_a \frac{\partial \lambda^a}{\partial \tau} \right\} d\sigma \quad . \tag{A25}$$

Using (A1) and (A2),

$$\frac{dC}{d\tau} = \oint \left\{ \Lambda_{ab} U^b \lambda^a + (\nabla_a \mu_b) U^b \lambda^a + \mu_a \frac{\partial U^a}{\partial \sigma} \right\} d\sigma \quad . \tag{A26}$$

Since we may write $\lambda^a \nabla_a \mu_b = \frac{\partial \mu_b}{\partial \sigma}$, the last two terms may be grouped, $\frac{\partial}{\partial \sigma}(\mu_a U^a)$, which contributes nothing around a closed contour. With (A12), equation (113)

$$\frac{dC}{d\tau} = \oint T(\nabla_a s)\, \lambda^a d\sigma \quad , \tag{A27}$$

is obtained. A sufficient condition for the circulation to be constant (with respect to proper time) is that the fluid be isentropic. This is not a necessary condition, however. The necessary and sufficient condition is that, by Stoke's theorem,

$$\nabla_b [T(\nabla_a s)] - \nabla_a [T(\nabla_b s)] = 0 \quad . \tag{A28}$$

Using (A9) this can be written as

$$\nabla_a p \nabla_b \rho - \nabla_b p \nabla_a \rho = 0 \quad . \tag{A29}$$

By the same argument as before (see equation (A13)) this is possible if and only if

$$\nabla_a p = f \nabla_a \rho \quad , \tag{A30}$$

i.e., the gradients are proportional with some function f. If the EOS is barotropic, $p = p(\rho)$, (A30) is satisfied and indeed we find $f = \frac{\partial p}{\partial \rho}$, the sound speed squared. If the EOS is of the form $p = p(\rho, s)$, taking the total differential shows (A30) cannot be satisfied. The circulation is therefore constant if the EOS is barotropic (e.g., eqn. (105)).

However, from (A28) if the circulation is to be driven ($\frac{dC}{d\tau} \neq 0$) it is not sufficient for the fluid to be only anisentropic but, from (A28), there must also be temperature gradients. Indeed, it must also be true that $\nabla_a T \neq g \nabla_a s$, where g is some scalar. This is equivalent to the argument given above regarding a non-barotropic

EOS violating (A30). This has the important consequence for shock driven vorticity changes that ΔC is maximized in regions where the shock propagates obliquely with respect to the density gradient.

If a temperature has not been defined, (A27) may be rewritten using the first law (A9):

$$\frac{dC}{d\tau} = -\oint \frac{1}{\rho}(\nabla_a p)\lambda^a \, d\sigma \quad . \tag{A31}$$

In our numerical simulations, if the EOS (105) is employed, $\frac{dC}{d\tau}$ will be nonvanishing only in regions where the artificial viscosity is operative. However the results (A27) and (A31) are not strictly valid in such situations since the locally adiabatic assumption (110) (dependent on the perfect fluid assumption), used in deriving (A12), will be violated.

A shock propagating through spacetime is represented by a three-dimensional discontinuity surface with a spacelike normal vector w^a. The equations of motion (92) and (94) give the jump conditions

$$[\rho U^a w_a] = 0 \quad , \quad \text{and}$$
$$[T^{ab} w_b] = 0 \quad , \tag{A32}$$

by integrating and using Gauss' Theorem. Here the bracket is the usual notation indicating the difference of the limits from above and below the discontinuity surface i.e., $[A] = A_+ - A_-$. We single out the invariant quantity

$$F = \rho_+ U_+^a w_a = \rho_- U_-^a w_a \quad , \tag{A33}$$

from (A32). Using the definition (80), the second condition can be written as

$$F(h_+ U_+^a - h_- U_-^a) = w^a(p_+ - p_-) \quad . \tag{A34}$$

Alternately, contracting with U_+^a and U_-^a, the fundamental relativistic Rankine-Hugoniot condition

$$h_+^2 - h_-^2 = \left(\frac{h_+}{\rho_+} + \frac{h_-}{\rho_-}\right)(p_+ - p_-) \tag{A35}$$

is obtained. In the limits $h \to 1$; ε, $p/\rho \to 0$, this reduces to the nonrelativistic result,[13,21]

$$\varepsilon_+ - \varepsilon_- = \frac{p_+ + p_-}{2\rho_+\rho_-}(\rho_+ - \rho_-) \quad . \tag{A36}$$

Equation (A35) can be cast in a dimensionless form

$$M^2 - 1 = \alpha^2(y - 1)\left(\frac{M}{\eta} + 1\right) \quad , \tag{A37}$$

where $M = \frac{h_+}{h_-}$, $y = \frac{p_+}{p_-}$, $\eta = \frac{\rho_+}{\rho_-}$, and $\alpha^2 = \frac{p_-}{\rho_- h_-}$. Note that the size of α^2 determines the degree to which the preshock gas is relativistic. The ratio of enthalpies, M, may be eliminated from (A37) upon substitution of an equation of state. Using the adiabatic EOS (105), yields the equation

$$[y(\Gamma - 1) + (\Gamma q + 1)]\eta^2 - q[y(\Gamma + 1) + (\Gamma - 1)]\eta$$

$$- (1 - q)y(y + \Gamma - 1) = 0 \quad , \tag{A38}$$

to be solved for the density ratio η in terms of the pressure ratio y. Here $q = h_-^{-1}$ is the factor determining the importance of relativity. The nonrelativistic limit is achieved by taking $q \to 1$ and we obtain from (A38) the familiar result for a "perfect gas"[13,21]:

$$\eta = \frac{y(\Gamma + 1) + (\Gamma - 1)}{y(\Gamma - 1) + (\Gamma + 1)} \quad . \tag{A39}$$

For strong shocks $y >> 1$, (A39) implies the usual maximum shock compression

$$\eta \to \frac{\Gamma + 1}{\Gamma - 1} \quad . \tag{A40}$$

For moderately relativistic configurations, (A38) must be solved fully; care must be taken to use the solution for which $s_+ - s_- > 0$ when $\eta > 1$ and $y > 1$. A second interesting limit results if the preshock gas is extremely relativistic. In this case $q \to 0$ and the compression satisfies

$$\eta = \left[\frac{y(y + \Gamma - 1)}{y(\Gamma - 1) + 1}\right]^{1/2} \quad . \tag{A41}$$

This has the interesting implication that for strong shocks, $y >> 1$, the compression ratio continues to rise with y, $\eta \to \left[\frac{y}{\Gamma - 1}\right]^{1/2}$, as opposed to (A40). For all such strongly relativistic systems it is

likely that the effective adiabatic index approaches $\Gamma \to 4/3$. Certainly for the sound speed

$$v_s^2 = \Gamma \frac{p}{\rho} \frac{1}{1 + \frac{\Gamma}{\Gamma - 1}\frac{p}{\rho}} \quad , \tag{A42}$$

to remain bounded by $v_s^2 \leq 1$ requires $\Gamma \leq 2$.

Obtaining a more familiar form for the *velocity* jump condition (A33) is difficult owing to the complete generality of the spacetime coordinates. We proceed to a degree by *defining* a shock velocity $U^a_{(s)}$:

$$U_{(s)}U^a_{(s)} = n^a + U_{(w)}w^a \quad , \tag{A43}$$

where $U_{(w)} = -n_a w^a$ and $U_{(s)} = -n_a U^a_{(s)}$. The vector $U^a_{(s)}$ is tangent to the discontinuity surface (i.e. $U^a_{(s)}w_a = 0$), timelike normalized, $U^a_{(s)}U_{(s)a} = -1$, and orthogonal to the two-surface formed by the intersection of the shock surface and the simultaneity $\Sigma(t)$. Note, however, that whereas the vector w^a has invariant meaning, the shock velocity depends upon the chosen time slicing and n^a. Contracting (A43) with n_a yields

$$U^2_{(s)} = 1 + U^2_{(w)} \quad . \tag{A44}$$

Using (A43) and (A44) to rewrite (A32) gives

$$[\rho U^a w_a] = \frac{1}{\sqrt{U^2_{(s)} - 1}}\left\{[\rho U] + U_{(s)}U_{(s)a}[\rho U^a]\right\} = 0 \quad , \tag{A45}$$

or

$$\rho_+ U_+ - \rho_- U_- + g_{ab} U_{(s)} U^a_{(s)} (\rho_+ U^b_+ - \rho_- U^b_-) = 0 \quad . \qquad \text{(A46)}$$

Without knowledge of the metric it is difficult to proceed beyond (A46). If, however, we use a local inertial frame or restrict the calculation to flat space, special relativity, (A46) becomes

$$\rho_+ \gamma_+ \{1 - \gamma^2_{(s)} (1 - V_{(s)} \cdot V_+)\} = \rho_- \gamma_- \{1 - \gamma^2_{(s)} (1 - V_{(s)} \cdot V_-)\} \quad , \qquad \text{(A47)}$$

where $U^a_+ = U^t_+ (1, V^i_+) = \gamma_+ (1, V^i_+)$. If relative velocities are assumed small, i.e. $V_{(s)}$, V_+, $V_- \ll 1$, and $\gamma^2_{(s)} = \frac{1}{1 - V_{(s)} \cdot V_{(s)}} \cong 1 + V_{(s)} \cdot V_{(s)} \to 1$, then (A47) reduces to

$$\rho_+ V_{(s)} \cdot (V_+ - V_{(s)}) = \rho_- V_{(s)} \cdot (V_- - V_{(s)}) \quad , \qquad \text{(A48)}$$

the usual Rankine-Hugoniot condition.

CHAPTER III

The ADM equations for the gravitational field (II74-77) and Wilson's formulation of the hydrodynamic equations (II101-103) were derived in the previous chapter. Here we consider how solutions to these equations are to be found (either "by hand" or with the computer). There are several identifiable steps to solving the Cauchy problem. First, a solution to the initial value problem (IVP) must be obtained. Then gauge conditions must be judiciously applied to construct a foliation of spacetime and a spatial coordinate congruence as the calculation unfolds. Finally, the equations of motion are integrated, propagating the initial data along the chosen spacetime coordinates. In this last aspect, we must decide in a numerical context whether to employ the constraints, which in an analytic sense are superfluous once the IVP has been solved, to produce a fully constrained solution. This chapter is devoted to a discussion of general aspects of the conformal approach to solving the IVP, to how the constraints are solved on subsequent time slices to provide a fully constrained evolution, and to several useful classes of gauge conditions.

a) Initial Value Problem

As has been mentioned previously, the IVP is embodied by the four constraint equations (II74,75). Starting values for the gravitational fields (γ_{ij},K^{ij}) must be found that are compatible with chosen initial matter fields (ρ_H,S^i). Once the IVP is solved, gauge conditions are imposed to determine the lapse function α ($(-g^{00})^{-\frac{1}{2}}$) and the shift vector β_i (g_{0i}). These are *kinematical*, not dynamical, quantities since the decomposed Einstein equations reveal no equations of motion for α or β_i. Once gauge conditions have been specified, a spacetime development is constructed using the equations of motion (II76,77) and (II101-103). It is important to notice that the solution of the IVP is quite independent of α and β_i, as can be seen by inspection of (II74,75). The lapse and shift affect only the development of the data off of Σ_o. Stated another way, the lapse does not determine the shape of the initial time slice, only the separation of subsequent slices. In the same way, the shift vector does not fix the spatial coordinates on the initial slice, only their propagation from slice to slice.

Insight to the structure of the IVP and dynamical problem of general relativity can be obtained by counting[1] the dynamical degrees of freedom in the gravitational field. The ADM method has resulted in a first order description of general relativity in terms of the twelve functions (γ_{ij},K^{ij}). In fact, these equations of motion (II76,77) are derived equally well from the variation of a properly

defined Hamiltonian.[2] The fields γ_{ij} and K^{ij} are thus considered independent. The three-metric γ_{ij} represents "configuration variables" canonically conjugate[3] to the "momenta" K^{ij} in this Hamiltonian picture. The constraints (II74,75) then reduce the freedom in γ_{ij} and K^{ij} from six degrees each. The momentum constraints (II75) remove three degrees of freedom in the extrinsic curvature (exactly what part of K^{ij} is fixed will be taken up below). The Hamiltonian constraint (II74) determines one part of the three-metric γ_{ij}, namely the scale of the three-space.

The remaining reductions follow from the need to impose conditions to fix the *initial* coordinates of the hypersurface Σ_o within the full spacetime. Choosing the initial simultaneity (the shape of the hypersurface) is equivalent to picking the initial time coordinate. York and Murchadha[4,5] have identified the trace, K, as naturally related to the choice of initial time coordinate. Specifying K initially leaves just two degrees of freedom in K^{ij}. Analogously, the three-fold spatial coordinate freedom in Σ_o can be removed by imposing three conditions on the components of γ_{ij}. This leaves two dynamical degrees of freedom in both γ_{ij} and K^{ij}, which represents precisely the two independent polarization states of gravity.

In passing, we note that when gauge conditions are considered, the *kinematical* degrees of freedom (α and β^i) will be fixed by setting four conditions on the "velocities" $\partial_t K$ and $\partial_t \gamma_{ij}$. It is clear that such gauge conditions do not interfere with the choice of initial coordinates on Σ_o.

We proceed to describe a technique to solve the IVP. In one sense, finding solutions to the IVP presents no problem. We can, for example, specify the entire three-metric γ_{ij} and extrinsic curvature K^{ij} and then use equations (II74,75) to deduce the required matter fields ρ_H and S^i. For reasonable choices of γ_{ij} and K^{ij} (ones which lead to matter fields satisfying the dominant energy condition for example), this procedure should work in providing initial data. Unfortunately, we would have little control over, or understanding of, the physical conditions of the source, which is of great importance in astrophysical applications. Additionally, there would be no control on the amount of gravitational radiation contained in the initial data. The problem then is to find a procedure which yields physically *sensible* solutions.

A fruitful technique for solving the constraints, the conformal approach, will be described. The pioneering application of conformal transformations to the IVP was made by Lichnerowicz.[6] This early work was restricted to only vacuum spacetimes with a particular (maximal) time slicing. In the past decade, largely through the efforts of York and his coworkers, the technique has been extended to include sources[5,7] (through conformal scalings of ρ_H, S^i), use of more arbitrary, nonmaximal ($K \neq 0$) time slicings,[4] and a covariant decomposition of the extrinsic curvature tensor.[8] In this last aspect, a natural constrained part of the extrinsic curvature is identified in the form of a vector potential W^i. Along with the

conformal factor ϕ (the scale function) providing the transformation, these form four "generalized potentials"[5] which are determined by the constraints. The remaining parts of γ_{ij} and K^{ij} are freely specifiable and fix both the initial coordinates and the "dynamical" part of the gravitational field.

A conformal transformation of the metric is introduced by

$$\gamma_{ij} = \phi^4 \hat{\gamma}_{ij} \quad , \tag{1}$$

where ϕ is a positive[9] scalar function, γ_{ij} is the physical metric and $\hat{\gamma}_{ij}$ is a conformally related metric. Our notation is that quantities appearing with a circumflex are conformally related while those without are physical quantities. We have referred to ϕ as a scale factor because it alters the scale of distances between the two manifolds but leaves unchanged distance ratios and angles.

York has emphasized[1,5] that the transformation (1) serves to define an equivalence class of manifolds and metrics all related by the *conformal metric*

$$\tilde{\gamma}_{ij} = \gamma^{-1/3} \gamma_{ij} \quad , \tag{2}$$

which is conformally invariant. We regard $\tilde{\gamma}_{ij}$ as carrying the dynamical information. Later, we define the conformal factor used in (1) in such a way that the conformally related metric, $\hat{\gamma}_{ij}$, has properties similar to $\tilde{\gamma}_{ij}$. The resulting conformally related metric plays a central part in our method.

The rule (1) immediately gives the transformation of the connection,

$$\Gamma^{i}{}_{jk} = \hat{\Gamma}^{i}{}_{jk} + 2\phi^{-1}\left[\delta^{i}{}_{j}\hat{D}_{k}\phi + \delta^{i}{}_{k}\hat{D}_{j}\phi - \hat{\gamma}_{jk}\hat{\gamma}^{i\ell}\hat{D}_{\ell}\phi\right] \quad , \tag{3}$$

and curvature quantities, of which the scalar curvature is,

$$R = \phi^{-4}\hat{R} - 8\phi^{-5}\hat{\Delta}\phi \quad . \tag{4}$$

Here $\hat{D}_k$, $\hat{R}$, and $\hat{\Delta} = \hat{\gamma}^{ij}\hat{D}_i\hat{D}_j$ are compatible with the metric $\hat{\gamma}_{ij}$. However, the transformation of the metric does not tell us how K^{ij}, S_i, ρ_H, etc., are to be treated. This is where the method gains its utility, since we are free, in many situations, to make up their conformal transformation rules. The guiding principle in inventing these rules is to facilitate the solution of the constraint equations.

We consider the extrinsic curvature tensor first. It has already been indicated that the trace K plays a special role in fixing the time coordinate. The trace-free part of K^{ij} is split off (irreducibly decomposed):

$$A^{ij} = K^{ij} - \frac{1}{3}\gamma^{ij}K \quad . \tag{5}$$

From a group theoretic standpoint, this is the spin-2 part of K^{ij} under rotations. We are particularly interested in how the divergence term of (II75) transforms. For a traceless tensor, use of (3) gives

$$D_i A^{ij} = \phi^{-10}\hat{D}_i(\phi^{10}A^{ij}) \quad . \tag{6}$$

If we assign to A^{ij} the conformal scaling rule

$$A^{ij} = \phi^{-10}\hat{A}^{ij} \quad , \tag{7}$$

(6) obtains the simple form

$$D_i A^{ij} = \phi^{-10}\hat{D}_i\hat{A}^{ij} \quad . \tag{8}$$

Note that if a tensor is *transverse-traceless* (TT), i.e. $\psi^{i}{}_{i} = 0$ and $D_i\psi^{ij} = 0$, and transforms by (7) this TT property is preserved.

We next consider how the trace, K, is to be transformed. One obvious choice is to transform the entire extrinsic curvature as was done for A^{ij} (7), i.e.

$$K^{ij} = \phi^{-10}\hat{K}^{ij} \quad . \tag{9}$$

Contracting with γ_{ij} and using (1) gives

$$K = \phi^{-6}\hat{K} \tag{10}$$

for the transformation of the trace. Using (10) and (8), the transformed momentum constraint (II75) becomes

$$\hat{D}_j\hat{A}^{ij} = \phi^{10}S^{i} + \frac{2}{3}\hat{\gamma}^{ij}\hat{D}_j\hat{K} - 4\hat{K}\phi^{-1}\hat{D}^{i}\phi \quad . \tag{11}$$

Momentarily ignoring the momentum density term $\phi^{10}S^{i}$, the remaining parts of the equation would be independent of ϕ were it not for the last term. It is somewhat convenient to eliminate this form of the

coupling, which involves the value of $\hat{K}$, particularly if time slicing conditions with $\hat{K} \neq 0$ are used.

To this end, we treat the trace as a conformal invariant instead, i.e. $K = \hat{K}$. The momentum constraints then become modified to read

$$\hat{D}_j \hat{A}^{ij} = \phi^{10} S^i + \frac{2}{3} \phi^6 \hat{\gamma}^{ij} \hat{D}_j \hat{K} \quad . \tag{12}$$

The coupling with the conformal factor has reappeared in the last term. However, in many problems one may choose to assume $\hat{D}_j \hat{K} = 0$, i.e. constant mean curvature, on the initial time slice. A special case is the "maximal slicing" condition, $\hat{K} = 0$, utilized in a number of applications including our own (discussed below). Leaping ahead somewhat, we note that it is possible to treat the momentum density term in (12) so that, when combined with constant mean curvature slicing, the momentum constraints become independent of ϕ. Thus, (12) can be decoupled from the Hamiltonian constraint, which is used to determine the conformal factor. This is somewhat useful though not strictly necessary in a numerical application.

The intent in so writing the transformed momentum constraints (12) is to allow the terms on the right-hand-side to be specified and thereby constrain the tracefree part of the extrinsic curvature. By removing the trace, $\hat{A}^{ij}$ contains only five independent components. The constraints (12) can fix only three, so a further splitting of $\hat{A}^{ij}$ is required. We apply York's[8] decomposition to the conformally

related extrinsic curvature. This decomposition is covariant, orthogonal and splits $\hat{A}^{ij}$ into transverse and longitudinal parts:

$$\hat{A}^{ij} = \hat{K}_T{}^{ij} + \hat{K}_L{}^{ij} \quad . \tag{13}$$

Here, by definition the transverse part satisfies

$$\hat{D}_j \hat{K}_T{}^{ij} = 0 \quad , \tag{14}$$

and the longitudinal part is derived from the gradient of a vector potential (properly symmetrized)

$$\hat{K}_L{}^{ij} = (\hat{L}W)^{ij} \equiv \hat{D}^i W^j + \hat{D}^j W^i - \frac{2}{3} \hat{\gamma}^{ij} \hat{D}_k W^k \quad . \tag{15}$$

The covariant nature of the splitting is obvious. The orthogonality will be demonstrated below.

Substituting (13) and (15) in (12) produces a second order operator defined by

$$(\hat{\Delta}_L W)^i \equiv \hat{D}_j (\hat{L}W)^{ij} = (\hat{\Delta} W)^i + \frac{1}{3} \hat{D}^i (\hat{D}_j W^j) + \hat{R}^i{}_j W^j \quad , \tag{16}$$

where $\hat{\Delta} = \hat{\gamma}^{\ell m} \hat{D}_\ell \hat{D}_m$ and $\hat{R}^i{}_j$ is the Ricci tensor constructed from $\hat{\gamma}_{ij}$. This operator, called the "vector Laplacian," is elliptic and maps vectors to vectors. A number of its other properties will be discussed shortly. The momentum constraints become

$$(\hat{\Delta}_L W)^i = \phi^{10} S^i + \frac{2}{3} \phi^6 \hat{\gamma}^{ij} \hat{D}_j \hat{K} \quad . \tag{17}$$

The transverse part $\hat{K}_T^{ij}$, which is TT, does not appear and is taken as the freely specifiable part of $\hat{K}^{ij}$ containing the two dynamical degrees of freedom. The trace, $\hat{K}$, is specified to fix the time slicing. The remaining three degrees are determined by solving (17) for the vector potential and using (15) to compute $\hat{K}_L^{ij} = (\hat{LW})^{ij}$.

We must now determine how the sources, ρ_H and S^i, are to be transformed. If these sources arise from another field theory, which is coupled to the gravitational field through the stress-energy tensor (such as the electromagnetic field), then it is likely that the scalings of ρ_H and S^i are predetermined.[7,10] This is not the case for a hydrodynamic source (i.e. a fluid) and we will consider here only this situation. We are free then to pick the conformal scalings to aid in simplifying the transformed constraints.

For the momentum density, S^i, the scaling

$$S^i = \phi^{-10}\hat{S}^i \tag{18}$$

is an obvious choice since, as has been noted before, the momentum constraints (17) decouple from ϕ for constant mean curvature slicing. Similar power-law scalings for ρ_H can be considered. It is important to note that, with constant mean curvature slicing, all the nonlinearity of the IVP has been lumped into the Hamiltonian constraint (as can be seen in (22) below). The nonlinearities produced by a scaling $\rho_H = \phi^{-n}\hat{\rho}_H$ will only allow solutions provided[10] $n > 5$. The case $n = 8$ has been argued for by ÓMurchadha and York.[5,10] This

scaling is most natural on dimensional grounds and because it guarantees that the local *dominance-of-energy* condition,

$$\hat{\rho}^2_H - \hat{\gamma}_{ij}\hat{S}^i\hat{S}^j \geq 0 \quad , \tag{19}$$

satisfied on the conformal manifold, continues to be satisfied by the physical source. Wilson and Dykema[11] and York[10] have pointed out that for the scaling,

$$\rho_H = \phi^{-6}\hat{\rho}_H \quad , \tag{20}$$

a "conservation of mass" results of the form

$$\int d^3x\, \gamma^{1/2}\rho_H = \int d^3x\, \hat{\gamma}^{1/2}\hat{\rho}_H \tag{21}$$

since from (1) $\gamma^{1/2} = \phi^6\hat{\gamma}^{1/2}$. This can be advantageous in astrophysical applications since it provides a finer control over specifying the initial energy content of the source. In sufficiently relativistic conditions, care must be exercised so as to not violate the energy condition (19) on the physical space. In our application, a more detailed description of the energy density ρ_H is made in terms of the rest energy density D and internal energy density E as discussed in Chapter II. As will be described in Chapter IV, we use different power-law scalings for D and E, thus obviating use of a power-law scaling for ρ_H. For the purposes of discussion we will, however, assume the scaling (20) for the remainder of this chapter.

With the source scalings now determined, the Hamiltonian constraint can be rewritten in terms of conformally related quantities and the conformal factor. Using (4), (5) and (20), (II74) becomes

$$\hat{\Delta}\phi = \frac{1}{8}\phi\left[\hat{R} - 2\hat{\rho}_H\phi^{-2} - \hat{A}_{ij}\hat{A}^{ij}\phi^{-8} + \frac{2}{3}\hat{K}^2\phi^4\right] \quad . \tag{22}$$

The equation is regarded as a quasilinear elliptic equation for the conformal factor. Given a solution, the Hamiltonian constraint has been used to fix the scale of the three-geometry.

Similarly, the momentum constraints become

$$(\hat{\Delta}_L W)^i = \hat{S}^i + \frac{2}{3}\phi^6\hat{\gamma}^{ij}\hat{D}_j\hat{K} \quad . \tag{23}$$

This system, (22) and (23), is a set of coupled elliptic equations for the conformal factor ϕ and vector potential W^i. Beyond the appearance of ϕ and W^i, their sources are entirely derived from conformally related data. The procedure for the IVP is as follows. First, specify the free data $\hat{\rho}_H$, $\hat{S}^i$, $\hat{\gamma}_{ij}$, $\hat{K}_T{}^{ij}$ and $\hat{K}$. Then solve the coupled system (22) and (23) for ϕ and W^i (decoupled equations if the coordinate condition $\hat{D}_i\hat{K} = 0$ is imposed). Finally, W^i is used with (15), (13) and (5) to give

$$K^{ij} = \phi^{-10}\left[(\hat{L}W)^{ij} + \hat{K}_T{}^{ij}\right] + \frac{1}{3}\phi^{-4}\hat{\gamma}^{ij}\hat{K} \quad , \tag{24}$$

which along with the transforms (18), (20) and (1) give a proper data set satisfying (II74,75). The IVP has been solved, provided adequate conditions are placed on the freely specifiable data

$(\hat{\rho}_H, \hat{S}^i, \hat{\gamma}_{ij}, \hat{K}_T{}^{ij}, \hat{K})$, i.e. sufficiently strong fall-off conditions for asymptotically flat spacetimes, and proper boundary conditions are imposed so that (22) and (23) yield unique solutions.

This method of solving the IVP has produced four "generalized potentials" ϕ and W^i. They are the general relativistic generalization of the single gravitational potential of Newtonian gravity. Just as the Newtonian potential carries information about the mass of its source into the distant, vacuum field, so the conformal factor ϕ carries information on the total *energy* of an isolated source in an asymptotically flat spacetime. Additionally, the vector potential now asymptotically supplies information about the linear and angular momentum of the source.

A set of standard two-surface integrals is given in Appendix A which compute the asymptotic energy-momentum four vector and angular momentum vector. These prove useful in deriving boundary conditions for (22) and (23) to be used in numerical applications. We consider next how such boundary conditions are obtained, examine the properties of the York decomposition, and discuss what fall-off conditions are required on the sources to provide unique solutions representing asymptotically flat spacetimes.

We consider the momentum constraints (23) first and assume in this discussion that $\hat{D}_j\hat{K} = 0$ slicing is used and that the manifold is topologically $\mathbb{R}^3$. A number of the properties given here will hold in any case. The momentum constraints are then a separate linear

system for W^i,

$$(\hat{\Delta}_L W)^i = \hat{S}^i \quad . \tag{25}$$

The vector Laplacian, $\hat{\Delta}_L$, has several interesting features which guarantee that (25) may be uniquely inverted.[8] To display these, we form the invariant function space inner product

$$\int d\hat{v}\ V_i(\hat{\Delta}_L W)^i \tag{26}$$

between two vectors V^i and W^i on the conformally related manifold. Here, $d\hat{v}$ is the invariant volume element on this space. Recalling the definition of $\hat{\Delta}_L$ (16) and using the identity

$$\hat{D}_i V_j = \frac{1}{2}(\hat{L}V)_{ij} + \hat{D}_{[i}V_{j]} + \frac{1}{3}\hat{\gamma}_{ij}\hat{D}_k V^k \quad , \tag{27}$$

integration by parts yields the first form of a *vector Greens theorem*

$$\int d\hat{v}\ V_i(\hat{\Delta}_L W)^i = -\frac{1}{2}\int d\hat{v}(\hat{L}V)_{ij}(\hat{L}W)^{ij} + \oint d\hat{A}_j\ V_i(\hat{L}W)^{ij} \quad . \tag{28}$$

The invariant surface element of the bounding two-surface is $d\hat{A}_j$. The second form of the vector Greens theorem can be obtained as well:

$$\int d\hat{v}[V_i(\hat{\Delta}_L W)^i - W_i(\hat{\Delta}_L V)^i] = \oint d\hat{A}_j[V_i(\hat{L}W)^{ij} - W_i(\hat{L}V)^{ij}] \quad . \tag{29}$$

Though we have kept the surface integral terms in (28) and (29), for asymptotically flat manifolds these will vanish in the limit $r \to \infty$ given sufficiently fast fall-off for solutions of (25): $W^i = \mathcal{O}(r^{-1})$

and $(\hat{L}W)^{ij} = \mathcal{O}(r^{-2})$. These rates of fall-off will in turn depend on the the rates assumed for the source.

To show that $\hat{\Delta}_L$ is elliptic, or has negative-definite eigenvalues, we use (28) with $V^i = W^i$ to obtain the inequality

$$\int d\hat{v}\ W_i(\hat{\Delta}_L W)^i = -\frac{1}{2}\int d\hat{v}(\hat{L}W)_{ij}(\hat{L}W)^{ij} \leq 0 \quad . \tag{30}$$

With (29), the vector Laplacian can be shown to be a symmetric, or self-adjoint, operator,

$$\int d\hat{v}\ V_i(\hat{\Delta}_L W)^i = \int d\hat{v}\ W_i(\hat{\Delta}_L V)^i \quad , \tag{31}$$

in the same way as the ordinary scalar Laplacian $\hat{\Delta}$.

The boundedness condition (30) contains $(\hat{L}W)^{ij} = 0$ as a potential special case with vanishing eigenvalue. The trivial solution, $W^i = 0$, is no problem, but it is necessary to examine the case $(\hat{L}W)^{ij} = 0$, $W^i \neq 0$. Such vectors, if they exist, are called *conformal Killing vectors* (CKV). The reason for this term is that C^i is a CKV if along it the metric satisfies a conformal isometry

$$\pounds_C \hat{\gamma}_{ij} = \hat{D}_i C_j + \hat{D}_j C_i = \lambda\hat{\gamma}_{ij} \quad . \tag{32}$$

This is the conformal Killing equation. Here, λ is not arbitrary, but follows from the trace of (32): $\lambda = \frac{2}{3}\hat{D}_k C^k$. Hence a CKV satisfies $(\hat{L}C)^{ij} = 0$. Using the conformal invariance of $\tilde{\gamma}_{ij}$ in (2) gives $\tilde{\gamma}_{ij} = \hat{\gamma}^{-1/3}\hat{\gamma}_{ij}$ which allows (32) to be rewritten in terms of the

conformal metric:

$$\pounds_C \tilde{\gamma}_{ij} = 0 \quad . \tag{33}$$

Conformal Killing vectors represent coordinate transformations which preserve the conformal three-geometry.

Just as Killing vectors do not always exist, CKV's will only be obtained for sufficiently special metrics. If they exist, the Kernel of $\hat{\Delta}_L$ is nontrivial and the solution of (25) will be unique only up to the addition of CKV's.

However if CKV's exist, they contribute nothing to the longitudinal part of the extrinsic curvature, since $(\hat{L}C)^{ij} = 0$. This might however pose a problem in a numerical application where one must find a unique vector potential that is a solution to (25). This is similar to the uniqueness problem of the ordinary Poisson equation when a Neumann boundary condition is used exclusively. The scalar solution is unique only up to an additive constant, which can be fixed by applying a Dirichlet condition at one point on the boundary. In any case, CKV's are not a concern in the asymptotically flat IVP, since, if they exist they do not vanish[5,12-14] at spatial infinity and are eliminated by the boundary condition $W^i \to 0$ as $r \to \infty$.

It is important to note, however, that in spatially closed applications (numerical cosmologies) CKV's may exist and, while again not contributing to the extrinsic curvature, they then represent the

existence of important integrability conditions[5,8] on allowable sources to (25) or (23).

Another result of (30) is that if a vector, V^i, exists such that $(\hat{\Delta}_L V)^i = \hat{D}_j(\hat{L}V)^{ij} = 0$, then it follows $(\hat{L}V)^{ij} = 0$. A corollary is that if M^{ij} is a TT tensor, i.e. $\hat{D}_i M^{ij} = 0$ and $M^i{}_i = 0$, then it cannot be represented by $(\hat{L}V)^{ij}$ for some vector V^i. Stated more completely, arbitrary longitudinal tensors $(\hat{L}W)^{ij}$ and transverse tensors $\hat{K}_T{}^{ij}$ are orthogonal in the global scalar product

$$\int d\hat{v}\ \hat{K}_T{}^{ij}(\hat{L}W)_{ij} = 0 \quad , \tag{34}$$

as can be demonstrated by integration by parts. This is the orthogonality of the York decomposition we have mentioned before. It must be noted, however, that this orthogonality exists only on the conformally related manifold. This can be seen by using the transformation (7) for $\hat{K}_T{}^{ij}$ and $(\hat{L}W)^{ij}$ and transforming the volume element to show

$$\int dv\ K_L{}^{ij}K_{Tij} = \int d\hat{v}\ \phi^{-6}\ \hat{K}_T{}^{ij}(\hat{L}W)_{ij} \neq 0 \quad , \tag{35}$$

in general.

We have already shown the TT property of $\hat{K}_T{}^{ij}$ is preserved under conformal transformation. The implication of (35) is that the "longitudinal" part of A^{ij} on the physical space, $K_L{}^{ij} = \phi^{-10}(\hat{L}W)^{ij}$, cannot be written as $(LV)^{ij}$ for some vector V^i with L the operator compatible with γ_{ij}. Therefore $K_L{}^{ij}$ contains some TT part, in

general, and the conformal transformation has mixed the components of the decomposition.

This has the unfortunate, though perhaps unavoidable, consequence that if one assumes, as is most natural, initial data with $\hat{\gamma}_{ij} = f_{ij}$ (flat metric) and $\hat{K}_T{}^{ij} = 0$, the physical data will still contain preexisting gravitational radiation. This has been vividly demonstrated in a numerical calculation[15] of moving black hole initial data. It also seems apparent in calculations of two black hole collisions[16,17] though in our application for hydrodynamic core collapse (see Chapter VI) the York decomposition minimizes to a great extent the initial radiation content. This is probably due to the fact that our configurations do not begin as *extremely* relativistic objects while black holes can hardly be considered anything else.

It has been indicated that the proper condition at spatial infinity for (23) and (25) is $W^i = 0$. However in most numerical applications for asymptotically flat systems, we will need to apply a condition on a finite radius boundary. This is true unless compactifying spatial coordinates are used, which, to my knowledge, has not been done in spacelike numerical calculations.[18] Applying $W^i = 0$ on a finite radius boundary would introduce large local errors in the solution.

In Appendix B we derive a new vacuum multipole moment expansion for the flat space vector Laplacian. The form of the expansion should be valid also for the non-flat $\hat{\Delta}_L$ at large radii.

This expansion, through the first two orders, is given by

$$W^k(x) = -\frac{7}{32\pi r}(\delta^{ki} + \frac{1}{7}n^k n^i)P_i + \frac{1}{16\pi r^2}(\delta^{ki}n^j - \delta^{kj}n^i)J_{ij}$$
$$+ \frac{1}{64\pi r^2}\left[3(n^j\delta^{ki} + n^i\delta^{kj}) - n^k(\delta^{ij} - 3n^i n^j)\right]D_{ij} \quad , \qquad (36)$$

in asymptotic cartesian coordinates with $n^i = r^{-1}x^i$. Here P_i and J_{ij} are constant moments representing, respectively, the isolated system's linear momentum vector and angular momentum tensor. The D_{ij} are symmetric moments related (in the weak field approximation) to $\partial_t I_{ij}$ where I_{ij} is the second moment of the mass distribution.

For systems with nonvanishing linear momentum P_i, York and Piran[15,14] have given a Robin boundary condition

$$(\hat{L}W)^{kj}n_j(\delta^i{}_k - \frac{1}{2}n^i n_k) + \frac{6}{7r_m}W^k(\delta^i{}_k - \frac{1}{8}n^i n_k) = \mathcal{O}(r_m^{-3}) \quad , \qquad (37)$$

suitable for obtaining unique (Appendix B) solutions for large radius r_m. This Robin condition utilizes a linear combination of $W^k(r_m)$ and $(\hat{L}W)^{ij}(r_m)$ to eliminate the explicit appearance of P_i from (36).

However, most numerical calculations will generally be done in the center of momentum frame. An exception is, of course, the moving black hole problem,[15] referred to earlier. For these systems, (37) cannot provide an accurate boundary condition. The task of finding a new boundary condition is complicated by the appearance of the two sets of moments (antisymmetric and symmetric) at order $\mathcal{O}(r^{-2})$ in (36). If $J_{ij} \neq 0$ and, in addition, $|J_{ij}| >> |D_{ij}|$ (e.g., a slowly

collapsing rotating object), then we have found a new Robin condition

$$(\hat{L}W)^{kj}n_j + \frac{3}{r_m}W^j(\delta^k{}_j + n^k n_j) = \mathcal{O}(r_m^{-4}) \quad , \tag{38}$$

which can be imposed to obtain unique solutions (see Appendix B for derivation and proof).

However a number of nontrivial problems can be posed (including our own application) for which both $P_i = 0$ and $J_{ji} = 0$. In these cases, the lowest order nonvanishing moments will be D_{ij} from (36). Because these are nonstationary moments, unlike P_i and J_{ij} which are conserved, we cannot find a corresponding Robin-type boundary condition. Instead, we propose using an approximate Dirichlet condition imposed by directly calculating the moments (in cartesian coordinates)

$$D_{ij} = -2\int d\hat{v}\ \hat{S}_{(i}x_{j)} \quad , \tag{39}$$

as if the conformal manifold were flat. To serve as a good approximation, it must be true that $|\hat{\gamma}_{ij} - f_{ij}| << |f_{ij}|$ globally. In our application of the ADM method to axisymmetric, nonrotating gravitational collapse, this condition has always been well satisfied even for extremely relativistic configurations. Use of this boundary condition will be demonstrated in Chapter IV.

We must next consider the Hamiltonian constraint equation (22) for the conformal factor. To do so, we first note some of the properties of ϕ. The condition that is required for asymptotically

flat slices is $\phi \to 1$ as $r \to \infty$. In fact, the condition is more completely stated as $\phi = 1 + \mathcal{O}(r^{-1})$, which along with the asymptotic condition

$$\hat{\gamma}_{ij} = f_{ik}(\delta^k{}_j + \hat{h}^k{}_j) \ , \quad \hat{h}^k{}_j = \mathcal{O}(r^{-1} \tag{40}$$

on the conformally related metric, guarantees the same approach

$$\gamma_{ij} = f_{ik}(\delta^k{}_j + h^k{}_j) \ , \quad h^k{}_j = \mathcal{O}(r^{-1}) \tag{41}$$

to flat space by the physical metric.

The monopole part of ϕ is identified in many situations with the total energy E of the isolated system:

$$\phi = 1 + \frac{E}{16\pi r} + \mathcal{O}(r^{-2}) \quad . \tag{42}$$

Recall our units are $G = (8\pi)^{-1}$, $c = 1$. In order for ϕ to have this physical association, several conditions are required on the initial data $\hat{\gamma}_{ij}$ (or equivalently on $\hat{h}_{ij}$). The first is that the trace of $\hat{h}_{ij}$ (with respect to f_{ij}) must satisfy

$$\hat{h}_{(f)} = f^{ij}\hat{h}_{ij} = \mathcal{O}(r^{-2}) \quad . \tag{43}$$

This is always possible. Recall that the conformal technique is used to split the metric into two parts: ϕ and $\hat{\gamma}_{ij}$. This is actually an entire class of splittings. Which element of the class is employed is only uniquely determined once a single condition is placed on $\hat{\gamma}_{ij}$.

Suppose data has been chosen such that $\hat{h}_{(f)} = \mathcal{O}(r^{-1})$. Using (1) and (40), we write

$$\gamma_{ij} = \phi^4(f_{ij} + \hat{h}_{ij}) \quad , \tag{44}$$

which has trace

$$\gamma_{(f)} = 3\phi^4 + \phi^4\hat{h}_{(f)} \quad . \tag{45}$$

We can then, for example, split (44) into its trace and tracefree parts:

$$\gamma_{ij} = \phi^4\left[1 + \frac{1}{3}\hat{h}_{(f)}\right]f_{ij} + \phi^4\left[\hat{h}_{ij} - \frac{1}{3}\hat{h}_{(f)}f_{ij}\right] \quad . \tag{46}$$

A redefinition of the conformal factor and $\hat{h}_{ij}$ by

$$\phi^4 \to \phi'^4 = \phi^4\left[1 + \frac{1}{3}\hat{h}_{(f)}\right] \quad ,$$

$$\hat{h}_{ij} \to \hat{h}'_{ij} = \left[1 + \frac{1}{3}\hat{h}_{(f)}\right]^{-1}\left[\hat{h}_{ij} - \frac{1}{3}\hat{h}_{(f)}f_{ij}\right] \quad , \tag{47}$$

then gives $\hat{h}'_{(f)} = 0$, which is clearly sufficient. This question of defining the splitting and the conformal factor is really most important at subsequent times during an evolution, so that the interpretation of (42) can be maintained.

The second requirement needed to place ϕ in the form (42) is that the tracefree part of γ_{ij},

$$\psi_{ij} \equiv h_{ij} - \frac{1}{3}h_f f_{ij} \quad , \tag{48}$$

satisfy the asymptotic divergence condition

$$\zeta^j{}_{(k)}D^i\psi_{ij} = \mathcal{O}(r^{-3}) \quad . \tag{49}$$

Here $\zeta^j{}_{(k)}$ are the three asymptotic translational Killing vectors (Killing vector of f_{ij}) introduced so that the fall-off can be made basis independent. For this same reason, we used the mixed-form tensors in (40) and (41). This condition, (49), can always be imposed on the initial data by employing the freedom to fix the three initial spatial coordinate conditions. We may then derive (Appendix A) the two-surface integral

$$E = \lim_{r\to\infty}(-4)\oint dA^i D_i\phi \quad , \tag{A7}$$

involving just the conformal factor, from the more general ADM[2] mass-energy integral (A2). For (A7) to remain valid throughout the evolution requires gauge conditions for the lapse and shift which maintain (49) in time. York has called these (49) *quasi-isotropic* coordinates[10] since they go over to the isotropic coordinates for Schwarzschild geometry. In our application, we use a gauge condition which maintains (49), as will be demonstrated in Chapter IV, and so (A7) remains applicable.

We maintain (43) by defining ϕ with the condition

$$\det(\hat{\gamma}_{ij}) = \det(f_{ij}) \equiv f \quad , \tag{50}$$

on the conformally related metric. To see (43), use the matrix

identity

$$\delta \ell n[\det(M)] = \mathrm{tr}(M^{-1}\delta M) \tag{51}$$

with (40), $\hat{\gamma}_{ij} = f_{ij} + \hat{h}_{ij}$, and, notice from (50), that $\delta\det(\hat{\gamma}_{ij}) = 0$. This is the special nature of our definition of the conformally related metric alluded to at the beginning of the chapter.

The energy so defined, along with the asymptotic linear momentum $\zeta^i{}_{(j)}P_i$ (see Appendix A), forms a Lorentz covariant four vector with respect to asymptotic boosts.[14,19] One can define an invariant mass[5,14] of the configuration, $M^2 = E^2 - P_iP^i$, which is a constant of the motion as are E and $\zeta^i{}_{(j)}P_i$. If coordinates are chosen which maintain $P_i = 0$, then the mass and energy are synonymous. This is the case in our application and we will often refer to them interchangeably.

As was the case with the momentum constraints, in numerical applications we often will require a boundary condition on ϕ for (22) at finite, but large radius. York and Piran[15] have shown that (42) can be used to derive a Robin boundary condition

$$\partial_r\phi + \frac{1}{r_m}(\phi - 1) = \mathcal{O}(r_m^{-3}) \tag{52}$$

which eliminates the explicit appearance of the energy.

Proving existence and uniqueness of solutions to (22) is much more difficult owing to the nonlinearity of the equation. Nonetheless, the equation is quasilinear (derivatives appearing linearly)

which has allowed a great deal of progress to be made. Powerful attacks on (22) have been made employing techniques of weighted Sobolev spaces introduced by Cantor[12,13,20] to general relativity. A number of results have been achieved[13,21] for asymptotically flat slices using the maximal slicing condition. York[14] has extended the arguments to nonmaximal slices. ÓMurchadha and York[7] have also examined compact slices.

At minimum, our initial data is required to satisfy acceptable fall-off rates to be admissible as representing a proper asymptotically flat slice and an embedding. Again, the metric is required to have the fall-off

$$h^i{}_j = \mathcal{O}(r^{-1}) \quad , \tag{53}$$

and successively higher powers for its derivatives,

$$\pounds_\zeta h^i{}_j = \mathcal{O}(r^{-2}) \quad , \quad \pounds_\zeta\pounds_\zeta h^i{}_j = \mathcal{O}(r^{-3}) \quad , \tag{54}$$

etc. Here, Lie derivatives along the asymptotic Killing vectors are used to state the conditions in a basis independent manner again. This is completely compatible with the usual notions of fall-off of cartesian components. These conditions apply at distances beyond any radiation wavefronts, which is necessary in writing (54).

Minimum rates of decay for the extrinsic curvature are

$$K^i{}_j = \mathcal{O}(r^{-2}) \quad , \quad \pounds_\zeta K^i{}_j = \mathcal{O}(r^{-3}) \quad , \tag{55}$$

etc. The sources, as can be seen from (22) and (23), must satisfy

$$\rho_H = \mathcal{O}(r^{-4}) \ , \qquad S_i\zeta^i{}_{(j)} = \mathcal{O}(r^{-4}) \quad . \tag{56}$$

Finally, the gauge variables must satisfy conditions such that

$$\alpha = 1 + \mathcal{O}(r^{-1}) \ , \qquad \beta_i\zeta^i{}_{(j)} = \mathcal{O}(r^{-1}) \quad , \tag{57}$$

in order to maintain the initial asymptotic flatness throughout an evolution. Obviously, faster rates of fall-off will occur for certain coordinate choices and source symmetries.

b) Fully Constrained Evolution

In solving the IVP, one often assumes for starting values $\hat{\gamma}_{ij} = f_{ij}$ and $\hat{K}_T{}^{ij} = 0$ (i.e. no wavelike momentum in the initial conformal gravitational field). Such an assumption is made for simplicity and the desire to minimize the amount of initial gravitational radiation in the problem; though recall there will still be transverse momentum in the physical initial data.

Equations (22) and (23) are in a form, however, that allows them to be solved in situations in which $\hat{\gamma}_{ij} \neq f_{ij}$ and $\hat{K}_T{}^{ij} \neq 0$. This will arise on subsequent slices during the evolution, so (22) and (23) provide the means to resolve the constraints on each slice and hereby construct a fully constrained evolution algorithm.

We have already indicated in Chapter II one reason for pursuing this method; that a free evolution will not in general maintain satisfaction of the constraints. It is not absolutely clear what difficulties may be encountered by evolving improper Einstein data. We may perhaps take a clue from the electromagnetic analogy. Solving that dynamical problem involves finding initial data to satisfy the single constraint, $\vec{\nabla}\cdot\vec{E} = 4\pi\rho_c$, and then evolving the dynamical equations for $\vec{E}$, ρ_c, and the vector potential, as well as fixing the scalar gauge field ϕ. Analytically, the constraint condition is preserved during an evolution; the conservation law ($\partial_t\rho_c$ equation) and field equations ($\partial_t\vec{E}$ equation) guarantee it. Numerically evolving the charge density and electric field will involve a drift out of the constraint surface in general. One immediate physical effect is that the charge measured by a distant observer examining the stationary part of the electric field will differ from the charge obtained by volume integrating the charge density.

It is clear that a similar problem can arise in general relativity. Here, the stationary multipoles of the gravitational field (yielding E, P^i, J^i) may not agree with the internal sources, which ostensibly conserve them. This may be a significant problem in numerical relativity since the stationary (and gauge) parts of the field are often much larger than the dynamical (wave) parts we are so interested in calculating.

We use a fully constrained evolution method to avoid many of the problems that may occur with improper Cauchy data. Similar schemes, though different in detail, were used by Dykema and Wilson[11] and Wilson and Smarr[22] in earlier versions of the code. An added feature of this method is that fewer evolution equations are integrated in time. This may be advantageous in reducing numerical high wave-number noise on the finite difference mesh.

When one adopts this approach and uses (22) and (23) on subsequent slices, then, of course, the sources $\hat{\gamma}_{ij}$, $\hat{K}_T{}^{ij}$, $\hat{\rho}_H$, and $\hat{S}^i$ are no longer freely specifiable but rather follow from the evolution. Leaving $\hat{K}_T{}^{ij}$ aside for the moment, how are $\hat{\gamma}_{ij}$, $\hat{\rho}_H$, and $\hat{S}^i$ to be obtained on a new slice when we have only derived evolution equations, (II77) and (II101-103), for γ_{ij}, ρ_H, and S^i and have yet to determine ϕ? The answer lies in using the definition (50), which fixes the relationship between ϕ and γ_{ij}; i.e.,

$$[\det(\gamma_{ij})]^{1/2} = \gamma^{1/2} = \phi^6 f^{1/2} \quad . \tag{58}$$

Taking the trace of (II77) and using (51) yields

$$\partial_t \ell n(\gamma^{1/2}) = -\alpha K + D_i \beta^i \quad , \tag{59}$$

which, using (58), gives an evolution equation for ϕ:

$$\partial_t \ell n(\phi^6) = -\alpha K + D_i \beta^i \quad . \tag{60}$$

Equations (II77), (60), and (1) then produce an equation for $\hat{\gamma}_{ij}$:

$$\hat{\gamma}^{ik} \partial_t \hat{\gamma}_{kj} = -2\alpha A^i{}_j + (L\beta)^i{}_j \quad . \tag{61}$$

Note that (60) and (61) represent the York-Lichnerowicz splitting of the metric; their sources involve, respectively, the trace and trace-free parts of K^{ij}.

Consider next the hydrodynamic equations (II101-103). If the scaling laws (18) and (20) are adopted, then (58) shows that these *are* evolution equations for $\hat{\rho}_H$ and $\hat{S}_i$. If different scalings had been chosen (for D and E for example), then use of (60) will allow (II101, 102) to be rewritten for $\hat{D}$ and $\hat{E}$. So, we will have these conformally related functions as input to (22) and (23) on a new time slice.

But what about $\hat{K}_T{}^{ij}$? The transverse extrinsic curvature forms part of the source for (22) and the solution of the momentum constraints (23) yields only the longitudinal part of $\hat{A}^{ij}$ in the decomposition (13): $(\hat{LW})^{ij}$. What we need are evolution equations for the transverse momentum. Unfortunately, no such equations exist. The decomposition (13) - (15) is nonlocal; one derives the transverse part from

$$\hat{K}_T{}^{ij} = \hat{A}^{ij} - (\hat{LW})^{ij} \tag{62}$$

only after having integrated the elliptic system (23) for W^i.

In a way similar to the splitting of (II77) into (60) and (61), we may also obtain dynamical equations for the conformally related trace, $\hat{K}$, and tracefree part, $\hat{A}^{ij}$, from (II76) using (60) and

the scalings (7) and $K = \hat{K}$. We can thus integrate $\hat{A}^{ij}$ forward in time, solve (23) for W^i, and use (62) to read off the new values of $\hat{K}_T{}^{ij}$. However, this violates one of the aims of solving the constraints on successive time slices, which is to avoid having to evolve the full extrinsic curvature. What we are after is a reduced evolution scheme that involves just dynamically evolving two of the components of the extrinsic curvature (representing the two "dynamical" degrees of freedom). The trace, $\hat{K}$, will be used to fix the time gauge and the remaining three components will come from solving (23).

The idea is then to use the evolution equations for $\hat{A}^{ij}$ to propagate forward two (specific) components. This may reduce to only one component if symmetries restrict the dynamical freedom (which is the case in our application). Then (23) is solved to obtain W^i and the entire longitudinal part of $\hat{A}^{ij}$. The transverse part is calculated for the two chosen dynamical components by using (62). Finally, these transverse components are used, along with solving the other half of the decomposed momentum constraints (14), to find the remaining transverse components and reconstruct the entire new $\hat{A}^{ij}$.

In practice, solving the first order system (14) proves numerically and conceptually difficult. The questions of how to pose proper boundary conditions and find convergent iterative finite difference algorithms are most naturally discussed in terms of second order equations. Fortunately, there exists[8] a means of finding a second order elliptic system for $\hat{K}_T{}^{ij}$.

Recalling the discussion before, if V^i and M^{ij} are a vector and a symmetric tracefree tensor with sufficient rates of fall-off, then the integral relation can be written,

$$\int d\hat{v}\, M_{ij}(\hat{L}V)^{ij} = -2 \int d\hat{v}\, V_j \hat{D}_i M^{ij} \quad , \tag{63}$$

with neglect of the surface terms (again with the assumption that the manifold is topologically R^3). Equation (63) implies that the operators $\hat{L}$ and $\hat{D}$ are in adjoint relation.[8,23] Two adjoint operators, applied successively, produce a self-adjoint operator, as is the case with the vector Laplacian $\hat{\Delta}_L = \hat{D}\hat{L}$ (31). The same is true of the dual operator, $\hat{\Delta}_T = \hat{L}\hat{D}$, formed by reversing the order, which takes symmetric tracefree (STF) two-tensors to STF two-tensors. This operator is called the *tensor Laplacian* and it is strongly elliptic.

We may work out the properties of this tensor Laplacian as was done for the vector Laplacian. Of primary importance will be the first form of the tensor Greens identity

$$\int d\hat{v}\, S_{ij}(\hat{\Delta}_T T)^{ij} = 2 \oint d\hat{A}^i S_{ij} \hat{D}_k T^{kj} - 2 \int d\hat{v} (\hat{D}_k T^{kj})(\hat{D}^i S_{ij}) \quad , \tag{64}$$

found with the use of (27) and application of Gauss' theorem. Here both S_{ij} and T_{ij} must be STF tensors. Before proceeding to apply (64), we give for completeness the second form of the tensor Greens theorem also:

$$\int d\hat{v} [S_{ij}(\hat{\Delta}_T T)^{ij} - T_{ij}(\hat{\Delta}_T S)^{ij}] = 2 \oint d\hat{A}^i [S_{ij} \hat{D}_k T^{kj} - T_{ij} \hat{D}_k S^{kj}] \quad . \tag{65}$$

The result we desire comes from the use of $S_{ij} = T_{ij} = \hat{K}_{ij}$ in (64) as well as the divergence-free condition (14) on $\hat{D}_k \hat{K}^{kj} = 0$ on the boundary to produce the inequality

$$\int d\hat{v}\ \hat{K}_{ij}(\hat{\Delta}_T \hat{K})^{ij} = -2 \int d\hat{v}(\hat{D}_k \hat{K}^{kj})(\hat{D}^i \hat{K}_{ij}) \leq 0 \quad . \tag{66}$$

It is immediately apparent from the form of the operator $\hat{\Delta}_T = \hat{L}\hat{D}$ (where $\hat{D}$ here implies the divergence) that if $\hat{K}_{ij}$ is transverse (i.e. satisfies equation (14)), then it also satisfies $(\hat{\Delta}_T \hat{K})^{ij} = 0$. Conversely, the inequality (66) implies that if $(\hat{\Delta}_T \hat{K})^{ij} = 0$, then $\hat{K}^{ij}$ is transverse everywhere (if it is on the boundary). Thus the tensor Laplacian has the remarkable property that the solutions to

$$(\hat{\Delta}_T \hat{K}_T)^{ij} = 0 \quad , \tag{67}$$

are identically the solutions to (14), the first order transverse part of the decomposed momentum constraints.

Using the transverse components which are known from the evolution, (67) provides a system of second order elliptic equations for the remaining transverse parts. The proper boundary conditions to be imposed on this second order system are precisely the transverse (radiation) conditions (14). A specific example of this method will be displayed in Chapter IV. To be used in the next chapter, the system (67) is simplified from the more explicit form

$$(\hat{\Delta}_T \hat{K}_T)^{ij} = \hat{D}^i \hat{D}_\ell \hat{K}_T^{\ell j} + \hat{D}^j \hat{D}_\ell \hat{K}_T^{\ell i} - \frac{2}{3} \hat{\gamma}^{ij} \hat{D}_m \hat{D}_\ell \hat{K}_T^{\ell m} = 0 \quad . \tag{68}$$

Before closing out this section, the above function space decomposition gives rise to an interesting global test of the orthogonality of the splitting, (34), which can be used in numerical applications. Defining the notation

$$(\hat{S},\hat{T}) = \int d\hat{v}\ \hat{S}_{ij}\hat{T}^{ij} \quad , \tag{69}$$

for the global inner product, the orthogonality of the longitudinal and transverse tensors in (34) is expressed simply as

$$(\hat{K}_T,(\hat{L}W)) = 0 \quad . \tag{70}$$

Now in a numerical setting, it can be expected that these quantities will not precisely satisfy (70). A global test of the degree of orthogonality can be made by calculating the function space angle ϕ_* from

$$\cos\left(\frac{\pi}{2} - \phi_*\right) = \frac{(\hat{K}_T,(\hat{L}W))}{(\hat{K}_T,\hat{K}_T)^{1/2}((\hat{L}W),(\hat{L}W))^{1/2}} \quad , \tag{71}$$

and requiring ϕ_* to be sufficiently small.

c) Kinematical Conditions

We consider in this section the kinematical conditions which must be imposed to determine the lapse, α, and shift, β^i. These thereby define the spatial time slices (the foliation) and a

coordinate congruence in the future of Σ_0, along which our initial data are propagated. We cannot improve here much upon the discussions of coordinate conditions in the ADM scheme previously given[11,16,22,24-28] in the literature. The gauge employed in the current code remains the same as that used by Wilson and Dykema.[11] This particular gauge will be fully described in Chapter IV, so the comments here will be of a more general nature to serve to highlight the advantages and limitations of our choice.

We have expressed the Einstein equations in the previous chapter in terms of the coordinate congruence, whose tangent vector is t^a (II49) and which depends on the lapse and shift, without yet discussing the geometrical significance of these quantities or how they are determined. The lapse determines the local orthogonal interval of proper time, $d\tau$, between adjacent slices, with coordinate time separation dt, by

$$d\tau = \alpha dt \quad . \tag{72}$$

The lapse function therefore determines the location of the "next" slice in the future of Σ_0, i.e. $\Sigma(t_0 + dt)$, and the normal vector field n^a on this new slice as well. From (II48), it is clear that αn^a is the vector field that orthogonally "connects" the slices $\Sigma(t)$ and $\Sigma(t + dt)$. Any spatial "shift" vector, β^a, defined by (II50) then defines an equivalent, though nonorthogonal, vector field t^a given by (II49). The observers carried along the worldlines with t^a as tangents are *coordinate observers*. Observers transported along

the curves with n^a as tangents are termed *Eulerian observers*; they are at rest relative to the time slices. The shift vector corresponds to a relative velocity between the coordinate observers and Eulerian observers given by

$$v^a = \frac{1}{\alpha} \beta^a \quad . \tag{73}$$

Since we will only consider asymptotically flat spacetimes, the lapse will be conventionally taken to satisfy $\alpha \to 1$ as $r \to \infty$ and the shift $\beta^a \to 0$ as $r \to \infty$ (57). This identifies asymptotic coordinate time with proper time and assumes the source is in the asymptotic rest frame. The ability to choose α and β^i (since $\beta^0 = 0$) quite arbitrarily otherwise reflects the coordinate freedom of general relativity.

In any constructive calculation, conditions must be imposed to determine the lapse and shift. The choice of the lapse function is of fundamental importance in calculations involving strong fields. If singularities arise (i.e. black holes), an improper choice for α may cause the time slices to advance into the singular region and terminate the calculation long before the effects of the strong-field dynamics (gravitational waves) can reach the weak-field region and be studied. Instead, the lapse can be reduced in strong-field regions to slow the advance of proper time there (72), while allowing a significant Cauchy development in the weak exterior.

How is the lapse to be determined? We can of course directly specify α; say by setting $\alpha = 1$ everywhere. This particular

choice is called *geodesic slicing*, since from (II33) the acceleration of the Eulerian observers vanishes. It is well known[24,29] that geodesic slicing fails to provide a significant development of the initial data in many strong-field problems. We can demonstrate the problem by calculating the rate of change of the trace of K_{ij} along αn^a using (II58) with (II46) and (II52):

$$\pounds_{\alpha n} K = -\Delta\alpha + \alpha\left[K_{ij}K^{ij} + \frac{1}{2}(\rho_H + S)\right] \quad , \tag{74}$$

and assuming geodesic slicing to obtain,

$$\pounds_n K = K_{ij}K^{ij} + \frac{1}{2}(\rho_H + S) \quad . \tag{75}$$

The right-hand-side is positive (or zero) if the strong energy condition[29] is satisfied and K will tend to grow without bound. From (59) using (II52) we find

$$\pounds_{\alpha n}\, \ell n \gamma^{1/2} = -\alpha K \quad , \tag{76}$$

and so, again given $\alpha = 1$, if K diverges then $\gamma \to 0$ implying a coordinate singularity. What has happened is that the Eulerian observers lie on geodesics in this gauge and these tend to focus upon encountering non-vanishing sources in (75) and subsequently cross (form caustics).

Of course, other direct specifications of the lapse may be better suited to avoiding coordinate singularities and real physical curvature singularities. The lapse might be controlled by monitoring

γ and some number of the Riemann curvature invariants. From the standpoint of exploring the structure of general relativity, this might provide a productive means of pushing the slicing ahead, arbitrarily close to the singularities that form from gravitational collapse, to achieve a *maximal development* of the initial data. The singularity structures that arise from nonspherical gravitational collapse could then be studied.[30] The *maximal slicing* condition, described below and used in our application, is known to halt the development in the interior of a black hole (at least in spherical symmetry) well short of the singularity, though it does provide a complete foliation of the exterior.[24,30-32]

A different route, which has been most fruitful in numerical applications and is by now fairly well explored, is to treat the gauge fixing in a way that is similar to the initial value problem. The lapse and shift in this method are determined indirectly by specifying conditions on components of the "velocities" $\pounds_t K^i{}_j$ (for the time slicing and lapse) and $\pounds_t \gamma_{ij}$ or $\pounds_t \tilde{\gamma}_{ij}$ (for the spatial coordinates and shift). Initial values of these chosen components are given on Σ_0 to fix the kinematical degrees there. For whichever component of $K^i{}_j$ and γ_{ij} (or $\tilde{\gamma}_{ij}$) are employed in the gauge conditions, the effect is to turn the corresponding equations of (II77,78) from a hyperbolic character to elliptic or parabolic for α and β^i.

We can consider examples of this approach for finding the lapse by treating the trace K as the kinematical part determining the time slicing. Then, using (5), (74) becomes the elliptic equation

$$\Delta\alpha = \alpha\left[A_{ij}A^{ij} + \frac{1}{3}K^2 + \frac{1}{2}(\rho_H + S)\right] + \beta^i D_i K - \partial_t K \quad , \qquad (77)$$

for α, dependent on K and its rate of change $\partial_t K$. On any subsequent slice, (77) requires that $\partial_t K = f(x^i,t)$ be specified; the value of $K = g(x^i,t)$ will itself have followed from the evolution of its initial value on Σ_0. The initial value of K on Σ_0 will fix the initial time coordinate.

One example of such slicing conditions is constant-mean-curvature slices, $K = K(t)$. These have the immediate advantage that the equation (77) for the lapse decouples from the shift vector, though this is only of secondary importance in a numerical calculation. Constant-mean-curvature slices however fail to satisfy our assumed fall-off conditions (55). This has the consequence that, though everywhere spacelike, these slices interact *null* infinity instead of spatial infinity, I^0. These spacelike slices are asymptotic to null slices. Slices with $K < 0$ intersect future null infinity, I^+, while those with $K > 0$ intersect past null infinity, I^-. This property of constant-mean-curvature slices may eventually be used to great advantage to allow the spacelike ADM scheme to incorporate the standard theory[33,34] of gravitational radiation and mass-energy at null infinity. One potential problem with this approach[30,35] is the question of whether these slices intersect null infinity in a *good cut*, i.e., whether the two-surface of intersection is sufficiently smooth.

The maximal slicing condition, which we employ, results in an equation for the lapse from (77) by demanding $\partial_t K = K = 0$:

$$\Delta\alpha = \alpha\left[A_{ij}A^{ij} + \frac{1}{2}(\rho_H + S)\right] \quad . \qquad (78)$$

Again, assuming the strong energy condition, i.e. $\rho_H + S \geq 0$, the term multiplying α on the right-hand-side is positive definite and so the standard maximum-minimum arguments on elliptic systems apply. Maximal slices intersect I^0. The maximal slicing condition was originally discussed and suggested by Lichnerowicz.[6] Its geometrical significance can be seen by considering the trace of equation (II32) giving $\nabla_a n^a = 0$. This result implies that the convergence of the Eulerian observers vanishes, i.e. the Eulerian observers behave like an incompressible fluid in this gauge.

While this property does not guarantee that maximal slices will always avoid physical curvature singularities that result from black hole formation, it has worked well in practice in a number of applications[11,16,22,36,37] to date. The effect of maximal slicing when a black hole forms (event horizon appears) is to decrease the lapse exponentially in the interior, thus forming a *limit slice* which, presumably, has some finite proper time interval away from the singularities. Proper energy densities will "freeze" in the interior.

An example of the collapse of the lapse function from our own calculations is given in Figures 1a,b. These are plots of the central value of the lapse during a spherical core collapse to a black

Figures 1a,b. Data from a spherical collapse to a black hole. Figure 1a gives the central value of the lapse function plotted versus coordinate time in units of M. An apparent horizon formed at roughly t = 52 M. The logarithm of the central value of α is shown in Figure 1b. The calculation proceeded for times in excess of 100 M past horizon formation. The exponential braking of the lapse is evident.

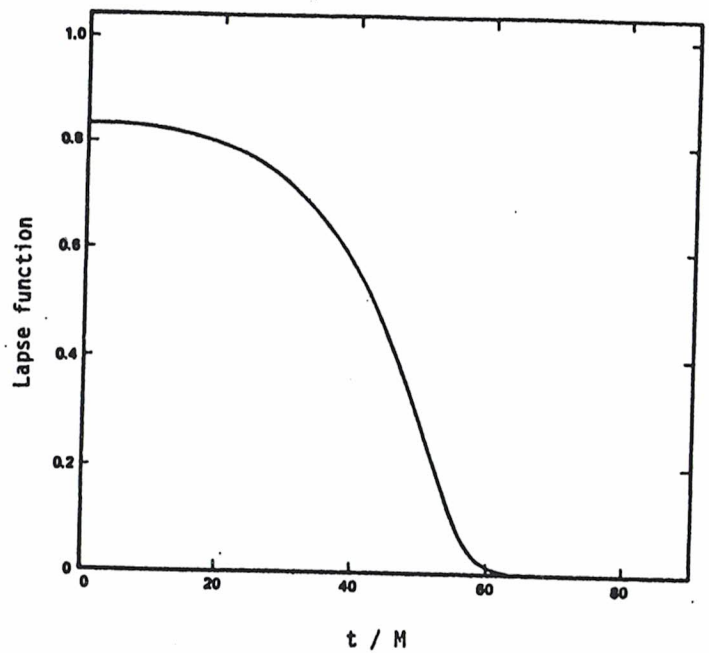

Figure 1a

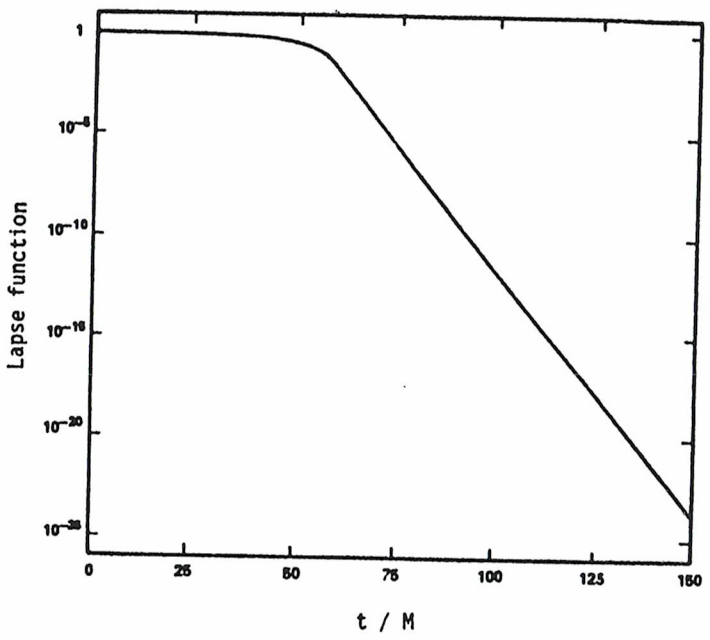

Figure 1b

hole. An apparent horizon was observed to form at approximately t = 52M where M is the mass of the system. In Figure 1b, at late times after horizon formation, the exponential decrease, e^{-t/t_e}, is clearly evident. This behavior confirms simplified arguments of Smarr and York,[24] results from maximally slicing vacuum Schwarzschild geometry,[24,31] and calculations of Shapiro and Teukolsky.[37] Interestingly, the measured e-folding rate for our *matter-filled* collapse is t_e = 1.80M; exceedingly close to the rate, t_e = 1.82M, obtained from maximally slicing a Schwarzschild black hole.[24] This is added confirmation of the conjecture[24] that the decrease of α is largely independent of the details of the strong field region during black hole formation.

We note also in Figure 1b that the calculation continued long after horizon formation (approximately 100M). This is the desired property of our time slicing when a black hole forms. From perturbation studies[38] of black holes and the two black hole collision,[16] it is known that the characteristic wavelength of gravitational radiation from black hole formation is likely to be roughly 17M. We will thus require our calculation to be able to continue for times on the order of hundreds of M after horizon formation. This allows the gravitational radiation pulse to propagate out into the wave-zone and to be measured as it passes through an edit two-surface at the edge of our mesh.

Finally before leaving the lapse, we point out that one need not restrict attention to K and (78) in using this method to

specify the lapse. Other combinations of components of $K^i{}_j$ will do also. Bardeen and Piran[26,39] and Eardley[40] have advanced the *polar slicing* condition

$$\partial_t(K^\theta{}_\theta + K^\phi{}_\phi) = 0 \quad \text{and} \quad K^\theta{}_\theta + K^\phi{}_\phi = 0 \quad , \tag{79}$$

in spherical coordinates, which has similar "singularity avoidance" properties. This condition results in a *parabolic* equation for the lapse, α, with significant computational speed advantages over (78). However, the condition (79) results in regularity problems at $r = 0$, which require modification of (79)[26,39] in practice.

Compared to the lapse, the specification of the shift vector is of less fundamental importance, since its use only amounts to a relabeling of the spatial coordinates on the time slices. Of course, the flow of the spatial coordinates from slice to slice must proceed in a sufficiently smooth manner or coordinate singularities can again arise.

We can take similar approaches to the shift as we did for the lapse. The shift vector components can be directly specified, as the case of geodesic slicing demonstrated for the lapse. The most obvious choice of this type is to take $\beta^i = 0$ (normal coordinates). There is no fundamental objection to this particular choice and it has been successfully applied in several problems including the calculation of the collision of two black holes.[16] This spatial gauge leads to a degree of simplification of the Einstein equations, by

eliminating terms in the evolution equations (II76-78). However, from the standpoint of achieving the greatest degree of simplification, there is a better course involving the use of a nonvanishing shift vector, as will be shown below.

Another useful example of directly specifying the shift is the Lagrangian gauge.[41] Here the idea is to choose the shift vector so that the spatial coordinates comove with the matter. This route leaves the lapse free to determine a smooth time slicing. In the Lagrangian gauge, the hydrodynamic equations (II101-103) then obtain a simplified form ($V^i = 0$). This technique has so far been used in spherical collapse calculations,[27,42] though it is also amenable to nonspherical situations.

It is important to distinguish this approach to constructing a Lagrangian gauge from a more commonly employed,[43-45] though less satisfactory, method. This older approach takes $\beta^i = 0$ and uses the lapse to distort the time slices in such a way that the matter velocity corresponds in direction with the surface normal, n^a, and therefore with the flow of the Eulerian and coordinate observers. This is only possible, however, if the fluid flow is irrotational since n^a is *surface-forming* only if condition (II9,29) is satisfied. The technique is therefore restricted to use only in spherical systems. Even in spherical collapse calculations however, this gauge breaks down[45] shortly after a black hole forms as the time slices intersect the singularity.

We can also indirectly specify the shift vector by setting conditions on components of the velocity of the three-metric, $\partial_t \gamma_{ij}$, or the velocity of the conformal metric, $\partial_t \tilde{\gamma}_{ij}$, in analogy to the time slicing conditions just discussed. These gauge conditions split into two types, which we call differential and simplifying (or algebraic). The attempt with these gauge conditions is to use the shift vector to, respectively, either minimize coordinate excitation in the presence of gravitational waves or to simplify the form of the three-metric in order to reduce the complexity of the Einstein equations.

The former course is most naturally pursued by use of the Smarr-York[24,25] minimal distortion shift vector condition in conjunction with the maximal slicing condition on α. Minimal distortion shift vector is an attempt to separate out and minimize the coordinate waves (coordinate shear) that appear in the presence of "true" gravitational waves. The idea is to use β^i to remove the longitudinal part of the time rate of change of the conformal three-metric, $\tilde{\gamma}_{ij}$. Using (59) and (II77), we obtain the evolution equation

$$\gamma^{1/3}\, \partial_t \tilde{\gamma}_{ij} = -2\alpha A_{ij} + (L\beta)_{ij} \equiv 2\, \Sigma_{ij} \quad , \tag{80}$$

with the definition (2) employed. Σ_{ij} is a shear-like quantity called the distortion tensor. It is obviously tracefree. Assuming our manifold is topologically $\mathbb{R}^3$, the covariant orthogonal decomposition, utilized previously, can be applied to Σ_{ij} giving

$$\Sigma_{ij} = \Sigma_{ij}{}^{T} + (LV)_{ij} \quad , \tag{81}$$

where $D^i \Sigma_{ij}{}^{T} = 0$. So $\Sigma_{ij}{}^{T}$ is TT. Note also that this decomposition is orthogonal on the *physical* manifold, as opposed to the earlier application on the conformally related manifold.

The longitudinal part of Σ_{ij} in (81) is, recalling the arguments of (32) and (33), also given by

$$(LV)_{ij} = \gamma^{1/3} \pounds_V \tilde{\gamma}_{ij} \quad , \tag{82}$$

which hence represents the part of $\partial_t \tilde{\gamma}_{ij}$ affected by coordinate changes. The minimal distortion shift vector gauge results from requiring this part of Σ_{ij} to vanish, thus making the time rate of change of $\tilde{\gamma}_{ij}$ pure TT:

$$D^i(\partial_t \tilde{\gamma}_{ij}) = 0 \quad . \tag{83}$$

From (80), this condition results in the system of second order elliptic equations on β^i,

$$(\Delta_L \beta)_j = D^i (L\beta)_{ij} = 2 D^i (\alpha A_{ij}) \quad , \tag{84}$$

which involves the use of the previously described vector Laplacian. The term differential shift condition comes from the use in (83) of the divergence operator on the velocity of the conformal metric.

This *radiation gauge*[25] (including the use of maximal slicing) has the nice property of maintaining throughout the evolution the initial fall-off rates (53) -(56). The shift condition (84) is also three-covariant, allowing freedom to specify the initial

spatial coordinates on Σ_0 as desired (recall that β^i only *propagates* spatial coordinates from slice to slice). This gauge gives a much cleaner asymptotic separation between the radiative and nonradiative parts of the gravitational field. However, it has yet to be employed in a multi-dimensional code. This fact owes much to the complexity of the Einstein equations in multi-dimensional problems and that the minimal distortion shift condition adds to this complexity, through the use of nonvanishing β^i, while making no corresponding simplification in the rest of the metric. It is likely that symbolic manipulation languages (such as MACSYMA, SHEEP, etc.) will have to be employed to derive and check the differential equations resulting from these "general metric" gauges.

Algebraic shift conditions are similar in type to the maximal and polar time slicing conditions. Conditions are directly placed on some number of components (up to three) of the velocity of the three-metric or on some number of time independent linear combinations of components of $\partial_t\gamma_{ij}$. Such conditions can be symbolically represented as

$$\sum_{p,q} c^m_{pq}(x^i)\partial_t\gamma_{pq} = \partial_t \sum_{p,q} c^m_{pq}(x^i)\gamma_{pq} = f^m(x^i,t) \quad , \qquad (85)$$

where m labels the gauge conditions imposed and $c^m_{pq}(x^i)$ are spatial coordinate dependent functions. These gauge conditions must be supplemented by initial values on Σ_0:

$$\sum_{p,q} c^m_{pq}(x^i)\gamma_{pq} = g^m(x^i) \quad . \qquad (86)$$

Note that these conditions are no longer three-covariant in contrast to the minimal distortion gauge.

Assuming the number of equations represented by (85) is equal to the number of nonvanishing shift vector components (or if less, then additional conditions are imposed on β^i), then (85) results in the equations

$$\sum_{p,q} c^m_{pq}(D_p\beta_q + D_q\beta_p - 2\alpha K_{pq}) = f^m(x^i,t) \qquad (87)$$

for β^i using (II77). This will be a system, in general, of first order PDE's.

The purpose behind these conditions is to simplify the differential equations in the algorithm. This is accomplished, even though nonvanishing β^i contributes kinematical terms to the evolution equations (II77,78), by reducing the number of independent components of γ_{ij}. Recall that the kinematical quantities α and β^i do not appear in the IVP, while γ_{ij} appears in both the evolution equations and the IVP equations as complicated second order covariant derivatives and Ricci tensor terms. The most general metric with six components can be reduced to three independent components using the full shift vector. Of the remaining three, one is determined by the Hamiltonian constraint (ϕ) and the last two represent the

two dynamical degrees of freedom. In certain problems with symmetry, the number of degrees of freedom may be reduced (as with our application).

Typically, for reasonable simplifications to result we take $f^m = 0$, $g^m = 0$. A number of these conditions are discussed in the literature,[11,16,26,36,37,39] but they are usually tailored to the particular coordinates and symmetries of the problem. We therefore defer further discussion until considering in Chapter IV the specific gauge we employ in our code.

Chapter III References

1. York (1971).
2. Arnowitt, Deser, and Misner (ADM) (1962).
3. In fact the conjugate momenta are $\pi^{ij} = \gamma^{\frac{1}{2}}(\gamma^{ij}K - K^{ij})$; see Ref. 2.
4. York (1972).
5. ŌMurchadha and York (1974).
6. Lichnerowicz (1944); see also Choquet-Bruhat (1962) for early work on the conformal approach.
7. ŌMurchadha and York (1973).
8. York (1973); see also Deser (1967), and Berger and Ebin (1969) for earlier work on decompositions of K^{ij}.
9. Cantor and Piran (1982).
10. York (1979).
11. Dykema (1980).
12. Cantor (1979a).
13. Cantor (1979b).
14. York (1983).
15. York and Piran (1982).
16. Smarr (1979).
17. Evans, Smarr, and Wilson (1984).
18. Welling (1983); Isaacson, Welling, and Winicour (1983).
19. York (1980).

20. Cantor (1974).
21. Chaljub-Simon and Choquet-Bruhat (1980).
22. Wilson (1979).
23. Hellwig (1967).
24. Smarr and York (1978b).
25. Smarr and York (1978a).
26. Bardeen and Piran (1983).
27. Eardley and Smarr (1979).
28. Piran (1982).
29. Hawking and Ellis (1973).
30. Eardley (1979).
31. Estabrook et al. (1973).
32. Reinhart (1973).
33. Bondi, van der Burg, and Metzner (1962).
34. Sachs (1962).
35. Goddard (1977).
36. Evans (1984).
37. Shapiro and Teukolsky (1980).
38. Davis, Ruffini, Press, and Price (1971).
39. Piran (1983).
40. Eardley (1984).
41. Taub (1978).
42. Chrzanowski (1977).
43. Tolman (1934); Bondi (1947); Oppenheimer and Snyder (1939).

44. Misner and Sharp (1964).
45. May and White (1966; 1967).
46. Hawking (1968).
47. Newman and Penrose (1962).
48. Bowen (1979).
49. Bowen and York (1980).
50. Choquet-Bruhat, DeWitt-Morette, and Dillard-Bleick (1977).

APPENDIX A

The fall-off conditions (41), (53), (54), and (55) guarantee that our slices intersect spatial infinity, I^0, and that a unique, well defined asymptotic energy-momentum four vector for our isolated system can be found there. Writing the metric (as in (41))

$$\gamma_{ij} = f_{ik}(\delta^k{}_j + h^k{}_j) \quad , \tag{A1}$$

where f_{ik} is the corresponding flat metric, allows the ADM energy energy[2,10,19] to be expressed in terms of the two-surface integral by (recalling our units $G = (8\pi)^{-1}$, $c = 1$)

$$E_{ADM} = \lim_{r \to \infty} \frac{1}{2} \oint dA^j \, D_i(h^i{}_j - \delta^i{}_j h^k{}_k) \quad . \tag{A2}$$

Here, the full D_i can be replaced by its flat space counterpart relative to f_{ij}.

Using the assumptions (43) and (49) discussed in the text, we can proceed to show the reduction of (A2) in terms of only the conformal factor ϕ. From (40) and (41),

$$h_{ij} = (\phi^4 - 1)f_{ij} + \phi^4 \hat{h}_{ij} \quad , \tag{A3}$$

with trace (relative to f_{ij})

$$h^k{}_k = 3(\phi^4 - 1) + \phi^4 \hat{h}^k{}_k \quad . \tag{A4}$$

We can write

$$\begin{aligned} h^i{}_j - \delta^i{}_j h^k{}_k &= \left(h^i{}_j - \frac{1}{3}\delta^i{}_j h^k{}_k\right) - \frac{2}{3}\delta^i{}_j h^k{}_k \\ &= \psi^i{}_j - \frac{2}{3}\delta^i{}_j h^k{}_k \quad , \end{aligned} \tag{A5}$$

using the definition (48) for the tracefree part. Then combining (A5) and (A4) gives

$$h^i{}_j - \delta^i{}_j h^k{}_k = \psi^i{}_j - 2(\phi^4 - 1)\delta^i{}_j - \frac{2}{3}\phi^4 \hat{h}^k{}_k \delta^i{}_j \quad , \tag{A6}$$

which with assumptions (43) and (49) allows (A2) to be rewritten as

$$E_{ADM} = \lim_{r \to \infty} (-4) \oint dA^i \, D_i\phi \quad . \tag{A7}$$

In the same way, the linear momentum of the system has a two-surface integral definition. Letting $\zeta^i{}_{(k)}$ be the k^{th} asymptotic translational Killing vector of f_{ij}, the component of the momentum along this direction is

$$P_i \zeta^i{}_{(k)} = \lim_{r \to \infty} \oint dA_i \, \zeta^j{}_{(k)}(K^i{}_j - \delta^i{}_j K) \quad . \tag{A8}$$

These results, (A2) and (A8), are asymptotically invariant under gauge changes that do not produce asymptotic Lorentz boosts (i.e. the allowed asymptotic coordinate changes are of the form $x^a \to x^{a'} = x^a + \varepsilon\xi^a$ where $\partial_b\xi^a = \mathcal{O}(r^{-1})$, $\partial_c\partial_b\xi^a = \mathcal{O}(r^{-2})$, etc.[10]).

An expression for the angular momentum of the system can also be produced by replacing the $\zeta^i{}_{(k)}$ in (A8) by rotational Killing

vectors $\zeta^i{}_{rot(k)}$:

$$J_i\zeta^i{}_{rot(k)} = \lim_{r\to\infty} \oint dA_i\, \zeta^j{}_{rot(k)}(K^i{}_j - \delta^i{}_j K) \quad . \tag{A9}$$

However, this result is asymptotically gauge invariant only if the relevant $\zeta^i{}_{rot(k)}$ are exact rotational Killing vectors of the full spacetime. If exact symmetries do not exist and the rotational Killing vectors of f_{ij} are used, the values produced by (A9) are ambiguous unless suitable further restrictions are made on the gauge and allowable gauge changes. Sufficient conditions on the asymptotic *gauge* are (49) (on the spatial coordinates) and

$$K = \mathcal{O}(r^{-3}) \quad , \tag{A10}$$

(asymptotically maximal slicing for the time coordinate), however further *physical* restrictions may also be necessary.[19]

The ADM surface integrals given above are defined at spatial infinity. In a typical numerical calculation, however, these quantities must be evaluated at the edge of a grid at a finite radius. Therefore, they will only approximate the ADM values at I^0. We can add to this list other quasilocal indicators that formally approach their ADM analogs as $r \to \infty$. One such indicator of the energy (or mass with mass-centered coordinates) is the Hawking mass[11,30,36,46]

$$M_H(r) = 8\pi\left[\frac{A(r)}{16\pi}\right]^{1/2}\left(1 - \int \frac{dA}{2\pi}\,\mu\rho\right) \quad , \tag{A11}$$

where $A(r) = \int dA$ is the proper area of a coordinate two-surface and μ and ρ are the Newman-Penrose spin coefficients[11,47]

$$\mu = -\bar{m}^a m^b \nabla_b k_a \quad , \tag{A12}$$

$$\rho = m^a \bar{m}^b \nabla_b \ell_a \quad . \tag{A13}$$

Here k_a and ℓ_a are, respectively, the ingoing and outgoing future directed null vectors orthogonal to the coordinate two-sphere of radius r. The interpretation of (A12) and (A13) is that $-\mu$ and ρ are the convergences of the null congruences associated with k_a and ℓ_a, respectively. Hence, μ and ρ measure the focussing of null rays due to the curvature of the two-surface and the presence of mass-energy. The surface integral in (A11) encompassing the isolated system attempts to remove the focussing due to just the two-surface curvature (on a metric sphere in flat space, $\mu = \frac{1}{2r}$ and $\rho = \frac{1}{r}$).

This points to one of the properties of $M_H(r)$; it vanishes in flat space on a sphere. The Hawking mass has several other nice features.[30] One property is that $\lim M_H(r) = M_{ADM}$ as $r \to \infty$ on a spatial slice. Secondly, it also gives $\lim M_H(r) = M_{BONDI}$[33,34] as $v = t + r \to \infty$ (i.e. on a cut of future null infinity). Thus, the radiation reaction effect on the mass of a system is potentially measurable using M_H. This indicator has worked well in our application, as will be demonstrated in Chapter VI.

We will also be interested in measuring the flux of gravitational radiation emitted during our calculations. This too must be

done at a finite radius as opposed to future null infinity I^+, where it is more rigorously defined.[33,34] To this end, we use the asymptotic expression for the rate of change of M_H with retarded time,[46]

$$\frac{dM_H}{du} = -\frac{1}{4\pi} \lim_{r \to \infty} \int dA \, |\lambda'|^2 \quad , \tag{A14}$$

where λ' is the Newman-Penrose coefficient[11,47]

$$\lambda' = -\bar{m}^a \bar{m}^b \nabla_b k_a \quad , \tag{A15}$$

equivalent to the Bondi *news* function.[33] It is clear from (A14) that a nonvanishing news function can only lead to a decrease in the Bondi mass with time. Expression (A14) for the flux is calculated in our applications at a large, but finite radius. Its value will therefore not be unique and will only approximate that which one would obtain at I^+. No rigorous error bounds are available, but it is expected that (A14) can be evaluated on a sufficiently large coordinate two-sphere to make such errors comparable to the truncation errors associated with the finite difference approximation.

APPENDIX B

Bowen and York[48,49] have derived a monopole (r^{-1}) singular solution to the vacuum, flat space vector Laplace equation

$$(\Delta_L{}^{(f)} W)^i = 0 \quad , \tag{B1}$$

given by

$$W^i(x) = -\frac{7}{32\pi r}\left[\delta^i{}_j + \frac{1}{7} n^i n_j\right] p^j \quad . \tag{B2}$$

Here p^j is a constant vector and $n^i = \frac{1}{r} x^i$. Flat space cartesian coordinates are used throughout this discussion unless otherwise noted. There are three independent solutions of (B2) corresponding to linearly independent $p^i{}_{(k)}$.

We can use these monopole solutions to produce a basis of vector Greens functions (bivectors) $g^i{}_{(k)}(x - x')$ of $\Delta_L{}^{(f)}$. Taking for $p^i{}_{(k)}$ the cartesian coordinate basis

$$e^i{}_{(k)} = \delta^i{}_k \quad , \tag{B3}$$

and replacing $x^i \to x^i - x^{i'}$ yields

$$g^i{}_{(k)}(x - x') = -\frac{7}{32\pi|x - x'|}\left[\delta^i{}_k + \frac{1}{7}\frac{(x^i - x^{i'})(x_k - x'_k)}{(x - x')^2}\right] \quad , \tag{B4}$$

from (B2). The L operator (15) applied to (B4) gives

$$(Lg_{(k)})^{ij} = \frac{3}{16\pi}(x - x')^{-2}\left[\delta^i{}_k \frac{x^j - x^{j'}}{|x - x'|} + \delta^j{}_k \frac{x^i - x^{i'}}{|x - x'|} - \frac{x_k - x'_k}{|x - x'|}\left(\delta^{ij} - \frac{(x^i - x^{i'})(x^j - x^{j'})}{(x - x')^2}\right)\right] \quad . \tag{B5}$$

Computing $\Delta_L^{(f)}$ (16) of $g^i{}_{(k)}(x - x')$ from (B5) produces

$$(\Delta_L^{(f)} g_{(k)})_i = \delta_{ik}\delta^3(x - x') \quad , \tag{B6}$$

where the coefficient of $\delta^3(x - x')$ is found by evaluating (28) using (B5) and $V_i = e_{i(k)}$ (B3). This justifies the use of the term vector Greens function. In evaluating (B5) and (B6) we have used

$$\frac{\partial r}{\partial x^i} = \frac{1}{r} x_i = n_i \quad , \quad \frac{\partial n^j}{\partial x^i} = \frac{1}{r}(\delta^j{}_i - n_i n^j) \quad , \tag{B7}$$

where n^i should not be confused with the time slice normals, and the surface integrals

$$\int d\Omega = 4 \quad , \quad \int d\Omega\, n^i n^j = \frac{4\pi}{3}\delta^{ij} \quad ,$$

and

$$\int d\Omega\, n^{\alpha_1} \cdots n^{\alpha_m} = 0 \qquad \text{for odd } m \quad . \tag{B8}$$

We are now in a position to calculate an integral solution of the flat space version of (25):

$$(\Delta_L^{(f)} W)^i = S^i \quad . \tag{B9}$$

Using (B9) in (29) with $V^i = g^i{}_{(k)}(x - x')$ gives

$$W^k(x) = \int d^3x'\, g^{(k)i}(x - x') S_i(x') \quad , \tag{B10}$$

where the surface terms vanish since $g^i{}_{(k)} = \mathcal{O}(r^{-1})$ and $W^k = \mathcal{O}(r^{-1})$.

The solution (B10) can now be employed to obtain a vacuum multipole moment expansion of W^k, valid for asymptotically flat manifolds as well, by expanding the vector Greens functions. Taking $r = |x| >> |x'| = r'$ gives

$$g^{(k)i}(x - x') \cong -\frac{7}{32\pi r}\left[\left(\delta^{ki} + \frac{1}{7} n^k n^i\right) + \frac{x^\ell x'^\ell}{r^2}\left(\delta^{ki} + \frac{3}{7} n^i n^i\right) - \frac{1}{7r}(n^i x^{k'} + n^k x^{i'})\right] \quad , \tag{B11}$$

through orders r^{-1} and r^{-2}. Then using (B11) in (B10) we obtain the expansion (36):

$$W^k(x) \cong -\frac{7}{32\pi r}\left(\delta^{ki} + \frac{1}{7} n^k n^i\right) P_i + \frac{1}{16\pi r^2}(\delta^{ki} n^j - \delta^{kj} n^i) J_{ij} + \frac{1}{64\pi r^2}\left[3(n^j \delta^{ki} + n^i \delta^{kj}) - n^k(\delta^{ij} - 3n^i n^j)\right] D_{ij} \quad , \tag{B12}$$

where the moments P_i, J_{ij}, and D_{ij} are given by

$$P_i = \int d^3x'\, S_i(x') \quad , \tag{B13}$$

$$J_{ij} = -2\int d^3x'\, S_{[i}(x')x'_{j]} \quad , \tag{B14}$$

$$D_{ij} = -2\int d^3x'\, S_{(i}(x')x'_{j)} \quad . \tag{B15}$$

In a sufficiently flat spacetime, (B13) - (B15) can be directly interpreted, with P_i being the linear momentum of the system, J_{ij} being the angular momentum tensor giving an angular momentum vector $J^m = \frac{1}{2}\epsilon^{mij}J_{ij}$, and symmetric moments D_{ij} representing some non-stationarity of the system.

The linear and angular momentum terms of (B12) continue to have the same interpretation for P_i and J_{ij} on an asymptotically flat space, as can be verified by calculation of $K^i{}_j = (LW)^i{}_j$ from (B12) and substitution in (A8) and (A9). We have not yet found an interpretation of D_{ij} on a non-flat manifold. However, in flat space, D_{ij} is the time rate of change of the quadrupole moment tensor. This can be shown by use of the conservation law $T^{ab}{}_{,b} = 0$:

$$\begin{aligned}\partial_t I_{ij} &= \partial_t \int d^3x\, T^{oo}\, x_i x_j = \int d^3x\, T^{oo}{}_{,o}\, x_i x_j \\ &= -\int d^3x\, T^{ok}{}_{,k}\, x_i x_j \\ &= \int d^3x (T^o{}_i x_j + T^o{}_j x_i) \\ &= -2\int d^3x\, S_{(i}x_{j)} = D_{ij} \quad , \end{aligned} \tag{B16}$$

where $S_i = -T^o{}_i$ from (II79) if $\alpha = 1$, $\beta^i = 0$.

Finally, we use (B12) to consider boundary conditions for (25) at finite radius. Assuming $P_i \neq 0$, (B12) can be used to derive the York-Piran Robin condition (37) for a moving source. We proceed to show the uniqueness of the solution to (25) using (37). By taking (37) and multiplying by $(\delta^m{}_i + n^m n_i)$ we obtain

$$(\hat{L}W)^{ij}n_j = -\frac{6}{7r}W_j\left(\delta^{ij} + \frac{3}{4}n^i n^j\right) \quad . \tag{B17}$$

We assume two solutions, $W_1{}^i$ and $W_2{}^i$, exist to (25). Their difference, $U^i = W_2{}^i - W_1{}^i$, satisfies $(\hat{\Delta}_L U)^i = 0$. Using this with (B17) in (28) with $V^i = W^i = U^i$ gives

$$\frac{1}{2}\int d\hat{v}(\hat{L}U)_{ij}(\hat{L}U)^{ij} + \frac{6}{7}\oint d\Omega r\, U_i U_j\left(\delta^{ij} + \frac{3}{4}n^i n^j\right) = 0 \quad . \tag{B18}$$

The first term is positive definite and, since the eigenvalues of $\left(\delta^{ij} + \frac{3}{4}n^i n^j\right)$ are (7/4,1,1), so is the second term. Therefore, $(\hat{L}U)^{ij} = 0$ everywhere interior and $U^i = 0$ on the boundary. The former condition allows the possibility that U^i is a CKV. The CKV's of three-dimensional flat space are[50]

$${}_{(0)}C^i = a^i + b^{ij}x_j + cx^i + d^j x_j x^i - \frac{1}{2}d^i x_j x^j \quad , \tag{B19}$$

in cartesian coordinates, where $b^{ij} = -b^{ji}$. The constants give the ten parameter conformal group. None of these vanish on a spheroidal boundary of nonzero radius, as required by the surface integral (B18). Suppose on an asymptotically flat manifold CKV's $C^i{}_{(k)}$ exist, differing from ${}_{(0)}C^i{}_{(k)}$ by

$$C^i{}_{(k)} = {}_{(0)}C^i{}_{(k)} + \epsilon^i{}_{(k)} \quad . \tag{B20}$$

Taking the metric in the form (41), with asymptotically cartesian coordinates ($f_{ij} = \delta_{ij}$), we obtain

$$\tilde{\gamma}_{ij} = \delta_{ij} + \psi_{ij} \quad , \tag{B21}$$

where ψ_{ij}, the tracefree part of γ_{ij}, is defined in (48). Then using the defining relations, $\pounds_c \tilde{\gamma}_{ij} = 0$ and $\pounds_{(0)c} \tilde{f}_{ij} = 0$, we find asymptotically that $\epsilon^i{}_{(k)}$ satisfies

$$(L^{(f)}\epsilon)_{ij} = -\pounds_{(0)c}\psi_{ij} = -{}_{(0)}C^{\ell}\partial_{\ell}\psi_{ij} - \psi_i{}^{\ell}\partial_{\ell(0)}C_j - \psi^{\ell}{}_j\partial_{\ell(0)}C_i \quad , \tag{B22}$$

where the k subscript has been dropped. Since we require $\psi^i{}_j = \mathcal{O}(r^{-1})$, (B22) implies $\epsilon^i{}_{(k)}/{}_{(0)}C^i{}_{(k)} = \mathcal{O}(r^{-1})$ as well. Thus on at sufficiently large radius, (B18) implies $U^i = 0$ everywhere and therefore uniqueness.

The new Robin boundary condition (38) is applicable to problems involving rotation and which employ center-of-momentum coordinates, $P_i = 0$. Additionally, it must be true that the symmetric moments, D_{ij}, are such that

$$|D_{ij}| \ll |J_{ij}| \quad . \tag{B23}$$

This condition should apply to slowly collapsing, rotating configurations; say, for example, initial data for rotating stellar collapse. If $P_i = 0$ and $D_{ij} = 0$ are assumed, (B12) becomes

$$\begin{aligned} W^k(x) &= \frac{1}{16\pi r^2}(\delta^{ki}n^j - \delta^{kj}n^i)J_{ij} + \mathcal{O}(r^{-3}) \\ &= -\frac{1}{8\pi r^2} n_j J^{jk} + \mathcal{O}(r^{-3}) \quad . \end{aligned} \tag{B24}$$

From this is obtained

$$(LW)^{k\ell} = \frac{3}{8\pi r^3}(n^k n_j J^{j\ell} + n^{\ell} n_j J^{jk}) + \mathcal{O}(r^{-4}) \quad , \tag{B25}$$

which, using (B24) and contracting with n_{ℓ}, gives (38):

$$(\hat{L}W)^{k\ell} n_{\ell} + \frac{3}{r}(\delta^{k\ell} + n^k n^{\ell})W_{\ell} = \mathcal{O}(r^{-4}) \quad . \tag{B26}$$

Assuming again two solutions, $W_1{}^k$ and $W_2{}^k$, to (25) using boundary condition (38; B26), with difference $U^k = W_2{}^k - W_1{}^k$ satisfying $(\hat{\Delta}_L U)^i = 0$, (B26) in (28) gives

$$\frac{1}{2}\int d\hat{v}(\hat{L}U)_{ij}(\hat{L}U)^{ij} + 3\oint d\Omega r\, U_k U\,(\delta^{k\ell} + n^k n^{\ell}) = 0 \quad . \tag{B27}$$

The eigenvalues of $(\delta^{k\ell} + n^k n^{\ell})$ are (2,1,1) and the same arguments apply showing uniqueness.

CHAPTER IV

Having discussed in Chapters II and III many of the general aspects of how general relativity is treated as an initial value and dynamical problem, we are now in a position to apply these techniques to model axisymmetric, nonrotating gravitational collapse. This chapter is devoted in large part to obtaining the partial differential equations to be solved through finite differencing (see Chapter V). Our particular spatial and time gauge conditions are implemented along with applying the assumed symmetries and reducing covariant to partial derivatives. We evaluate expressions for mass-energy and energy flux (Chapter III) that are used to obtain results on gravitational radiation from our calculations.

Boundary conditions are formulated for the derived equations. These include physical conditions at large but finite radius, as well as conditions produced by the symmetry assumptions at the origin, along the symmetry axis, and on the equatorial plane. To aid in understanding the physical conditions at large radius, expansions are given for some of the longitudinal, gauge, and radiative parts of the gravitational field. Symmetry conditions follow from a thorough examination of the regularity of geometrical quantities near the singular points ($r = 0$, $\theta = 0$) of our spherical polar coordinates. These considerations also help to determine a pair of variables formed from combinations of the coordinate components of γ_{ij} and $K^i{}_j$ which

have particularly nice radiative features. Using the simplifying gauge approach and fully constrained evolution, these are the only components of the gravitational field, representing the single dynamical degree of freedom allowed by our symmetry assumptions, that need to be evolved using (II77,78).

a) Spatial Gauge, Shift, and Metric

Axisymmetry implies that the metric admits a rotational Killing vector $\tilde{\phi}^a$. We assume in addition that the space has equatorial plane reflection symmetry. It is possible therefore to choose the computational frame that is momentum and mass centered. Assuming no axial rotation leads to vanishing angular momentum at infinity, $J_i\tilde{\phi}^i = 0$, from (IIIA9). Even if the technique is extended to allow axial rotation, the calculation of (IIIA9) will be unambiguous owing to the exact rotational Killing vector. In this case, the boundary condition (III38) can be used to determine a precise value (to lowest order) of J_ϕ at large radius.

To proceed much further, we must make a specification of the spatial basis $\{e_i\}$. As mentioned in Chapter II, it is most practical to take a holonomic, or coordinate, basis. We produce this basis by taking the tangent vectors of the topological spherical polar coordinates (r,θ,ϕ). The Killing vector is identified with $\tilde{\phi} = \partial_\phi$, while the symmetry axis is at $\theta = 0, \pi$ and the equatorial plane is at

$\theta = \pi/2$. We assume $r = 0$ has the topology of a point (the three-manifold is diffeomorphic to $\mathbb{R}^3$) and that the center of mass is located there.

The Killing vector generates isometry in the metric and other geometrical quantities under the action of $\pounds_\phi$. Hence, with our coordinates defined as above, ϕ is an ignorable coordinate. The resulting two-dimensionality is the primary reason the problem is numerically tractable using current resources. The assumption of no axial rotation implies that the gravitational and matter fields are invariant under the change $\phi \to \phi_0 - \phi$ for arbitrary ϕ_0. In our coordinate basis, this results in the vanishing of any tensor component having an odd number of ϕ indices. In particular, we have

$$\beta^\phi = \gamma_{r\phi} = \gamma_{\theta\phi} = 0 \quad . \tag{1}$$

This initial reduction of the metric gives the line element

$$ds^2 = -\alpha^2 dt^2 + \gamma_{rr}(dr + \beta^r dt)^2 + \gamma_{\theta\theta}(d\theta + \beta^\theta dt)^2 + \gamma_{\phi\phi} d\phi^2 + 2\gamma_{r\theta}(dr + \beta^r dt)(d\theta + \beta^\theta dt) \quad , \tag{2}$$

from (II73).

We must next impose our spatial gauge conditions. Our gauge is the same as the last one of several tried by Wilson and Dykema.[1] The two conditions

$$\partial_t \gamma_{r\theta} = 0 \qquad \text{and} \qquad \partial_t(r^2\gamma_{rr} - \gamma_{\theta\theta}) = 0 \quad , \tag{3a,b}$$

of the simplifying type (III85), are introduced. In addition initial values

$$\gamma_{r\theta} = 0 \qquad \text{and} \qquad r^2\gamma_{rr} - \gamma_{\theta\theta} = 0 \quad , \tag{4a,b}$$

are taken on Σ_0 (III86) leading to a greatly simplified line element

$$ds^2 = -\alpha^2 dt^2 + A^2(dr + \beta^r dt)^2 + A^2 r^2(d\theta + \beta^\theta dt)^2 + B^2 r^2 \sin^2\theta \, d\phi^2 \quad , \tag{5}$$

where we have introduced $\gamma_{rr} = A^2$ and $\gamma_{\phi\phi} = B^2 r^2 \sin^2\theta$. The three-metric is

$$\gamma_{ij} = \mathrm{diag}(A^2, A^2 r^2, B^2 r^2 \sin^2\theta) \quad . \tag{6}$$

In writing down (3) and (4), we have used the freedom embodied in the two nonvanishing shift components, β^r and β^θ. These gauge conditions result in equations for the shift vector from (III87). Using

$$\pounds_\beta \gamma_{ij} = D_i\beta_j + D_j\beta_i = \beta^k \partial_k \gamma_{ij} + \gamma_{ik}\partial_j\beta^k + \gamma_{jk}\partial_i\beta^k \quad , \tag{7}$$

in the coordinate basis gives

$$r\partial_r\beta^\theta + \partial_\theta\left(\frac{\beta^r}{r}\right) = 2\alpha\frac{K^r{}_\theta}{r} \quad , \tag{8}$$

for (3a) and

$$r\partial_r\left(\frac{\beta^r}{r}\right) - \partial_\theta\beta^\theta = \alpha(2K^r{}_r + K^\phi{}_\phi) \quad , \tag{9}$$

from (3b). Note that the extrinsic curvature is used in mixed form throughout our discussion.

Equation (8) and (9) form a first order system for the two shift components. This system is elliptic as can be shown by calculating the *symbol* of the differential operator. We take $\partial_r \to k_r$ and $\frac{1}{r}\partial_\theta \to k_\theta$ to replace derivatives in (8) and (9) giving a symbol matrix operating on β^i. The determinant

$$\det \begin{bmatrix} k_r & -k_\theta \\ k_\theta & k_r \end{bmatrix} = k_r^2 + k_\theta^2 \geq 0 \quad , \tag{10}$$

is positive (nonvanishing is sufficient) for all nonvanishing k^i, indicating that the system admits no real characteristics. We will consider at a later point how this system is to be solved for the shift vector.

This gauge, giving three-metric (6), is called quasi-isotropic because in static spherical symmetry it reduces to the isotropic coordinates for Schwarzschild geometry. It has also been referred to as the *isothermal* gauge.[1-3] There appears to be one other two component choice for the three-metric with these symmetries.[3] The *radial* gauge, which reduces to Schwarzschild coordinates, has been recommended by Bardeen and Piran.[3-5] Gauge conditions of this type were first considered, in this context, by Wilson and Smarr.[2,6] An earlier version[6] of this work used the quasi-isotropic

form of the metric but in topological cylindrical coordinates. Wilson and Dykema[1] examined several other choices, radial-cylindrical and radial-spherical polar, before settling on the current gauge: quasi-isotropic-spherical polar. As pointed out by Wilson,[6] the use of cylindrical coordinates is satisfactory for core bounce calculations but very zone inefficient if a black hole forms. This is due to the "grid-sucking" effect produced by use of these gauges when a hole forms.[7] Spherical polar coordinates are much better numerically suited in this regard.

The connection associated with (6) is

$$\Gamma^r_{rr} = \frac{1}{A}\partial_r A \quad , \qquad \Gamma^r_{r\theta} = \Gamma^r_{\theta r} = \frac{1}{A}\partial_\theta A \quad ,$$

$$\Gamma^r_{\theta\theta} = -\frac{r}{A}\partial_r(Ar) \quad , \qquad \Gamma^r_{\phi\phi} = -\frac{Br}{A^2}\sin^2\theta\,\partial_r(Br) \quad ,$$

$$\Gamma^\theta_{rr} = -\frac{1}{Ar^2}\partial_\theta A \quad , \qquad \Gamma^\theta_{r\theta} = \Gamma^\theta_{\theta r} = \frac{1}{Ar}\partial_r(Ar) \quad ,$$

$$\Gamma^\theta_{\theta\theta} = \frac{1}{A}\partial_\theta A \quad , \qquad \Gamma^\theta_{\phi\phi} = -\frac{B\sin\theta}{A^2}\partial_\theta(B\sin\theta) \quad ,$$

$$\Gamma^\phi_{r\phi} = \Gamma^\phi_{\phi r} = \frac{1}{Br}\partial_r(Br) \quad , \qquad \Gamma^\phi_{\theta\phi} = \Gamma^\phi_{\phi\theta} = \frac{1}{B\sin\theta}\partial_\theta(B\sin\theta) \quad , \tag{11}$$

where all other coefficients vanish. The orthonormal and coordinate Riemann tensor components are

$$R^{\hat{r}}{}_{\hat{\theta}\hat{r}\hat{\theta}} = R^{r\theta}{}_{r\theta} = -\frac{1}{A^2_r}\left\{\partial_r\left[\frac{1}{A}\partial_r(Ar)\right] + \frac{1}{r}\partial_\theta\left[\frac{1}{A}\partial_\theta A\right]\right\} \quad ,$$

$$R^{\hat{r}}{}_{\hat{\phi}\hat{r}\hat{\phi}} = R^{r\phi}{}_{r\phi} = -\frac{1}{ABr}\left\{\partial_r\left[\frac{1}{A}\partial_r(Br)\right] + \frac{1}{A^2 r\sin\theta}(\partial_\theta A)\cdot\partial_\theta(B\sin\theta)\right\} \quad ,$$

$$R^{\hat{\theta}}{}_{\hat{\phi}\hat{\theta}\hat{\phi}} = R^{\theta\phi}{}_{\theta\phi} = -\frac{1}{ABr^2\sin\theta}\left\{\partial_\theta\left[\frac{1}{A}\partial_\theta(B\sin\theta)\right] + \frac{\sin\theta}{A^2}\partial_r(Br)\cdot\partial_r(Ar)\right\} \quad ,$$

$$R^{\hat{r}}{}_{\hat{\theta}\hat{\theta}\hat{\phi}} = \frac{1}{r}R^{r\phi}{}_{\theta\phi} = -\frac{1}{ABr^2\sin\theta}\left\{\partial_\theta\left[\frac{\sin\theta}{A}\partial_r(Br)\right] - \frac{1}{A^2}\partial_r(Ar)\cdot\partial_\theta(B\sin\theta)\right\} \quad , \tag{12}$$

with others found from algebraic symmetry. The Ricci tensor becomes

$$R^{r}{}_{r} = -\frac{1}{A^2_r}\left\{\partial_r\left[\frac{1}{A}\partial_r(Ar)\right] + \frac{1}{r}\partial_\theta\left[\frac{1}{A}\partial_\theta A\right]\right\}$$

$$- \frac{1}{ABr}\left\{\partial_r\left[\frac{1}{A}\partial_r(Br)\right] + \frac{1}{A^2 r\sin\theta}(\partial_\theta A)\cdot\partial_\theta(B\sin\theta)\right\} \quad ,$$

$$R^{\theta}{}_{\theta} = -\frac{1}{A^2_r}\left\{\partial_r\left[\frac{1}{A}\partial_r(Ar)\right] + \frac{1}{ABr}\partial_r(Br)\cdot\partial_r(Ar)\right\}$$

$$- \frac{1}{A^2_r}\left\{\frac{1}{A}\partial_\theta\left[\frac{1}{A}\partial_\theta A\right] + \frac{1}{B\sin\theta}\partial_\theta\left|\frac{1}{A}\partial_\theta(B\sin\theta)\right|\right\} \quad ,$$

$$R^{\phi}{}_{\phi} = -\frac{1}{A^2B^2r^2}\left\{\partial_r\left[r\partial_r(Br)\right] + \frac{1}{\sin\theta}\partial_\theta{}^2(B\sin\theta)\right\} \quad ,$$

$$R^{r}{}_{\theta} = -\frac{1}{ABr\sin\theta}\left\{\partial_\theta\left[\frac{\sin\theta}{A}\partial_r(Br)\right] - \frac{1}{A^2}\partial_r(Ar)\cdot\partial_\theta(B\sin\theta)\right\} \quad , \tag{13}$$

giving the Ricci scalar

$$R = -\frac{2}{A^2_r}\left\{\partial_r\left[\frac{r}{A}\partial_r A\right] + \frac{1}{r}\partial_\theta\left[\frac{1}{A}\partial_\theta A\right]\right\}$$

$$- \frac{2}{A^2B^2r^2}\left\{\partial_r\left[r\partial_r(Br)\right] + \frac{1}{\sin\theta}\partial_\theta{}^2(B\sin\theta)\right\} \quad . \tag{14}$$

Armed with the orthonormal curvature components (12), we can now examine the boundary conditions and regularity of the metric functions (6) on the symmetry axis. From examination of (12), for $R^{\hat{r}}{}_{\hat{\phi}\hat{r}\hat{\phi}}$ to be finite across the axis requires A to be an even function there:

$$\partial_\theta A = 0 \quad . \tag{15}$$

Similarly $R^{\hat{\theta}}{}_{\hat{\phi}\hat{\theta}\hat{\phi}}$ leads to the same condition on B at $\theta = 0, \pi$. The component $R^{\hat{r}}{}_{\hat{\phi}\hat{\theta}\hat{\phi}}$ taken along $\theta = 0$ gives

$$R^{\hat{r}}{}_{\hat{\phi}\hat{\theta}\hat{\phi}} \to \frac{1}{A^2B^2r}\cot\theta\,\partial_r\,\ell n\left(\frac{A}{B}\right) \quad , \tag{16}$$

so, for the metric to be regular, requires $\frac{A}{B}$ = constant on axis. From (6), for our gauge to go over to isotropic coordinates in spherical symmetry and asymptotically to spherical polar coordinates necessitates

$$\frac{A}{B} = 1 \quad , \qquad \text{for} \qquad \theta = 0, \pi \quad . \tag{17}$$

Reflection symmetry across $\theta = \frac{\pi}{2}$ requires

$$\partial_\theta A = \partial_\theta B = 0 \quad , \tag{18}$$

there. Reflection symmetry of the metric ($\theta \to \frac{\pi}{2} - \theta$) combined with axisymmetry, $\phi \to \phi + \pi$, is equivalent to isometry under $r \to -r$. So at the origin, in order for $R^{\hat{r}}{}_{\hat{\theta}\hat{r}\hat{\theta}}$ and $R^{\hat{r}}{}_{\hat{\phi}\hat{r}\hat{\phi}}$ to be finite, we have

$$\partial_r A = \partial_r B = 0 \quad . \tag{19}$$

These considerations lead to the recognition of

$$T = \frac{A}{B} \quad , \tag{20}$$

as an alternate metric variable with the important property that T = 1 everywhere is spherical symmetry from (17). Therefore, ℓnT can be used as a measure of the anisotropy of space and the deviation from spherical symmetry.

We define the conformal factor ϕ, a second alternate metric variable, by demanding the condition (III50) on the conformally related metric. This gives

$$\phi^6 = A^2B \quad , \tag{21}$$

since

$$\gamma^{\frac{1}{2}} = A^2Br^2\sin\theta \quad . \tag{22}$$

These definitions allow the metric (6) to be rewritten as

$$\gamma_{ij} = \phi^4 \, \mathrm{diag}(T^{2/3}, T^{2/3}r^2, T^{-4/3}r^2\sin^2\theta) = \phi^4\hat{\gamma}_{ij} \quad , \tag{23}$$

with ϕ and T satisfying the same symmetry conditions as A and B, with the additional knowledge that T = 1 for $\theta = 0, \pi$ and $r = 0$.

With the definition (21) for the conformal factor, the conformally related metric $\hat{\gamma}_{ij}$ (23) satisfies (III50), since

$$\det(\hat{\gamma}_{ij}) = r^2\sin\theta \quad . \tag{24}$$

Therefore (III43), which is one of the assumptions necessary to associate the monopole part of ϕ with the energy, holds.

Our simplifying three-gauge conditions have reduced the metric down to two functions. One, ϕ, gives the scale of the three-geometry and is determined by the Hamiltonian constraint (III22). The other, T, is the single variable entering the conformally related metric $\hat{\gamma}_{ij}$ (23) and represents the single dynamical degree of freedom operative in our problem. (If rotation had been allowed, the metric, of necessity, would contain an off-diagonal component representing the second polarization state.) Since ℓnT provides a measure of the deviation of $\hat{\gamma}_{ij}$ relative to f_{ij}, we might expect it to have nice properties as a radiative variable. That this is the case is shown later when the radiation flux indicators are considered.

b) Time Slicing, Extrinsic Curvature, and Field Evolution

We now turn to the implications of the choice for the remaining kinematical freedom: the time slicing. We employ the maximal slicing condition described in Chapter III. The condition K = 0 allows one of the diagonal components of $K^i{}_j$ to be eliminated:

$$K^\theta{}_\theta = -K^r{}_r - K^\phi{}_\phi \quad . \tag{25}$$

The only remaining independent components are $K^r{}_r$, $K^\phi{}_\phi$, and $K^r{}_\theta$. Using (25), the first order momentum constraints (III12) become

$$\frac{1}{r^3}\partial_r(r^3\hat{K}^r{}_r) + \hat{K}^\phi{}_\phi\cdot\partial_r\,\ell nT + \frac{1}{r^2\sin\theta}\partial_\theta(\sin\theta\hat{K}^r{}_\theta) = \hat{S}_r \quad , \qquad (26a)$$

$$-\frac{1}{\sin\theta}\partial_\theta(\sin\theta\hat{K}^r{}_r) - \frac{T}{\sin^2\theta}\partial_\theta\left(\frac{\sin^2\theta}{T}\hat{K}^\phi{}_\phi\right) + \frac{1}{r^2}\partial_r(r^2\hat{K}^r{}_\theta) = \hat{S}_\theta \ . \qquad (26b)$$

Here we have also employed (III18), $S_\phi = 0$, and make no distinction between $A^i{}_j$ and $K^i{}_j$ since $K = 0$. Examination of (26a) leads to the condition

$$K^r{}_\theta = 0 \ , \qquad \text{for} \qquad \theta = 0, \pi \ , \qquad (27)$$

for regularity on the axis. In fact, axisymmetry implies isometry under $\theta \to -\theta$ *at* $\theta = 0$ leading to the vanishing of any tensor component on axis having an odd number of θ indices. Such components are odd functions across the axis. With $K^r{}_\theta$ odd, equation (26a) implies S_r, $K^r{}_r$, $K^\phi{}_\phi$ are even functions across the axis. Evaluation of (26b) requires $K^r{}_r$ and $K^\phi{}_\phi$ to be differentiable at $\theta = 0, \pi$. Hence

$$\partial_\theta K^r{}_r = \partial_\theta K^\phi{}_\phi = \partial_\theta S_r = 0 \ , \qquad (28)$$

for $\theta = 0, \pi$.

Consideration of (26b) results in a second condition as well:

$$\lambda \equiv K^r{}_r + 2K^\phi{}_\phi = 0 \qquad \text{for} \qquad \theta = 0, \pi \ . \qquad (29)$$

Since this new variable vanishes on axis, it vanishes identically in spherical symmetry, even though $K^r{}_r$ and $K^\phi{}_\phi$ do not typically.

Therefore, λ shares this feature with ℓnT and, we will show, it has similar good properties in describing gravitational radiation.

The conditions resulting from equatorial plane reflection symmetry follow in like fashion:

$$K^r{}_\theta = S_\theta = 0 \qquad \text{at} \qquad \theta = \frac{\pi}{2} \ , \qquad (30)$$

and

$$\partial_\theta K^r{}_r = \partial_\theta K^\phi{}_\phi = \partial_\theta\lambda = \partial_\theta S_r = 0 \qquad \text{at} \qquad \theta = \frac{\pi}{2} \ . \qquad (31)$$

The symmetry conditions at the origin will be considered momentarily.

The new variable λ is adopted in place of $K^r{}_r$ in most of what follows. Hence, the rewritten momentum constraints (26a,b) are

$$-\frac{2T^{1/2}}{r^2}\partial_r\left[\frac{r^3}{T^{1/2}}\hat{K}^\phi{}_\phi\right] + \frac{1}{\sin\theta}\partial_\theta\left(\sin\theta\,\frac{\hat{K}^r{}_\theta}{r}\right) = r\hat{S}_r - \frac{1}{r^2}\partial_r(r^3\hat{\lambda}) \ , \qquad (32a)$$

$$\frac{1}{T}\partial_\theta(T\hat{K}^\phi{}_\phi) + \frac{1}{r^2}\partial_r\left(r^3\cdot\frac{\hat{K}^r{}_\theta}{r}\right) = \hat{S}_\theta + \frac{1}{\sin\theta}\partial_\theta(\sin\theta\,\hat{\lambda}) \ . \qquad (32b)$$

However, as we discussed in Chapter III, these constraints are not solved in first order form.

The evolution equations for the metric, (II77,78) and (III60,61) can be evaluated:

$$\partial_t(\phi^6) = \frac{1}{r^2}\partial_r\left[r^2\phi^6\beta^r\right] + \frac{1}{\sin\theta}\partial_\theta\left[\sin\theta\phi^6\beta^\theta\right] \ , \qquad (33)$$

$$\partial_t\,\ell nT = \beta^r\partial_r\,\ell nT + \beta^\theta\partial_\theta\,\ell nT + \partial_\theta\beta^\theta - \beta^\theta\cot\theta + \alpha\lambda \ , \qquad (34)$$

and

$$\partial_t A = \beta^r \partial_r A + \beta^\theta \partial_\theta A + A\partial_r \beta^r - \alpha A(\lambda - 2K^\phi{}_\phi) \quad , \tag{35}$$

$$\partial_t B = \beta^r \partial_r B + \beta^\theta \partial_\theta B + B\left(\frac{\beta^r}{r}\right) + B\beta^\theta \cot\theta - \alpha B K^\phi{}_\phi \quad . \tag{36}$$

We note that the right-hand-side of (33) is in *divergence form* from (III60) and that the right-hand-side of (34) contains only λ from the extrinsic curvature. The latter again indicates that λ and ℓnT are related in a fairly deep fashion. We have given the evolution equations for both metric components, as well as their alternate forms, for completeness even though with the fully constrained approach only (34) need be evolved.

The evolution equations for the mixed form of the extrinsic curvature (II78) are

$$\begin{aligned}\partial_t K^r{}_r = {} & \beta^r \partial_r K^r{}_r + \beta^\theta \partial_\theta K^r{}_r - \tfrac{1}{2}\alpha(\rho + \rho\varepsilon - p) - S_r(V^r + \beta^r) \\ & + \alpha R^r{}_r - \frac{1}{A}\partial_r\left[\frac{1}{A}\partial_r\alpha\right] - \frac{1}{A^3 r^2}(\partial_\theta A)(\partial_\theta \alpha) \\ & + \frac{K^r{}_\theta}{r}\left[r\partial_r\beta^\theta - \partial_\theta\left(\frac{\beta^r}{r}\right)\right] \quad ,\end{aligned} \tag{37}$$

$$\begin{aligned}\partial_t K^\phi{}_\phi = {} & \beta^r \partial_r K^\phi{}_\phi + \beta^\theta \partial_\theta K^\phi{}_\phi - \tfrac{1}{2}\alpha(\rho + \rho\varepsilon - p) + \alpha R^\phi{}_\phi \\ & - \frac{1}{A^2 Br}\partial_r(Br)\partial_r\alpha - \frac{1}{A^2 Br^2 \sin\theta}\partial_\theta(B\sin\theta)\cdot\partial_\theta\alpha \quad ,\end{aligned} \tag{38}$$

$$\begin{aligned}\partial_t K^r{}_\theta = {} & \beta^r \partial_r K^r{}_\theta + \beta^\theta \partial_\theta K^r{}_\theta - S_\theta(V^r + \beta^r) + \alpha R^r{}_\theta \\ & + K^r{}_\theta(\partial_\theta\beta^\theta - \partial_r\beta^r) + (2K^r{}_r + K^\phi{}_\phi)\partial_\theta\beta^r \\ & - \frac{1}{A}\partial_\theta\left[\frac{1}{A}\partial_r\alpha\right] + \frac{1}{A^3 r}\partial_r(Ar)\cdot\partial_\theta\alpha \quad ,\end{aligned} \tag{39}$$

where we have retained momentarily the component $K^r{}_r$. In (37) - (39), the energy densities and stresses follow from (II81,84-86,90) and could, alternatively, be given by D and E (II99). The equation for $K^\theta{}_\theta$ is superfluous from (25) and is not given here (see however Dykema[1]).

Combining (37) and (38) with the definition (29) of λ and using (33) allows us to write an equation for the conformally related λ, $\hat{\lambda} = \phi^6\lambda$:

$$\begin{aligned}\partial_t\hat{\lambda} = {} & \frac{1}{r^2}\partial_r(r^2\beta^r\hat{\lambda}) + \frac{1}{\sin\theta}\partial_\theta(\sin\theta\beta^\theta\hat{\lambda}) + \frac{\alpha B S^2{}_\theta}{r^2(\rho + \rho\varepsilon + p)U^2} \\ & + \frac{\hat{K}^r{}_\theta}{r}\left[r\partial_r\beta^\theta - \partial_\theta\left(\frac{\beta^r}{r}\right)\right] + \frac{1}{r^2}\partial_r[\alpha B r^2 \partial_r\, \ell nT] \\ & + \frac{AB^2\sin\theta}{r^2}\partial_\theta\left[\frac{1}{AB\sin\theta}\partial_\theta\alpha\right] + \frac{\alpha B^2\sin\theta}{r^2}\partial_\theta\left[\frac{1}{AB\sin\theta}\partial_\theta A\right] \quad .\end{aligned} \tag{40}$$

Again, if the fully constrained approach is adopted, (40) is the only evolution equation for the extrinsic curvature that need be employed. In (37) - (40), we have used whichever metric variables provide the simplest expressions. The terms in the right-hand-side of (40) have

been carefully chosen so that each vanishes separately in spherical symmetry. This is an important consideration in numerical applications.

The maximal slicing condition results in the linear elliptic equation (III78) for the lapse, which reduces in our model to

$$\frac{1}{r^2}\partial_r(Br^2\partial_r\alpha) + \frac{1}{r^2\sin\theta}\partial_\theta(B\sin\theta\partial_\theta\alpha)$$
$$= \alpha\phi^6\left\{2\lambda^2 - 6\lambda K^\phi{}_\phi + 6K^\phi{}_\phi{}^2 + 2\left(\frac{K^r{}_\theta}{r}\right)^2\right.$$
$$\left. + (\rho + \rho\varepsilon)(U^2 - \tfrac{1}{2}) + p(U^2 + \tfrac{1}{2})\right\} \quad . \qquad (41)$$

Here, the reductions (II84,90) and (25) have been employed. The symmetry boundary conditions for α across the axis and equator and at the origin are the same as those for A and B. We defer until later, when the lapse equation is written in a different form, the question of an asymptotic boundary condition for α.

c) Regularity

Before discussing the constraints and the initial value equations, we first consider *regularity*. By regular, we mean here that a scalar or tensor is sufficiently differentiable at each point in the manifold *in locally cartesian coordinates*. To avoid discussing degrees of continuity, we simply take regular tensors to mean those whose cartesian components are analytic, i.e. expandable in a Taylor series in the neighborhood of each point. We define as our cartesian

coordinates those related to our gauge by

$$x = r\cos\phi\sin\theta \ , \quad y = r\sin\phi\sin\theta \ , \quad z = r\cos\theta \quad . \qquad (42)$$

The idea is first to express the tensor components in the cartesian system as Taylor series in (x,y,z) and eliminate certain coefficients in the series by enforcing the symmetry conditions, then to transform back to spherical polar coordinates to uncover the functional dependence near the singular points, $r = 0$ and $\theta = 0$, of the coordinate system.

We first examine scalars. Upon application of the symmetry conditions, a scalar, b, is expandable in powers of $\rho^2 = x^2 + y^2 = r^2\sin^2\theta$ and $z^2 = r^2\cos^2\theta$, or,

$$b = b(\rho^2, z^2) \quad . \qquad (43)$$

We refer to such a function as being an *even* function. Use of these even functions will form the basis for considering higher rank tensors. Note in particular that from (II7) the lapse, a scalar, is of the form (43).

We consider vectors next. Each cartesian component is Taylor expanded about $r = 0$. Axisymmetry and vanishing rotation require $W^\phi = 0$, so transforming,

$$W^\phi = 0 = -\frac{1}{r\sin\theta}[\sin\phi W^x - \cos\phi W^y] \quad , \qquad (44)$$

shows W^x and W^y related by $yW^x = xW^y$. Upon reflection, it is clear

that the general form of W^i, consistent with the symmetries, is

$$W^x = xf_1(\rho^2,z^2) \ , \quad W^y = yf_1(\rho^2,z^2) \ , \quad W^z = zf_2(\rho^2,z^2) \ . \qquad (45)$$

As expected there are only two independent components. The spherical polar components become

$$W^r = r(\sin^2\theta f_1 + \cos^2\theta f_2) \ , \quad W^\theta = \sin\theta\cos\theta(f_1 - f_2) \ , \qquad (46)$$

after transforming (45). Note that $\frac{W^r}{r}$ and W^θ typically have angular dependence at the point $r = 0$. This is an example of the peculiar functional behavior in tensor components due to the coordinate singularity at the origin of spherical polar coordinates. A numerically generated example of this multi-valued behavior at $r = 0$ is shown in Figure 1a,b.

Axisymmetry and vanishing rotation imply $T_{r\phi} = T_{\theta\phi} = 0$ for a second rank tensor T_{ij}. If we transform these to cartesian components we obtain

$$rT_{r\phi} = 0 = (x^2 - y^2)T_{xy} - xy(T_{xx} - T_{yy}) + z[xT_{yz} - yT_{xz}] \ , \qquad (47)$$

$$T_{\theta\phi} = 0 = z[xy(T_{yy} - T_{xx}) + (x^2 - y^2)T_{xy}] + (x^2 + y^2)[yT_{xz} - xT_{yz}] \ . \qquad (48)$$

Figures 1a,b. The local behavior near $r = 0$ for $\frac{W^r}{r}$ is shown in Figure 1a. This is a projected plot of the functional surface, represented by the numerical mesh, over the polar coordinate quadrant. The equatorial plane is to the left; the symmetry axis to the right. The multivalued behavior $a + b\cos2\theta$, with a and b constants, is evident at $r = 0$. Figure 1b gives the local appearance of W^θ near $r = 0$. W^θ behaves like $-2b\sin\theta\cos\theta$ at $r = 0$.

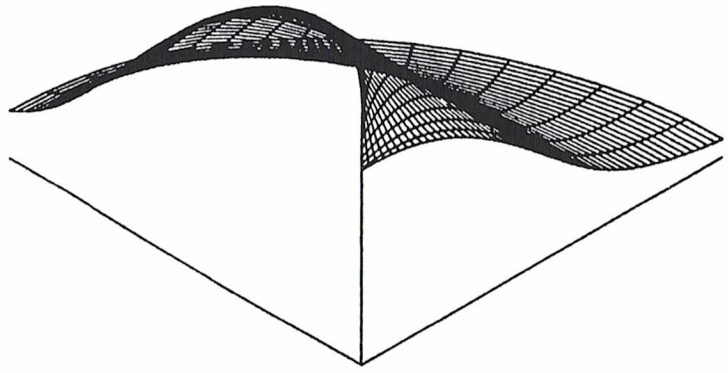

Figure 1a

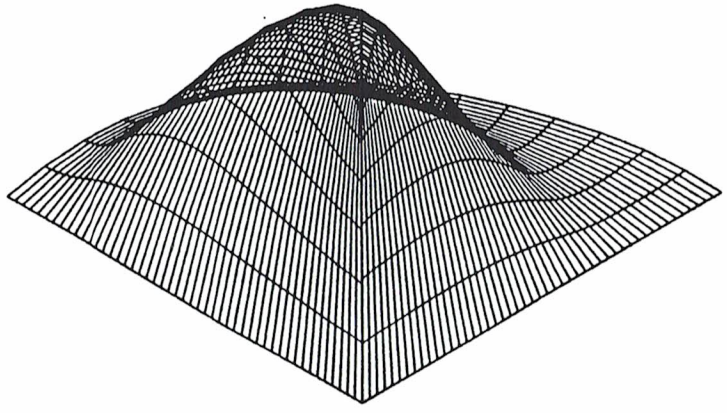

Figure 1b

Only one of these is needed to show that the cartesian coordinate tensor has the general form in the vicinity of the origin,

$$T_{xx} = g_1(\rho^2,z^2) + g_3(\rho^2,z^2)\, x^2 \quad , \tag{49a}$$

$$T_{yy} = g_1(\rho^2,z^2) + g_3(\rho^2,z^2)\, y^2 \quad , \tag{49b}$$

$$T_{zz} = g_2(\rho^2,z^2) \quad , \tag{49c}$$

$$T_{xy} = g_3(\rho^2,z^2)\, xy \quad , \tag{49d}$$

$$T_{xz} = g_4(\rho^2,z^2)\, xz \quad , \tag{49e}$$

$$T_{yz} = g_4(\rho^2,z^2)\, yz \quad , \tag{49f}$$

if it is to satisfy the symmetries. We recover four independent functions. Transforming back to spherical polar coordinates gives

$$T_{rr} = g_1\sin^2\theta + g_2\cos^2\theta + g_3 r^2\sin^4\theta + 2g_4 r^2\cos^2\theta\sin^2\theta \quad , \tag{50a}$$

$$T_{\theta\theta} = r^2(g_1\cos^2\theta + g_2\sin^2\theta) + (g_3 - 2g_4)r^4\cos^2\theta\sin^2\theta \quad , \tag{50b}$$

$$T_{\phi\phi} = g_1 r^2\sin^2\theta \quad , \tag{50c}$$

$$T_{r\theta} = (g_1 - g_2 + g_3 r^2\sin^2\theta + g_4 r^2\cos 2\theta)\, r\cos\theta\sin\theta \quad . \tag{50d}$$

This latter form can be used to reexamine the regularity of the metric components A and B. Before using (50a-d) however, we note that our gauge conditions (3) and (4) interrelate the functions, $g_{(i)}$. Applying (3) and (4) to (50a-d) gives

$$g_4 = 0 \ , \qquad \text{and} \qquad g_3 r^2 \sin^2\theta = g_2 - g_1 \ . \tag{51}$$

These, in turn, lead to the consistent identification of

$$A^2 = g_2 \ , \qquad B^2 = g_1 \ , \tag{52}$$

and the immediate demonstration of regularity of our quasi-isotropic gauge. The alternate variable T has the form

$$T^2 - 1 = \rho^2 \frac{g_3}{g_1} \ , \tag{53}$$

found from (51) and (52). Provided $\lim_{r \to 0} g_1 \neq 0$, which would otherwise produce a pathology in the metric, then

$$T = 1 + g_5 r^2 \sin^2\theta \ , \tag{54}$$

is also regular, where $g_1 g_5 (g_5 \rho^2 + 2) = g_3$.

Finally, let us apply equations (50a-d) to the extrinsic curvature. We first convert these equations to mixed form,

$$K^r{}_r = h_1 \sin^2\theta + h_2 \cos^2\theta + h_3 r^2 \sin^4\theta + 2h_4 r^2 \cos^2\theta \sin^2\theta \ , \tag{55a}$$

$$K^\theta{}_\theta = h_1 \cos^2\theta + h_2 \sin^2\theta + (h_3 - 2h_4) r^2 \cos^2\theta \sin^2\theta \ , \tag{55b}$$

$$K^\phi{}_\phi = h_1 T^2 \ , \tag{55c}$$

$$K^r{}_\theta = [h_1 (T^2 + 2) + 2h_3 r^2 \sin^2\theta + h_4 r^2 \cos 2\theta] r \cos\theta \sin\theta \ , \tag{55d}$$

where A^2 has been absorbed into the definition of $h_{(i)}$. The time

slicing condition will typically interrelate these components. Applying the maximal slicing condition, K = 0, leads to the elimination of one even function in terms of the others:

$$h_2 = -h_1 (T^2 + 1) - h_3 r^2 \sin^2\theta \ . \tag{56}$$

The right-hand-side is separately made up of even, analytic functions, so we conclude that maximal slicing is consistent with regularity.

Consider, instead, the polar time slicing condition (III79). This leads to

$$h_2 \sin^2\theta + h_1 (1 + \cos^2\theta) \ . \tag{57}$$

The explicit angular dependence appearing above cannot be written in terms of an expansion in ρ^2 and z^2. Hence this gauge produces an *irregular* extrinsic curvature at r = 0. The lapse function determined by this gauge will be irregular as well.[3]

Making use of the maximal slicing condition (56) alters only $K^r{}_r$ in (55):

$$K^r{}_r = -h_1 (\cos 2\theta + T^2 \cos^2\theta) - h_3 r^2 \sin^2\theta \cos 2\theta + 2h_4 r^2 \cos^2\theta \sin^2\theta \ , \tag{58}$$

and (55b) for $K^\theta{}_\theta$ is superfluous. Combining (58) and (55c) yields

$$\lambda = h_1 [T^2 (2 - \cos^2\theta) - \cos 2\theta] - h_3 r^2 \sin^2\theta \cos 2\theta + 2h_4 r^2 \cos^2\theta \sin^2\theta \ . \tag{59}$$

Considering the components of $K^i{}_j$ as expanded in powers of r^2, the

lowest order radial terms are

$$K^{\phi}{}_{\phi} = h_1{}^{(0)} + \mathcal{O}(r^2) \quad , \tag{60a}$$

$$\lambda = 3h_1{}^{(0)}\sin^2\theta + \mathcal{O}(r^2) \quad , \tag{60b}$$

$$\frac{K^{r}{}_{\theta}}{r} = 3h_1{}^{(0)}\sin\theta\cos\theta + \mathcal{O}(r^2) \quad , \tag{60c}$$

where $h_1{}^{(0)} = \lim_{r \to 0} h_1$ and λ and $K^{r}{}_{\theta}/r$ display angular dependence at the origin (are multivalued). The local behavior near $r = 0$ for λ, $K^{\phi}{}_{\phi}$ and $K^{r}{}_{\theta}/r$ is shown in Figs. 2a,b,c constructed on a finite difference mesh.

d) Constraints and Initial Value Equations

We solve the Hamiltonian constraint in a form somewhat different than that given by (III22). This equation is rewritten so that the solution obtains the variable $\psi \equiv B^{1/2}$ instead of ϕ. The connection between the two quantities is

$$\psi = \phi T^{-1/3} \quad . \tag{61}$$

The reason for this change is that the differential operators involving ψ and T have a simpler form as we will show below.

In retrospect, it would perhaps be better to solve for yet a different variable:

Figures 2a,b,c. The local behavior near $r = 0$ for extrinsic curvature quantities λ, $K^{\phi}{}_{\phi}$, and $K^{r}{}_{\theta}/r$ are shown in Figures 2a,b,c, respectively. In Figure 2a, λ has the multivalued behavior $3a\sin^2\theta$ at $r = 0$. Figure 2b shows $K^{\phi}{}_{\phi}$ to be an analytic function at the origin and it has the value a at $r = 0$ related to λ and $K^{r}{}_{\theta}/r$. The multivalued behavior $3a\sin\theta\cos\theta$ in $K^{r}{}_{\theta}/r$ at the origin is displayed in Figure 2c.

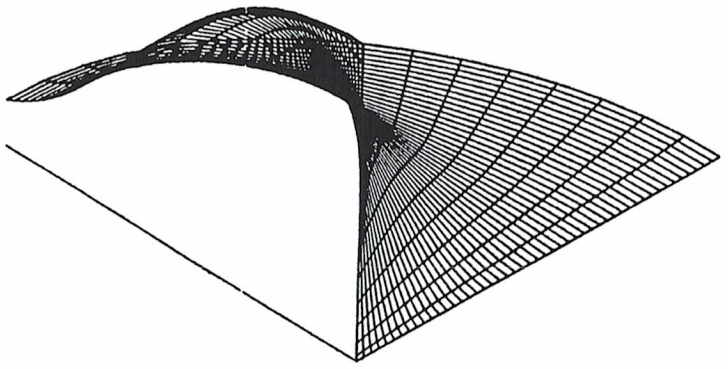

Figure 2a

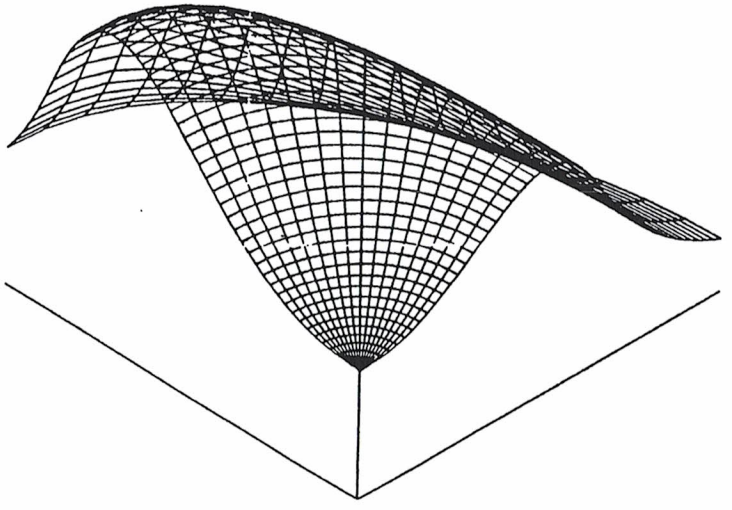

Figure 2b

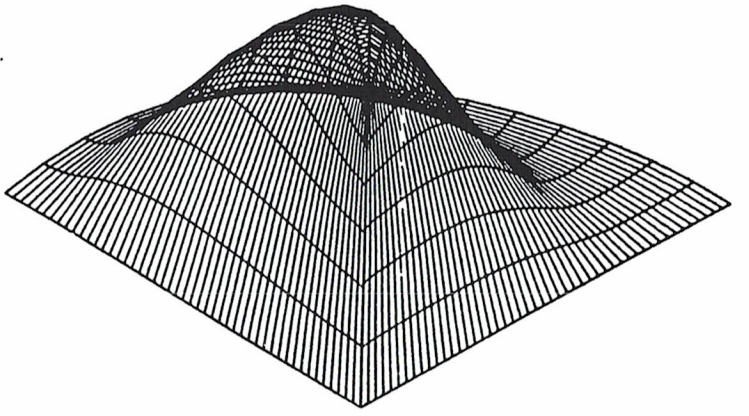

Figure 2c

$$\psi' = (AB)^{1/4} = \phi T^{-1/12} \quad . \tag{62}$$

As the results of Appendix B show, for a weak-field transverse-traceless gravitational wave transformed into our gauge, the combination (62) is the only one linear in the conformal factor *and* for which the wave vanishes to linear order. In contrast, the leading spherical wave term shows up in both ϕ and B. This renders somewhat inaccurate, or complicates, the solution of (III22) when a gravitational wave reaches the edge of the mesh. Our numerical method will likely undergo refinement in this area.

The Hamiltonian constraint equation using (61) is reduced to

$$\begin{aligned} &\frac{1}{r^2}\partial_r(r^2\partial_r\psi) + \frac{1}{r^2\sin\theta}\partial_\theta(\sin\theta\partial_\theta\psi) \\ &= -\frac{1}{4}\psi\Big[\frac{1}{r}\partial_r(r\partial_r\,\ell nT) + \frac{1}{r^2}\partial_\theta\partial_\theta\,\ell nT \\ &\quad + T^{-2}\psi^{-8}\Big(\hat{\lambda}^2 - 3\hat{\lambda}\hat{K}^\phi{}_\phi + 3\hat{K}^\phi{}_\phi{}^2 + \Big(\frac{\hat{K}^r{}_\theta}{r}\Big)^2\Big) \\ &\quad + \psi^{-2}\hat{D}U + T^{2(1-\Gamma)}\,\psi^{4-6\Gamma}\,\hat{E}\Big(\Gamma U + \frac{1-\Gamma}{U}\Big)\Big] \quad , \end{aligned} \tag{63}$$

where, unlike (III20), the rest energy density and internal energy density have separate conformal scalings:

$$D = \phi^{-6}\hat{D} \quad , \tag{64}$$

$$E = \phi^{-6\Gamma}\hat{E} \quad . \tag{65}$$

Here Γ is the adiabatic index (II105) and the scalings (64) and (65) are chosen under the assumption that such an adiabatic equation of state is employed. The reasons for these choices will be more fully discussed as we consider the hydrodynamic equations below. Notice that the use of ψ in (61) has produced flat space three- and two-dimensional Laplacians in (63) operating on ψ and ℓnT, respectively.

When (63) is used in the initial value problem, as was discussed in Chapter III, the terms appearing in the right-hand-side are all freely specifiable data or conformally related quantities. For use on subsequent slices in a fully constrained method, the source terms must follow from the evolution. In either case, once the solution of (63) is obtained, (61) gives ϕ and the physical values can be produced.

The symmetry boundary conditions for ψ are the same as (15), (18), and (19) for A. The physical condition at large radius is the York-Piran[8] Robin condition (III52) applied to ψ

$$\partial_r\psi + \frac{1}{r}(\psi - 1) = 0 \quad , \tag{66}$$

at $r = r_m$. The same condition applies to ψ because the asymptotic expansions of ϕ (III42) and ψ differ only at $\sigma(r^{-2})$. This is demonstrated below in Section IVe.

We now proceed to write down the longitudinal part of the momentum constraints (III25). In our model $W^\phi = S_\phi = 0$, so (III25) yields only two equations for the components W^r and W^θ. These are

$$\frac{4}{3}\frac{1}{r^2}\partial_r\left[r^4\partial_r\left(\frac{W^r}{r}\right)\right] + \frac{1}{\sin\theta}\partial_\theta\left[\sin\theta\left(\frac{W^r}{r}\right)\right] + F_1\left(\frac{W^r}{r}\right)$$

$$+ \frac{2}{3}r^4T\partial_r\left[\frac{1}{r^3T}\partial_\theta W^\theta\right] - \frac{1}{3}T^2r\sin\theta\partial_\theta\left[\frac{1}{T^2\sin\theta}\partial_r W^\theta\right] + F_2W^\theta = r\hat{S}_r \quad , \qquad (67a)$$

$$\frac{1}{r^2}\partial_r\left[r^4\partial_r W^\theta\right] + \frac{4}{3}\frac{1}{\sin\theta}\partial_\theta\left[\sin\theta\partial_\theta W^\theta\right] + F_3W^\theta$$

$$+ \frac{2}{3}rT\partial_\theta\left[\frac{1}{T}\partial_r\left(\frac{W^r}{r}\right)\right] - \frac{1}{3}r^{10}T^2\partial_r\left[\frac{1}{r^9T^2}\partial_\theta\left(\frac{W^r}{r}\right)\right] + F_4\left(\frac{W^r}{r}\right) = \hat{S}_\theta \quad , \qquad (67b)$$

where the functions $F_{(i)}$ are curvature terms:

$$F_1 = \frac{2}{3}\frac{T^2}{r^2}\partial_r\left[\frac{r^4}{T^2}\partial_r \ell nT\right] \quad , \qquad (68a)$$

$$F_2 = \frac{2}{3}r\left[\partial_r\partial_\theta \ell nT + \partial_r \ell n\left(\frac{r^3}{T^2}\right)\cdot\partial_\theta \ell n\left(\frac{T}{\sin\theta}\right)\right] \quad , \qquad (68b)$$

$$F_3 = \frac{2}{3}\frac{T^2}{\sin^3\theta}\partial_\theta\left[\frac{\sin^3\theta}{T^2}\partial_\theta \ell n\left(\frac{T}{\sin\theta}\right)\right] \quad , \qquad (68c)$$

$$F_4 = \frac{2}{3}r\frac{T^2}{\sin^3\theta}\partial_\theta\left[\frac{\sin^3\theta}{T^2}\partial_r \ell nT\right] \quad . \qquad (68d)$$

The symmetry boundary conditions for W^i derive from consideration of (46). We see that both components satisfy

$$\partial_r\left(\frac{W^r}{r}\right) = \partial_r W^\theta = 0 \quad , \qquad (69)$$

at $r = 0$. In addition, W^r is an even function across the axis and equator,

$$\partial_\theta W^r = 0 \ , \qquad \text{for} \qquad \theta = 0, \frac{\pi}{2} \quad , \qquad (70)$$

and W^θ is odd,

$$W^\theta = 0 \ , \qquad \text{for} \qquad \theta = 0, \frac{\pi}{2} \quad . \qquad (71)$$

These conditions on $\frac{W^r}{r}$ and W^θ hold even though both are multivalued at the origin (46). The boundary condition applied at large, but finite r is the (approximate) Dirichlet condition (III36,39) discussed before. In our model the symmetric moment tensor D_{ij} has only two independent components. We form from these two linear combinations, D_0 and D_2, as shown in Appendix A. These are related to the trace part and tracefree part of D_{ij}, respectively. In sufficiently special circumstances (Chapter III, Appendix B), these can be related to the decomposition of the time rate of change of the second moment of the mass distribution. These are given by the integrals

$$D_0 = -\int_0^{r_0}\int_0^{\pi/2} dr\, d\theta \sin\theta r^3 \hat{S}_r \quad , \qquad (72)$$

$$D_2 = -\int_0^{r_0}\int_0^{\pi/2} dr\, d\theta \sin\theta(\sin^2\theta - 2\cos^2\theta)r^3 \hat{S}_r$$

$$- 3\int_0^{r_0}\int_0^{\pi/2} dr\, d\theta \cos\theta\sin^2\theta\, r^2\hat{S}_\theta \quad , \qquad (73)$$

where r_0 encompasses the support of S_i. The Dirichlet condition (III36) at large $r = r_m$ then becomes

$$\left(\frac{W^r}{r}\right)_{r_m} = \frac{1}{8r_m^3}\left[(2D_0 - 3D_2) + \frac{9}{2}D_2\sin^2\theta\right] \quad , \qquad (74)$$

$$(W^\theta)_{r_m} = \frac{3}{8r_m^3} D_2 \sin\theta\cos\theta \quad . \tag{75}$$

These moments and boundary values are shown derived from (III36,39) in Appendix A and the longitudinal contributions to other parts of the gravitational field are shown. Once the solution for the vector potential has been obtained, equation (III15) gives the conformally related, longitudinal components of $K^i{}_j$:

$$\hat{\lambda}_L = -2r\left(\frac{W^r}{r}\right)\cdot\partial_r \ell nT - 2\frac{\sin\theta}{T}\partial_\theta\left(\frac{T}{\sin\theta}W^\theta\right) \quad , \tag{76}$$

$$\hat{K}_L{}^\phi{}_\phi = -\frac{2}{3}\frac{r}{T^2}\partial_r\left[T^2\left(\frac{W^r}{r}\right)\right] - \frac{2}{3}\frac{\sin^2\theta}{T^2}\partial_\theta\left[\frac{T^2}{\sin^2\theta}W^\theta\right] \quad , \tag{77}$$

$$\frac{1}{r}\hat{K}^r{}_{L\theta} = r\partial_r W^\theta + \partial_\theta\left(\frac{W^r}{r}\right) \quad . \tag{78}$$

If only the solution of the IVP is desired, i.e. if an unconstrained approach to the extrinsic curvature evolution is adopted, then the solution of (67a,b) and (76) - (78) suffices to produce a physically reasonable initial $\hat{K}^i{}_j$ leading to a small initial radiation content, when the free data is taken to be $\hat{K}_T{}^i{}_j = 0$ and $\hat{\gamma}_{ij} = f_{ij}$. In modelling stellar core collapse, however, we typically attempt to pick up the collapse just prior to the relativistic regime or to the bounce phase. What is missing in this approach to the initial data is a way to input the small, but noticeable amount of radiation that would have been produced during the infall prior to this time. This is likely to be a fruitful area for further work.

If (67a,b) and (76) - (78) are to be used in the fully constrained approach to the extrinsic curvature, then the second step is to find the transverse part of $\hat{K}^i{}_j$. Use of the longitudinal part from (76) - (78) then allows the entire extrinsic curvature to be reconstructed on each successive slice. Since $\hat{\lambda}$ is evolved using (40), the longitudinal result (76) can be used to calculate the transverse part of $\hat{\lambda}$, $\hat{\lambda}_T = \hat{\lambda} - \hat{\lambda}_L$. This then serves as the source with which to solve (III68) for the remaining two transverse components $\hat{K}_T{}^\phi{}_\phi$ and $\hat{K}_T{}^r{}_\theta$. Then (77) and (78) give the entire $\hat{K}^i{}_j$ on the new slice.

The second-order tensor Laplacian can be reduced to a pair of coupled equations for $\hat{K}_T{}^\phi{}_\phi$ and $\hat{K}_T{}^r{}_\theta$ by taking the (r,r) and (r,θ) components of (III68):

$$\begin{aligned} &4T^{2/3}\partial_r\left[\frac{r^2}{T^{2/3}}\partial_r\hat{K}_T{}^\phi{}_\phi\right] + \frac{T^{2/3}}{\sin\theta}\partial_\theta\left[\frac{\sin\theta}{T^{2/3}}\partial_\theta\hat{K}_T{}^\phi{}_\phi\right] + G_1\hat{K}_T{}^\phi{}_\phi \\ &- \frac{r}{T^{5/3}\sin\theta}\partial_\theta\left[\sin\theta T^{5/3}\partial_r\left(\frac{\hat{K}^r{}_{T\theta}}{r}\right)\right] + \left(7 + \frac{r}{3T}\partial_r T\right)\partial_\theta\left(\frac{\hat{K}^r{}_{T\theta}}{r}\right) + G_2\left(\frac{\hat{K}^r{}_{T\theta}}{r}\right) \\ &= 2T^{1/6}\partial_r\left[\frac{r^2}{T^{1/6}}\partial_r\hat{\lambda}_T\right] + \frac{T^{5/3}}{\sin^2\theta}\partial_\theta\left[\frac{\sin^2\theta}{T^{5/3}}\partial_\theta\hat{\lambda}_T\right] + G_3\hat{\lambda}_T \quad , \end{aligned} \tag{79a}$$

$$T^{2/3}\partial_r\left[\frac{r^2}{T^{2/3}}\partial_r\left(\frac{\hat{K}^r{}_{T\theta}}{r}\right)\right] + \frac{T^{2/3}}{\sin\theta}\partial_\theta\left[\frac{\sin\theta}{T^{2/3}}\partial_\theta\left(\frac{\hat{K}^r{}_{T\theta}}{r}\right)\right] + G_4\left(\frac{\hat{K}^r{}_{T\theta}}{r}\right)$$

$$- T^{7/3}r\partial_\theta\left[T^{-7/3}\partial_r\hat{K}_T{}^\phi{}_\phi\right] + \left(-8 + \frac{r}{3T}\partial_r T\right)\partial_\theta\hat{K}_T{}^\phi{}_\phi + G_5\hat{K}_T{}^\phi{}_\phi$$

$$= \frac{r}{T^{2/3}\sin\theta}\partial_\theta(\sin\theta T^{2/3})\cdot\partial_r\hat{\lambda}_T - \left(5 + \frac{2r}{3T}\partial_r T\right)\cdot\partial_\theta\hat{\lambda}_T + G_6\hat{\lambda}_T \quad . \tag{79b}$$

Here $\hat{\lambda}_T$ acts as the source and the functions $G_{(i)}$ are

$$G_1 = 12r^3T^{1/6}\partial_r\left[\frac{1}{r^2}\partial_r\left(\frac{r}{T^{1/6}}\right)\right] + \frac{T^{5/3}}{\sin\theta}\partial_\theta\left[\frac{\sin\theta}{T^{8/3}}\partial_\theta T\right] \quad , \tag{80a}$$

$$G_2 = \left(7 + \frac{r}{3T}\partial_r T\right)\cot\theta - \frac{5}{T}\partial_\theta T \quad , \tag{80b}$$

$$G_3 = -\frac{6}{rT^{1/6}}\partial_r\left[r^2T^{1/6}\right] + \frac{T^{5/3}}{\sin\theta}\partial_\theta\left[\frac{\cos\theta}{T^{5/3}}\right] \quad , \tag{80c}$$

$$G_4 = -\frac{6}{T^{1/3}}\partial_r\left[rT^{1/3}\right] + T^{2/3}\partial_\theta\left[\frac{\cot\theta}{T^{2/3}}\right] \quad , \tag{80d}$$

$$G_5 = r^3T^{2/3}\partial_r\left[\frac{1}{r^2T^{5/3}}\partial_\theta T\right] - \frac{3T^{2/3}}{r}\partial_\theta\left[\frac{1}{T^{1/3}}\partial_r\left(\frac{r^2}{T^{1/3}}\right)\right] \quad , \tag{80e}$$

$$G_6 = \frac{2}{T}\partial_\theta T - 2\frac{\cot\theta}{T^{1/3}}\partial_r\left[rT^{1/3}\right] \quad . \tag{80f}$$

The symmetry conditions for this elliptic system comes from (55c,d). These imply that

$$\partial_r K^\phi{}_\phi = \partial_r\left(\frac{K^r{}_\theta}{r}\right) = 0 \quad , \tag{81}$$

at $r = 0$, that $K^\phi{}_\phi$ is even, so

$$\partial_\theta K^\phi{}_\phi = 0 \quad , \qquad \text{for} \qquad \theta = 0, \frac{\pi}{2} \quad , \tag{82}$$

and that $K^r{}_\theta$ is odd,

$$K^r{}_\theta = 0 \quad , \qquad \text{for} \qquad \theta = 0, \frac{\pi}{2} \quad . \tag{83}$$

Both λ and $K^r{}_\theta/r$ are multivalued at the origin from (60b,c) while $K^\phi{}_\phi$ is single-valued and analytic (60a). This latter point forms an important test of the *numerical regularity* of the finite difference equations used for (79a,b) and (80a,f). This will be an important topic of Chapter V.

The asymptotic boundary condition for $\hat{K}_T{}^i{}_j$ is the radiation, or transverse condition (III14). At large radii this can be replaced by

$$n_i\hat{K}_T{}^i{}_j = 0 \quad , \tag{84}$$

where n_i is the outward directed coordinate two-sphere normal. This produces the conditions

$$\hat{K}_T{}^\phi{}_\phi = \frac{1}{2}\hat{\lambda}_T \quad , \tag{85}$$

$$\frac{\hat{K}^r{}_{T\theta}}{r} = \mathcal{O}(r^{-2}) \quad , \tag{86}$$

which result when $\omega r >> 1$, where ω is the characteristic frequency. Asymptotically, (85) and (86) can be verified by the structure of the

radiation field in our gauge displayed in Appendix B. Alternatively, these results can be used to improve the boundary values applied to (79a,b).

e) Shift and Lapse Revisited

The numerical treatment of elliptic systems is generally simpler in terms of second order equations which admit iterative numerical solution algorithms. Hence to solve the first order system (8) and (9) for the shift vector, potentials χ and Φ are introduced by

$$\frac{\beta^r}{r} = r\partial_r\chi + \partial_\theta\Phi \quad , \tag{87a}$$

$$\beta^\theta = r\partial_r\Phi - \partial_\theta\chi \quad . \tag{87b}$$

Writing the right-hand-sides appearing in (8) and (9) as

$$P = \alpha(2\lambda - 3K^\Phi{}_\Phi) \quad , \tag{88a}$$

$$Q = 2\alpha \frac{K^r{}_\theta}{r} \quad , \tag{88b}$$

and using (87a,b) produces the second order equations

$$\Delta_2^{(f)}\chi = r^{-2} P \quad , \tag{89a}$$

$$\Delta_2^{(f)}\Phi = r^{-2} Q \quad , \tag{89b}$$

where $\Delta_2^{(f)} = r^{-1}\partial_r(r\partial_r) + r^{-2}\partial_\theta\partial_\theta$ is the flat space two-dimensional Laplacian. The potentials have decoupled in (89a,b). The behavior of P and Q near r = 0 can be found from (60a-c):

$$P = -3\alpha^{(0)}h_1{}^{(0)} \cos 2\theta + \mathcal{O}(r^2) \quad , \tag{90a}$$

$$Q = 6\alpha^{(0)}h_1{}^{(0)} \sin\theta\cos\theta + \mathcal{O}(r^2) \quad . \tag{90b}$$

Despite the singular nature of the sources (89a,b) implied by (90a,b), solutions appear obtainable (we have not proven existence, except through direct numerical construction).

The local behavior of the source (90a,b) implies the shift vector components satisfy locally

$$\frac{\beta^r}{r} = a + 3\alpha^{(0)}h_1{}^{(0)} \sin^2\theta + \mathcal{O}(r^2) \quad , \tag{91a}$$

$$\beta^\theta = 3\alpha^{(0)}h_1{}^{(0)} \sin\theta\cos\theta + \mathcal{O}(r^2) \quad . \tag{91b}$$

Here $\alpha^{(0)} = \lim_{r \to 0} \alpha$. This multivalued dependence is completely consistent with the expected form (46) of a regular vector field near r = 0. The constant a is only determined once the global integration of (8) and (9) is performed. The definitions (87a,b) for the potentials then give a local dependence for χ and Φ of

$$\chi = \left(a + \frac{3}{2}\alpha^{(0)}h_1{}^{(0)}\right) \ell nr + \frac{3}{4}\alpha^{(0)}h_1{}^{(0)} \cos 2\theta + \mathcal{O}(r^2) \quad , \tag{92a}$$

$$\Phi = -\frac{3}{2}\alpha^{(0)}h_1{}^{(0)} \sin\theta\cos\theta + \mathcal{O}(r^2) \quad , \tag{92b}$$

with similar multivaluedness and a singularity in χ. This singularity is, however, in a potential, with no intrinsic physical meaning. Provided the numerical treatment of this term is appropriately careful, we see nothing to impede the solution of (89a,b). The reason for using potentials of the form (87a,b) is that, not only do the potentials separate in the resulting equations (89a,b), but the flat space two-dimensional Laplacians allow the second order equations to be decomposed with the finite Fourier transform. This makes possible a very fast numerical solution (see Chapter V).

Symmetry considerations show that χ is an even angular function,

$$\partial_\theta \chi = 0 \ , \qquad \text{at} \qquad \theta = 0, \frac{\pi}{2} \ , \tag{93}$$

and that Φ is odd,

$$\Phi = 0 \ , \qquad \text{at} \qquad \theta = 0, \frac{\pi}{2} \ . \tag{94}$$

Assuming the singular ($\ell n r$) part of χ is removed, leaving $\chi_{(reg)}$, the radial boundary conditions are

$$\partial_r \chi_{(reg)} = \partial_r \Phi = 0 \ , \qquad \text{at} \qquad r = 0 \ . \tag{95}$$

Again, the details of how this is accomplished are dealt with in Chapter V as a numerical technique.

We next consider the asymptotic form of the shift and, in turn, the potentials χ and Φ. First, since $K^i{}_j$ is the source for

(8) and (9), the dominant longitudinal asymptotic term (III36) in the extrinsic curvature $\sigma(r^{-3})$ shows up in β^i also at $\sigma(r^{-3})$:

$$\left(\frac{\beta^r}{r}\right)_L = \frac{1}{r^3}\left[\left(\frac{1}{2} D_0 - \frac{3}{4} D_2\right) + \frac{9}{8} D_2 \sin^2\theta\right] \ , \tag{96a}$$

$$\beta^\theta{}_L = \frac{3}{4r^3} D_2 \sin\theta\cos\theta \ , \tag{96b}$$

in terms of the moments D_0 and D_2 (72), (73). The corresponding behavior in χ and Φ is

$$\chi_L = \frac{1}{r^3}\left[\left(-\frac{1}{6} D_0 + \frac{1}{4} D_2\right) - \frac{3}{8} D_2 \sin^2\theta\right] \ , \tag{97a}$$

$$\Phi_L = \sigma(r^{-4}) \ . \tag{97b}$$

However, (96a,b) is not the dominant asymptotic part of β^i. Rather, we note that the operator for the system (8) and (9) admits homogeneous solutions, which vanish at infinity, of the form

$$\frac{\beta^r}{r} = \dot{n}_m(t) \frac{\cos m\theta}{r^m} \ , \qquad \beta^\theta = -\dot{n}_m(t) \frac{\sin m\theta}{r^m} \ . \tag{98}$$

With the required angular symmetries on the shift, a lowest order *gauge* term multipole of the form

$$\frac{\beta^r}{r} = \dot{n}_2(t) \frac{\cos 2\theta}{r^2} \ , \qquad \beta^\theta = -\dot{n}_2(t) \frac{\sin 2\theta}{r^2} \ , \tag{99}$$

can be excited by the sources P and Q.

Before considering how this term is calculated, we first show its effect on the asymptotic structure of the rest of the gravitational field. It is assumed in what follows that all radii considered are beyond any gravitational wavefronts, so that only gauge and longitudinal dependence is present in the field. Hence, we have $K^i{}_j = \mathcal{O}(r^{-3})$ and the evolution equations (35) and (36) give

$$\partial_t \ell n A = - \dot{\eta}_2(t) \frac{1}{r^2} \cos 2\theta + \mathcal{O}(r^{-3}) \quad , \tag{100}$$

$$\partial_t \ell n B = - \dot{\eta}_2(t) \frac{1}{r^2} + \mathcal{O}(r^{-3}) \quad . \tag{101}$$

Integrating we find

$$A = 1 + \frac{M}{r} + \frac{1}{r^2}\left(\frac{1}{4} M^2 - \eta_2 \cos 2\theta\right) + \mathcal{O}(r^{-3}) \quad , \tag{102}$$

$$B = 1 + \frac{M}{r} + \frac{1}{r^2}\left(\frac{1}{4} M^2 - \eta_2\right) + \mathcal{O}(r^{-3}) \quad , \tag{103}$$

where the static terms (constants of integration) are chosen to match static isotropic coordinates. From the definitions (20) and (21), we in turn find asymptotically

$$\phi = 1 + \frac{M}{2r} - \frac{\eta_2}{6r^2}(1 + 2\cos 2\theta) + \mathcal{O}(r^{-3}) \quad , \tag{104}$$

$$T = 1 + 2\eta_2 \frac{1}{r^2} \sin^2\theta + \mathcal{O}(r^{-3}) \quad . \tag{105}$$

Note that the monopole term does not arise in T (105). We can see in

(104) that the conformal factor actually has a static monopole term, apparently related to the mass. Indeed, we will show below that the dependence in T (105) indicates that condition (III49) is satisfied, guaranteeing the interpretation made in (III42). This gauge piece, produced by η_2, shows up as an immediate correction to the metric at the next order of $\frac{M}{r}$. For precise measurements of mass and energy flux, it is likely that this term will have to be taken into account.

To obtain $\dot{\eta}_2(t)$, we see that (89a,b) allow separate homogeneous solutions of the form

$$\chi = \sigma_m^{(1)} \frac{\cos m\theta}{r^m} \quad , \tag{106}$$

$$\Phi = \sigma_m^{(2)} \frac{\sin m\theta}{r^m} \quad . \tag{107}$$

Combining these in the definitions of the potentials (87a,b) gives

$$\dot{\eta}_m = m(\sigma_m^{(2)} - \sigma_{\dot{m}}^{(1)}) \quad . \tag{108}$$

The Greens function for $\Delta_2^{(f)}$ in (89a,b) in polar coordinates is

$$g(x - x') = \frac{1}{2\pi} \ell n r - \frac{1}{2\pi} \sum_{m=1}^{\infty} \frac{1}{m} \left(\frac{r'}{r}\right)^m \cos[m(\theta - \theta')] \quad , \tag{109}$$

for $r > r'$. This splits into even and odd angular parts

$$g_{even}(x - x') = \frac{1}{2\pi} \ell n r - \frac{1}{2\pi} \sum_{\text{even } m}^{\infty} \frac{1}{m} \left(\frac{r'}{r}\right)^m \cos m\theta \cos m\theta' \quad , \tag{110}$$

$$g_{odd}(x - x') = \frac{1}{2\pi} \sum_{even\ m}^{\infty} \frac{1}{m} \left(\frac{r'}{r}\right)^m \sin m\theta \sin m\theta' \quad , \qquad (111)$$

using $\cos[m(\theta - \theta')] = \cos m\theta \cos m\theta' + \sin m\theta \sin m\theta'$. The expansions of the Greens functions, (110) and (111), can be used in integral solutions of (89a,b)

$$\chi = \int dr'\, d\theta' r' \frac{P'}{r'^2} \left[\frac{1}{2\pi} \ell nr - \frac{1}{2\pi} \sum_{even\ m}^{\infty} \frac{1}{m} \left(\frac{r'}{r}\right)^m \cos m\theta \cos m\theta'\right] \quad , (112)$$

$$\Phi = \int dr'\, d\theta' r' \frac{Q'}{r'^2} \left(\frac{1}{2\pi}\right) \sum_{even\ m}^{\infty} \frac{1}{m} \left(\frac{r'}{r}\right)^m \sin m\theta \sin m\theta' \quad , \qquad (113)$$

to obtain multipole solutions for χ and Φ. However, P and Q will not have compact support and so, for sufficiently large m, the radial integrals will diverge (the solution is no longer a vacuum multipole moment). Since $K^i{}_j = \mathcal{O}(r^{-3})$, with the same dependence for P and Q, the integrals converge for $m \leq 2$. But this is sufficient to calculate $\dot{\eta}_2$ and hence using (106) - (108), (112), and (113)

$$\dot{\eta}_2 = \frac{1}{2\pi} \int dr'\, d\theta' r' \left[\cos 2\theta' \cdot \alpha \cdot (2\lambda - 3K^{\phi}{}_{\phi}) + \sin 2\theta' \cdot 2\alpha \frac{K^r{}_{\theta}}{r'}\right] \quad . \qquad (114)$$

Since P and Q do not have finite support, if the radial integration in (114) extends from $r' = 0$ to $r' = r$, r some large but finite radius, the result will be in error by an $\mathcal{O}(r^{-1})$ residual.

Note that had we relaxed the equatorial plane symmetry requirement, the $m = 1$ multipole would *no* longer be ruled out by angular symmetry. From (98), this would lead to an asymptotic shift

vector dependence

$$\zeta_1{}^{(j)}{}_{\beta}{}^{i} = \mathcal{O}(1) \quad , \qquad (115)$$

in violation of the assumptions (III57). This may either indicate the quasi-isotropic gauge is inappropriate for systems with mass dipole moments and axial linear momentum *or* that we have neglected terms, in writing these solutions, in previously applying equatorial plane symmetry.

The ℓnr part of (112) is related to the singular part of χ already described (92a). How this is handled is discussed in Chapter V.

We have indicated previously that we use a different form of the lapse equation than (41). This new equation is found by combining (41) and the Hamiltonian constraint equation (63). After some amount of calculation, we find

$$\frac{1}{r^2} \partial_r\left[r^2 \partial_r(\alpha\psi)\right] + \frac{1}{r^2 \sin\theta} \partial_{\theta}\left[\sin\theta \partial_{\theta}(\alpha\psi)\right]$$

$$= \frac{1}{4} \alpha\psi\left[-\frac{1}{r} \partial_r(r \partial_r\, \ell nT) - \frac{1}{r^2} \partial_{\theta}\partial_{\theta}\, \ell nT\right.$$

$$+ A^2\left\{7\left[\lambda^2 - 3\lambda K^{\phi}{}_{\phi} + 3K^{\phi}{}_{\phi}{}^2 + \left(\frac{K^r{}_{\theta}}{r}\right)^2\right]\right.$$

$$\left.\left. + (\rho + \rho\varepsilon)(3U^2 - 2) + p(3U^2 + 3)\right\}\right] \quad , \qquad (116)$$

which is an equation for $\alpha\psi = \alpha B^{\frac{1}{2}}$. This equation for the lapse is used in our code. Again the reason for this choice (116) is the simple flat space form of the three-dimensional Laplacian.

The symmetry conditions on $\alpha B^{1/2}$ are the same as mentioned before for α. With the lowest order gauge dependence in B (103) and T (105) known, we can examine the asymptotic form of the lapse. Using (105), we find

$$\Delta_2^{(f)}\, \ell n T = 4\eta_2 \frac{1}{r^4} + \mathcal{O}(r^{-5}) \quad , \tag{117}$$

for the source term in (116). The other source terms in (116) are $\mathcal{O}(r^{-6})$ or less. Then, taking as an *ansatz* the expression

$$\alpha B^{1/2} = 1 + \frac{a}{r} + \frac{b}{r^2} + \mathcal{O}(r^{-3}) \quad , \tag{118}$$

we find

$$b = -\frac{1}{2}\eta_2 \quad , \tag{119}$$

and the monopole term is, of course, a homogeneous solution. Then using (103) gives

$$B^{-1/2} = 1 - \frac{M}{2r} + \frac{1}{r^2}\left(\frac{1}{4}M^2 + \frac{1}{2}\eta_2\right) \quad , \tag{120}$$

and substituting in (118) implies $a = -\frac{M}{2}$ to give the correct monopole term in α and hence we obtain,

$$\alpha = 1 - \frac{M}{r} + \frac{M^2}{2r^2} \quad , \tag{121}$$

which is consistent with the first two leading terms for the lapse in static isotropic coordinates. We see that for maximal slicing the

asymptotic form of α is insensitive to both the gauge terms in lowest order and, as shown in Appendix B, to the gravitational wave to linear order. The boundary condition on $\alpha B^{1/2}$ can be taken from

$$\alpha B = 1 - \frac{1}{r^2}\left(\frac{1}{4}M^2 + \eta_2\right) \quad , \tag{122}$$

which is the form eliminating the explicit appearance of the monopole term.

f) Hydrodynamics

The inviscid hydrodynamic equations (II101-103) can now be obtained in our gauge. The equation for rest mass conservation (II101) is

$$\partial_t(\phi^6 D) + \frac{1}{r^2}\partial_r(r^2\phi^6 D V^r) + \frac{1}{\sin\theta}\partial_\theta(\sin\theta\phi^6 D V^\theta) = 0 \quad . \tag{123}$$

where $\gamma^{1/2} = \phi^6 r^2 \sin\theta$ is used. The internal energy equation (II102) can also be immediately written down,

$$\partial_t(\phi^6 E) + \frac{1}{r^2}\partial_r(r^2\phi^6 E V^r) + \frac{1}{\sin\theta}\partial_\theta(\sin\theta\phi^6 E V^\theta)$$
$$= -p\left[\partial_t(\phi^6 U) + \frac{1}{r^2}\partial_r(r^2\phi^6 U V^r) + \frac{1}{\sin\theta}\partial_\theta(\sin\theta\phi^6 U V^\theta)\right] \quad . \tag{124}$$

In order to write the momentum transport equations, (II103), the coordinate and gravitational acceleration terms, $U_a U_b \partial_j(g^{ab})$, must be evaluated. These two components are

$$\frac{1}{2} U_a U_b \partial_r(g^{ab}) = U^2 \partial_r \ell n\alpha + (1 - U^2)\partial_r \ell nA - \frac{U^2_\theta}{A^2 r^3}$$

$$- \frac{U}{\alpha} (U_r \partial_r \beta^r + U_\theta \partial_r \beta^\theta) \quad , \tag{125}$$

$$\frac{1}{2} U_a U_b \partial_\theta(g^{ab}) = U^2 \partial_\theta \ell n\alpha + (1 - U^2)\partial_\theta \ell nA$$

$$- \frac{U}{\alpha} (U_r \partial_\theta \beta^r + U_\theta \partial_\theta \beta^\theta) \quad . \tag{126}$$

With these, equations (II103) become

$$\partial_t(\phi^6 S_r) + \frac{1}{r^2} \partial_r(r^2 \phi^6 S_r V^r) + \frac{1}{\sin\theta} \partial_\theta(\sin\theta \phi^6 S_r V^\theta)$$

$$= -\alpha\phi^6 \Big[\partial_r p + (D + E + pU)(U\partial_r \ell n\alpha + (\frac{1}{U} - U)\partial_r \ell nA)$$

$$- \frac{S_\theta^2}{(D + E + pU) U r^3 A^2} \Big] + \phi^6 (S_r \partial_r \beta^r + S_\theta \partial_r \beta^\theta) \quad , \tag{127}$$

$$\partial_t(\phi^6 S_\theta) + \frac{1}{r^2} \partial_r(r^2 \phi^6 S_\theta V^r) + \frac{1}{\sin\theta} \partial_\theta(\sin\theta \phi^6 S_\theta V^\theta)$$

$$= -\alpha\phi^6 \Big[\partial_\theta p + (D + E + pU)(U\partial_\theta \ell n\alpha + (\frac{1}{U} - U)\partial_\theta \ell nA) \Big]$$

$$+ \phi^6 (S_r \partial_\theta \beta^r + S_\theta \partial_\theta \beta^\theta) \quad , \tag{128}$$

where in (123) - (128) we use the definitions (II99,100). The implicit equation (II104) for U becomes

$$A^2 (D + E + pU)^2 (U^2 - 1) = S_r^2 + \frac{1}{r^2} S_\theta^2 \quad . \tag{129}$$

The transport terms in equations (123), (127) and (128) are in the form of the divergence of a flux. This allows these terms to be conservatively differenced (see Dykema[1]). The implication in the case of equation (123) is that the total particle number

$$\int dr\, d\theta r^2 \sin\theta \phi^6 D = \text{constant} \quad , \tag{130}$$

can be globally conserved throughout a numerical evolution. This identifies the natural conformal scaling for the rest energy density

$$\hat{D} = \phi^6 D \quad , \tag{131}$$

shown before (64). Equations (127) and (128) in the same way strongly suggest using

$$\hat{S}_i = \phi^6 S_i \quad , \tag{132}$$

which has already been chosen (III18) in any case in order to help decouple the constraints (III22,23).

The internal energy equation (124) is handled differently. Since E appears implicitly through the pressure, p, we cannot preserve E as was done with D in (130). However, we note[1] that with an adiabatic equation of state

$$pU = (\Gamma - 1)E \quad , \tag{133}$$

equation (124) can be rewritten in the conservative form

$$\partial_t(\phi^6 E^{1/\Gamma} U^{1-1/\Gamma}) + \frac{1}{r^2}\partial_r(r^2\phi^6 E^{1/\Gamma} U^{1-1/\Gamma} V^r)$$

$$+ \frac{1}{\sin\theta}\partial_\theta(\sin\theta\phi^6 E^{1/\Gamma} U^{1-1/\Gamma} V^\theta) = 0 \quad , \tag{134}$$

in the absence of shocks. Where shocks are present, an artificial viscosity (Dykema[1]) is added in the numerical algorithm, altering (134). As we did before, the conservative form (134) indicates the natural conformal transformation of E to be

$$\hat{E} = \phi^{6\Gamma} E \quad , \tag{135}$$

which was used before (65) as the scaling in the Hamiltonian constraint. The combination of the scalings (131) and (135) help to maintain motion along the adiabat in regions free of shocks by enforcing (III10) under compression. This is the source of the separate power law scalings for D and E.

To complete the specification of the hydrodynamic equations we need to give the expressions for the coordinate velocity components V^r and V^θ. These are

$$V^r = \frac{\alpha}{A^2}\frac{S_r}{(D + E + pU)U} - \beta^r \quad , \tag{136}$$

$$V^\theta = \frac{\alpha}{A^2 r^2}\frac{S_\theta}{(D + E + pU)U} - \beta^\theta \quad . \tag{137}$$

g) Mass and Flux Indicators

We next consider the form of the mass and flux indicators, described in general terms in Chapter III (Appendix A), in our gauge and with the assumed symmetries. As was discussed in Chapter III, several assumptions are necessary for the validity of the simplified ADM mass integral (IIIA7) written in terms of the conformal factor. The first, (III43), depends upon the definition of the conformal splitting (III1) of the metric. Our choice of defining ϕ and $\hat{\gamma}_{ij}$, (21) and (24), is sufficient to guarantee (III43). The second condition (III49) is related to the choice of spatial coordinates on Σ_0, but the gauge conditions that are used must also maintain (III49) in time. Using the definition (6) of the metric, (III41) and (III48) we find the tracefree part of γ_{ij} is

$$\psi^i{}_j = \frac{1}{3}(A^2 - B^2)\mathrm{diag}[1,1,-2] \quad . \tag{138}$$

So $\psi^i{}_j$ is uniquely characterized by $(A^2 - B^2)$. This reduces to

$$A^2 - B^2 = B^2(T^2 - 1) = \phi^4 T^{-4/3}(T + 1)(T - 1) \quad ,$$

$$= 2\,\ell n T[1 + \mathcal{O}(r^{-1})] \quad , \tag{139}$$

and using (105),

$$A^2 - B^2 = 4\eta_2 \frac{1}{r^2}\sin^2\theta + \mathcal{O}(r^{-3}) \quad . \tag{140}$$

Equations (138) and (140) then imply the maintenance of (III49).

Hence, the ADM mass integral (IIIA7) can be written as

$$M_{ADM} = - \lim_{r \to \infty} \int d\theta \, r^2 \sin\theta \, AB \, \partial_r \phi \quad , \tag{141}$$

so that (141) expresses the gravitational mass (this differs from (IIIA7) by a factor 8π due to our choice of units.) Since in our numerical calculations the mass-energy must be evaluated on a finite radius mesh, we can expect the integral in (141), expressed as $M_A(r)$, to differ from M_{ADM} asymptotically by terms of order $\mathcal{O}(r^{-1})$. Fortunately, the analysis of the gauge effects in Section IVe allows the next order correction terms to be explicitly calculated.

Using (102) and (103), we obtain

$$AB = 1 + \frac{2M}{r} + \frac{1}{r^2}\left[\frac{3}{2}M^2 - \eta_2 - \eta_2 \cos 2\theta\right] + \mathcal{O}(r^{-3}) \quad , \tag{142}$$

which is expressed in terms of the gravitational mass as well. Calculating $\partial_r \phi$ from (104) and substituting (142) in (141) gives

$$M_A(r) = M\left[1 + \frac{1}{r}\left(2M - \frac{2}{9}\frac{\eta_2}{M}\right)\right] \quad , \tag{143}$$

to lowest order. In the limit

$$\lim_{r \to \infty} M_A(r) = M = M_{ADM} \quad . \tag{144}$$

Hence, errors in using (141) at finite radius are formally of order $\frac{M}{r}$. It should be possible to correct the finite radius result of (141)

to calculate M accurate to order $\frac{M^2}{r^2}$. This might be accomplished by explicitly integrating (115) for $\dot{\eta}_2$ and time integrating to produce η_2 to be used in (143). Conversely, one might consider evaluating (IIIA7) on a different coordinate two-sphere related by an asymptotic infinitesimal gauge transformation. The idea would be to use some *geometric* condition in constructing the new two-surface which eliminates to lowest order the built-up distortion, η_2, resulting from our quasi-isotropic gauge. These issues are under active consideration.

In order to express the Hawking mass (IIIA11) in our gauge and with our symmetries, the Newman-Penrose coefficients (IIIA12, A13) must be evaluated. These have been calculated by Dykema[1]:

$$\mu = -\bar{m}^a m^b \nabla_b k_a = \frac{1}{4}\left[\frac{1}{A^2 B r^2}\partial_r(r^2 AB) - K^r{}_r\right] \quad , \tag{145}$$

$$\rho = m^a \bar{m}^b \nabla_b \ell_a = \frac{1}{2}\left[\frac{1}{A^2 B r^2}\partial_r(r^2 AB) + K^r{}_r\right] \quad , \tag{146}$$

and we note that in axisymmetry the Newman-Penrose coefficients are all real. Equations (145) and (146) when combined give

$$\mu\rho = \frac{1}{8}\left\{\frac{1}{A^2}\left[\partial_r \ell n(r^2 AB)\right]^2 - K^r{}_r{}^2\right\} \quad , \tag{147}$$

which can be used in (IIIA11) for the Hawking mass,

$$M_H(r) = \left[\frac{A(r)}{16\pi}\right]^{\frac{1}{2}}\left(1 - \int \frac{dA}{2\pi}\mu\rho\right) \quad . \tag{148}$$

Here the gravitational mass is calculated by (148) and

$$A(r) = \int dA = \int d\Omega\, r^2 AB \qquad (149)$$

is used in (148).

In the same way as with the ADM mass above, the lowest order gauge effects in $M_H(r)$ can be derived. From (145) and (146), we see that

$$\mu = \frac{1}{2}\rho + \mathcal{O}(r^{-3}) \quad . \qquad (150)$$

Using (142) and (102) we obtain

$$\rho = \frac{1}{r}\left[1 - \frac{2M}{r} + \frac{1}{r^2}\left(\frac{21}{4}M^2 + 3\eta_2 - 4\eta_2 \sin^2\theta\right) + \mathcal{O}(r^{-3})\right] \quad , \qquad (151)$$

which used with (150) in (148), after some calculation, gives

$$M_H(r) = M\left[1 - \frac{3M}{r}\right] \quad , \qquad (152)$$

for the deviations at finite r from the ADM mass at I^0. Interestingly the Hawking mass suffers only a static (constant) lowest order correction.

The Bondi-Sachs flux (IIIA14) uses the Newman-Penrose coefficient[1] (IIIA15):

$$\lambda' = -\bar{m}^a \bar{m}^b \nabla_b k_a = \frac{1}{4}\left[\frac{1}{A}\partial_r \ell n T - \lambda\right] \quad , \qquad (153)$$

here expressed in our variables. This asymptotically gives the Bondi news function and the outgoing waveform at future null infinity, I^+. The flux becomes

$$\frac{dM_H}{du} = -\frac{1}{64\pi}\int d\Omega\, r^2 AB\left[\frac{1}{A}\partial_r \ell n T - \lambda\right]^2 \quad , \qquad (154)$$

giving a negative rate of change of the configuration mass if the outgoing waves are nonvanishing. Note the very clear appearance of the components $\ell n T$ and λ which we chose as our dynamical variables in the fully constrained, simplifying gauge approach.

The calculation of the Bondi-Sachs flux (154) at a finite radius will result in an approximate value for the radiated mass-energy. Asymptotically vanishing correction terms to (154) will exist. These will include for example corrections to the spherical wave, due to measuring at a finite distance into the wave zone, of order $\mathcal{O}\left(\frac{\lambda}{r}\right)$ where λ is a characteristic wavelength. We can also expect gauge terms due to the appearance of η_2 in (102), (103) and (105). At the time of this writing, these terms have not yet been calculated, though, this surely can be done using the results of Section IVe and Appendix B.

Examination of the results of Appendix B shows that (154) responds only to the outgoing wave amplitude (r^{-1} part). Appendix B also indicates, that using the simplifying gauge conditions, $\ell n T$ is asymptotically directly related to the usual transverse-traceless, weak-field gravitational wave amplitude h_+^{TT} by

$$\ell nT = h_+^{TT} + \sigma(r^{-2}) \quad . \tag{155}$$

This can be used to derive the usual TT radiation flux[10]

$$\frac{dE}{dt} = \frac{1}{16\pi}\int dA\ (\dot{h}_+^{TT})^2 = \frac{1}{16\pi}\int d\Omega\ r^2 AB\ \lambda^2 \quad , \tag{156}$$

using (34). However, as can be verified by reference to Appendix B, equation (156) responds both to outgoing and incoming radiation.

Chapter IV References

1. Dykema (1980).
2. Smarr (1979).
3. Bardeen and Piran (1983).
4. Bardeen (1983).
5. Piran (1983).
6. Wilson (1979).
7. Estabrook et al. (1973).
8. York and Piran (1982).
9. Morse and Feshbach (1953).
10. Misner, Thorne, and Wheeler (1973).
11. Teukolsky (1982).
12. Mathews (1962).
13. Zerilli (1970).
14. Thorne (1980b).

APPENDIX A

We derive here the lowest order asymptotic dependence in the vector potential compatible with our model assumptions. The corresponding longitudinal dependence in the extrinsic curvature is shown as well as the longitudinal effects in other parts of the gravitational field.

Our starting point is the symmetric $\mathcal{O}(r^{-2})$ vacuum multipole solution (III36)

$$W^k = \frac{1}{64\pi r^2}\left[3(n^j\delta^{ki} + n^i\delta^{kj}) - n^k(\delta^{ij} - 3n^in^j)\right]D_{ij} \quad , \qquad (A1)$$

given in asymptotic cartesian coordinates. Under axisymmetry, we have from (49a-f):

$$D_{xy} = D_{xz} = D_{yz} = 0 \quad , \qquad (A2)$$

and

$$D_{xx} = D_{yy} \quad , \qquad (A3)$$

since D_{ij} are constants. This leaves only D_{zz} and D_{xx} independent. The trace of D_{ij} is

$$D_0 = D_{kk} = D_{zz} + 2D_{xx} \quad . \qquad (A4)$$

The tracefree part of D_{ij} is

$$D_{ij} - \frac{1}{3}\delta_{ij}D_0 = 2(D_{xx} - D_{zz})\,\mathrm{diag}\left[\frac{1}{6}, \frac{1}{6}, -\frac{1}{3}\right] \quad , \qquad (A5)$$

and we define a second linear combination

$$D_2 = 2(D_{xx} - D_{zz}) \quad . \qquad (A6)$$

In terms of D_0 and D_2, we have

$$D_{xx} = \frac{1}{6}D_2 + \frac{1}{3}D_0 \quad , \qquad D_{zz} = \frac{1}{3}D_0 - \frac{1}{3}D_2 \quad . \qquad (A7)$$

We also have use for the intermediate result

$$n^in^jD_{ij} = \frac{1}{3}D_0 - \frac{1}{3}D_2\left(\frac{3}{2}\cos^2\theta - \frac{1}{2}\right) \quad ,$$

$$= \frac{1}{3}D_0 - \frac{1}{3}D_2P_2(\theta) \quad , \qquad (A8)$$

appearing in (A1). These result in the cartesian components

$$W^x = \frac{x}{8r^3}\left[2D_0 + D_2(1 - P_2(\theta))\right] \quad , \qquad (A9a)$$

$$W^y = \frac{y}{8r^3}\left[2D_0 + D_2(1 - P_2(\theta))\right] \quad , \qquad (A9b)$$

$$W^z = \frac{z}{8r^3}\left[2D_0 - 2D_2\left[1 + \frac{1}{2}P_2(\theta)\right]\right] \quad . \qquad (A9c)$$

Using the transformation from (45) to (46) we obtain

$$\frac{W^r}{r} = \frac{1}{8r^3}\left[(2D_0 - 3D_2) + \frac{9}{2}D_2\sin^2\theta\right] \quad , \qquad (A10a)$$

$$W^{\theta} = \frac{3}{8r^3} D_2 \sin\theta\cos\theta \quad , \tag{A10b}$$

with $W^{\phi} = 0$. These are the results (74) and (75) given before.

In the same way, if the integrals (III39) are used to approximate the moments D_{ij}, we can express D_0 and D_2 in terms of spherical polar coordinate quantities. Using (42), (45) and (46) produces in (A4) and (A6)

$$D_0 = -\frac{1}{2}\int dr\, d\theta\, r^3 \sin\theta\, \hat{S}_r \quad , \tag{A11}$$

$$D_2 = -\frac{1}{2}\int dr\, d\theta\, r^3 \sin\theta(\sin^2\theta - 2\cos^2\theta)\, \hat{S}_r$$

$$-\frac{3}{2}\int dr\, d\theta\, r^2 \cos\theta \sin^2\theta\, \hat{S}_{\theta} \quad , \tag{A12}$$

which have been given in (72) and (73).

Using (76), (77) and (78), the longitudinal dependence in the extrinsic curvature is found to be

$$\lambda_L = \frac{3}{4r^3} D_2 \sin^2\theta \quad , \tag{A13a}$$

$$K_L{}^{\phi}{}_{\phi} = \frac{1}{r^3}\left[\frac{1}{2}(D_0 - D_2) + \frac{9}{8} D_2 \sin^2\theta\right] \quad , \tag{A13b}$$

$$\frac{K^r{}_{L\theta}}{r} = \mathcal{O}(r^{-4}) \quad , \tag{A13c}$$

from (A10a,b). Here, the longitudinal dependence in $K^r{}_{\theta}/r$ vanishes

at $\mathcal{O}(r^{-3})$. From (A13a,b,c), we can derive the asymptotic longitudinal dependence in the functions P and Q (88a,b) used in the spatial gauge equations (8) and (9). We find

$$P_L = -\frac{1}{r^3}\left[\frac{3}{2}(D_0 - D_2) + \frac{15}{8} D_2 \sin^2\theta\right] \quad , \tag{A14a}$$

$$Q_L = \mathcal{O}(r^{-4}) \quad , \tag{A14b}$$

the latter following from (A13c). The subscripts on P and Q remind us there are only the longitudinal parts of these functions. From the spatial gauge equations (8) and (9), (A14a,b) give the longitudinal part of the shift

$$\left(\frac{\beta^r}{r}\right)_L = \frac{1}{r^3}\left[\left(\frac{1}{2} D_0 - \frac{3}{4} D_2\right) + \frac{9}{8} D_2 \sin^2\theta\right] \quad , \tag{A15a}$$

$$\beta^{\theta}{}_L = \frac{3}{4r^3} D_2 \sin\theta\cos\theta \quad , \tag{A15b}$$

which have previously appeared in (96a,b). With the definitions (87a,b) of the shift potentials, equations (A15a,b) require the asymptotic longitudinal dependence:

$$X_L = \frac{1}{r^3}\left[\left(-\frac{1}{6} D_0 + \frac{1}{4} D_2\right) - \frac{3}{8} D_2 \sin^2\theta\right] \quad , \tag{A16a}$$

$$\Phi_L = \mathcal{O}(r^{-4}) \quad , \tag{A16b}$$

where, again, Φ_L vanishes at $\mathcal{O}(r^{-3})$.

As we have done with the gauge term in Section IVe, the longitudinal effects in the metric can be uncovered by using the evolution equations (33) and (34). We find the longitudinal effects cancel in ℓnT at $\mathcal{O}(r^{-3})$. However, using (33), they do contribute to the conformal factor:

$$\partial_t\left(\phi^6_L\right) = \frac{3}{2r^3} D_2 P_2(\theta) \quad . \tag{A17}$$

Integrating, and using the notation

$$D_2^{(-1)}(t) = \int D_2 \, dt \quad , \tag{A18}$$

for the time integral, gives the longitudinal contribution

$$\phi_L = 1 + \frac{1}{4r^3} D_2^{(-1)} P_2(\theta) \quad . \tag{A19}$$

This is the form of a vacuum *quadrupole* moment and should be expected to appear in ϕ from the analysis of (IIIB16). However, (A19) will not express the total $\mathcal{O}(r^{-3})$ dependence in ϕ, since the static (r^{-1}) and gauge (r^{-2}) terms in (104) will likely mix at order $\mathcal{O}(r^{-3})$.

APPENDIX B

We present here the properties of a weak-field quadrupole gravitational wave in our gauge and which obeys our symmetry conditions. Such an analytic solution is useful both for testing our computer code as well as deriving proper wave boundary conditions. Our starting point is the quadrupole solution to the linearized theory worked out in spherical polar coordinates by Teukolsky.[11] The transverse-traceless gauge, in which the wave is described, has four-metric components, g_{oa},

$$\alpha^{TT} = 1 \, , \qquad \beta_i{}^{TT} = 0 \quad . \tag{B1}$$

With the three-metric perturbation expressed by

$$\gamma_{ij} = f_{ij} + h_{ij} \quad , \tag{B2}$$

with f_{ij} the flat spherical coordinate metric, the spatial metric perturbation satisfies

$$h^k{}_k = 0 \quad , \tag{B3}$$

$$D_i h^{ij} = 0 \quad , \tag{B4}$$

where D_i is the flat space covariant derivative compatible with f_{ij}. The field equations, in vacuum, in the transverse-traceless gauge are

$$D^a D_a h_{ij} = 0 \quad . \tag{B5}$$

In spherical coordinates, h_{ij} is decomposed in terms of *tensor spherical harmonics*.[12-14] For $\ell = 2$ (quadrupole), $m = 0$ (axisymmetric), and even parity (vanishing current modes from no rotation), we have the line element

$$\begin{aligned} ds^2 = &-dt^2 + [1 + (2 - 3\sin^2\theta)G]dr^2 \\ &+ 6Hr\cos\theta\sin\theta\, dr d\theta + [1 + 3\sin^2\theta I - G]\, r^2 d\theta^2 \\ &+ [1 - 3\sin^2\theta I + (3\sin^2\theta - 1)G] r^2 \sin^2\theta d\phi^2 \end{aligned} \tag{B6}$$

where

$$G = 3\left[\frac{F^{(2)}}{r^3} + 3\,\frac{F^{(1)}}{r^4} + 3\,\frac{F}{r^5}\right] \quad , \tag{B7a}$$

$$H = \left[\varepsilon\,\frac{F^{(3)}}{r^2} + 3\,\frac{F^{(2)}}{r^3} + 6\varepsilon\,\frac{F^{(1)}}{r^4} + 6\,\frac{F}{r^5}\right] \quad , \tag{B7b}$$

$$I = \frac{1}{4}\left[\frac{F^{(4)}}{r} + 2\varepsilon\,\frac{F^{(3)}}{r^2} + 9\,\frac{F^{(2)}}{r^3} + 21\varepsilon\,\frac{F^{(1)}}{r^4} + 21\,\frac{F}{r^5}\right] \quad , \tag{B7c}$$

$$F = F(t - \varepsilon r) \ , \qquad F^{(n)} = \frac{d^n F}{dx^n} \quad , \tag{B7d}$$

and where $x = t - \varepsilon r$ and $\varepsilon = +1, -1$ representing outgoing and incoming waves, respectively. $F(t - \varepsilon r)$ is a general function of retarded or advanced time; the solution is not Fourier transformed in time. The spatial TT components written out are

$$g_{rr}^{TT} = 1 + (2 - 3\sin^2\theta)G \quad , \tag{B8a}$$

$$g_{\theta\theta}^{TT} = (1 + 3\sin^2\theta\ I - G)r^2 \quad , \tag{B8b}$$

$$g_{\phi\phi}^{TT} = [1 - 3\sin^2\theta\ I + (3\sin^2\theta - 1)G]\, r^2\sin^2\theta \quad , \tag{B8c}$$

$$g_{r\theta}^{TT} = 3H\, r\sin\theta\cos\theta \quad , \tag{B8d}$$

which along with the shift and lapse (B1) give the entire metric.

Equations (B1) and (B8a-d) do not however represent the gravitational wave in our metric since the gauge conditions differ. To obtain the form of the quadrupole gravitational wave in our gauge we need to find the infinitesimal gauge transformation linking TT gauge to our maximal slicing and quasi-isotropic gauge. This infinitesimal gauge transformation has generators ξ^a such that

$$g_{ab}^{TT} = g_{ab} + D_a\xi_b + D_b\xi_a \quad , \tag{B9}$$

where g_{ab} represents the metric in our gauge. Taking the properties (B1) and (6), Equations (B9) reduce to

$$-1 = -\alpha^2 + 2D_0\xi_0 = -\alpha^2 + 2\partial_t\xi_t \quad , \tag{B10a}$$

$$0 = \beta_i + D_i\xi_0 + D_0\xi_i = \beta_i + \partial_i\xi_t + \partial_t\xi_i \quad , \tag{B10b}$$

$$g_{rr}^{TT} = A^2 + 2D_r\xi_r = A^2 + 2\partial_r\xi_r \quad , \tag{B10c}$$

$$g_{\theta\theta}^{TT} = A^2r^2 + 2D_\theta\xi_\theta = A^2r^2 + 2\partial_\theta\xi_\theta + 2r\xi_r \quad , \tag{B10d}$$

$$g_{\phi\phi}^{TT} = B^2r^2\sin^2\theta + 2D_\phi\xi_\phi = B^2r^2\sin^2\theta + \xi_r r\sin^2\theta + \xi_\theta\sin\theta\cos\theta \ , \tag{B10e}$$

$$g_{r\theta}{}^{TT} = D_r\xi_\theta + D_\theta\xi_r = \partial_r\xi_\theta + \partial_\theta\xi_r - \frac{2}{r}\xi_\theta \quad . \tag{B10f}$$

Combining (B10c) and (B10d) to eliminate A^2 (fixing this gauge condition) gives

$$r\partial_r\left(\frac{\xi^r}{r}\right) - \partial_\theta\xi^\theta = \frac{1}{2}\left(g_{rr}{}^{TT} - \frac{1}{r^2}\, g_{\theta\theta}{}^{TT}\right) \quad . \tag{B11}$$

Rewriting (B10f),

$$r\partial_r\xi^\theta + \partial_\theta\left(\frac{\xi^r}{r}\right) = \frac{1}{r}\, g_{r\theta}{}^{TT} \quad . \tag{B12}$$

Equations (B11) and (B12) are of the same form as our spatial gauge equations (8) and (9). Taking the known forms of the right-hand-side in (B11) and (B12) and using (B8a,b,d) produces solutions

$$\frac{\xi^r}{r} = -\frac{9}{4}\,\varepsilon\,\frac{F^{(1)}}{r^4} - \frac{9}{4}\,\frac{F}{r^5} - \frac{1}{2}\,\frac{b_2}{r^2} + \sin^2\theta\left[\frac{3}{8}\,\varepsilon\,\frac{F^{(3)}}{r^2} + \frac{27}{8}\,\varepsilon\,\frac{F^{(1)}}{r^4} + \frac{27}{8}\,\frac{F}{r^5} + \frac{b_2}{r^2}\right] \quad , \tag{B13}$$

$$\xi^\theta = \sin\theta\cos\theta\left[-\frac{9}{4}\,\frac{F^{(2)}}{r^3} - \frac{9}{4}\,\varepsilon\,\frac{F^{(1)}}{r^4} - \frac{9}{4}\,\frac{F}{r^5} + \frac{b_2}{r^2}\right] \quad , \tag{B14}$$

after some amount of calculation. The terms with $b_2(t)$ represent the homogeneous solution of (B11) and (B12) with quadrupolar angular dependence and this is related to the term (99) in the shift vector involving $\dot{\eta}_2$.

We next consider (B10a) to derive ξ^t. Since $\alpha \cong 1$, we obtain

$$\alpha = 1 + \partial_t\xi_t \quad , \tag{B15}$$

to linear order. The lapse must satisfy the (vacuum) maximal slicing condition, or

$$\Delta\alpha = \Delta\partial_t\xi_t = \partial_t\Delta\xi_t = 0 \quad . \tag{B16}$$

This yields for ξ^t, up to quadrupole angular dependence,

$$\xi^t = \frac{a_0(t)}{r} + \frac{a_2(t)P_2(\theta)}{r^3} \quad . \tag{B17}$$

These are just the vacuum monopole and quadrupole solutions of the Laplace equation. Equations (B13), (B14), and (B17) specify completely the infinitesimal coordinate transformation.

These generators can now be used to obtain the structure of the wave in our metric in maximal slicing, quasi-isotropic gauge. From (B15),

$$\alpha = 1 + \frac{\dot{a}_0}{r} + \frac{\dot{a}_2P_2(\theta)}{r^3} \quad , \tag{B18}$$

and we see that the maximal slicing condition leaves the lapse insensitive to the wave in linear order. Using (B10b), we find that the shift components are

$$\frac{\beta^r}{r} = \frac{9}{4}\varepsilon\frac{F^{(2)}}{r^4} + \frac{9}{4}\frac{F^{(1)}}{r^5} + \frac{1}{2}\frac{\dot{b}_2}{r^2} + \frac{a_0}{r^3} + 3\frac{a_2}{r^5}$$

$$+ \sin^2\theta\left[-\frac{3}{8}\varepsilon\frac{F^{(4)}}{r^2} - \frac{27}{8}\varepsilon\frac{F^{(2)}}{r^4} - \frac{27}{8}\frac{F^{(1)}}{r^5} - \frac{\dot{b}_2}{r^2} - \frac{9}{2}\frac{a_2}{r^5}\right] \quad , \qquad (B19)$$

$$\beta^\theta = \sin\theta\cos\theta\left[\frac{9}{4}\frac{F^{(3)}}{r^3} + \frac{9}{4}\varepsilon\frac{F^{(2)}}{r^4} + \frac{9}{4}\frac{F^{(1)}}{r^5} - \frac{\dot{b}_2}{r^2} + 3\frac{a_2}{r^5}\right] \quad . \qquad (B20)$$

We see from these last results that, with (99),

$$\dot{\eta}_2 = \frac{1}{2}\dot{b}_2 \quad .$$

The perturbation in A is

$$A - 1 = \frac{3}{4}\frac{F^{(2)}}{r^3} - \frac{b_2}{2r^2} + \sin^2\theta\left[\frac{3}{8}\frac{F^{(4)}}{r} + \frac{3}{8}\varepsilon\frac{F^{(3)}}{r^2} - \frac{9}{8}\frac{F^{(2)}}{r^3} + \frac{b_2}{r^2}\right] \quad , \qquad (B21)$$

found from (B10c). The corresponding result in B using (B10e) is

$$B - 1 = \frac{3}{4}\frac{F^{(2)}}{r^3} - \frac{b_2}{2r^2} + \sin^2\theta\left[-\frac{3}{8}\frac{F^{(4)}}{r} - \frac{9}{8}\varepsilon\frac{F^{(3)}}{r^2} - \frac{9}{8}\frac{F^{(2)}}{r^3}\right] . \qquad (B22)$$

We can now calculate the amplitude present in ℓnT:

$$\ell nT = \sin^2\theta\left[\frac{3}{4}\frac{F^{(4)}}{r} + \frac{3}{2}\varepsilon\frac{F^{(3)}}{r^2} + \frac{b_2}{r^2}\right] \quad , \qquad (B23)$$

and in ϕ:

$$\phi = 1 + \frac{3}{8}\frac{F^{(2)}}{r^3} - \frac{1}{4}\frac{b_2}{r^2}$$

$$+ \sin^2\theta\left[\frac{1}{16}\frac{F^{(4)}}{r} - \frac{1}{16}\varepsilon\frac{F^{(3)}}{r^2} - \frac{9}{16}\frac{F^{(2)}}{r^3} + \frac{1}{3}\frac{b_2}{r^2}\right] \quad . \qquad (B24)$$

Note that the radiative part of the wave ($F^{(4)}/r$) appears in the conformal factor. The combination AB however gives

$$AB = 1 + \frac{3}{2}\frac{F^{(2)}}{r^3} - \frac{b_2}{r^2} + \sin^2\theta\left[-\frac{3}{4}\varepsilon\frac{F^{(3)}}{r^2} - \frac{9}{4}\frac{F^{(2)}}{r^3} + \frac{b_2}{r^2}\right] \quad , \qquad (B25)$$

and here the radiative part of the solution vanishes.

Finally, we also obtain the wave dependence in λ using (34):

$$\lambda = \sin^2\theta\left[\frac{3}{4}\frac{F^{(5)}}{r} + \frac{3}{2}\varepsilon\frac{F^{(4)}}{r^2} + \frac{9}{4}\frac{F^{(3)}}{r^3} + \frac{9}{4}\varepsilon\frac{F^{(2)}}{r^4} + \frac{9}{4}\frac{F^{(1)}}{r^5} + 3\frac{a_2}{r^5}\right] , \qquad (B26)$$

with comparable results obtainable for the other components of $K^i{}_j$. Clearly using (B23) and (B26), the higher order terms correcting the leading spherical wave dependence can be obtained in the Bondi-Sachs flux integral evaluated at finite radius. Noting that $h_+{}^{TT} = h_{\theta\theta}{}^{TT}$, from (B8b) and (B23) we obtain the connection

$$\ell nT = h_+{}^{TT} + \mathcal{O}(r^{-2}) \quad , \qquad (B27)$$

for our radiative variable ℓnT.

CHAPTER V

In this chapter, we will discuss some of the numerical aspects of treating the equations derived in the previous chapters. Our numerical approach can be generally described as two-dimensional time explicit, Eulerian finite differencing with an adaptive mesh. By the usual ideas of considering truncated Taylor expansions, the differencing of spatial derivatives in the elliptic equations we solve (IV63, 67a,b, 79a,b, 89a,b, 116) is typically second order accurate through the use of a five point *coupling* (i.e. differences are computed using adjacent, neighboring values, in each spatial direction). Some deviation from second order accuracy will occur due to the use of nonuniform zoning on the spatial mesh typically. Such *grid stretching* is employed to increase the span of physical length scales that can be covered by a mesh using a fixed number of zones. However, for the sake of numerical accuracy there is some bound to the degree of stretching of the mesh that can be tolerated. Ultimately, there is no substitute for a sufficient number of zones when attempting to simulate a problem with several disparate length scales. This question of adequate resolution has been at least in part responsible for the slow rate of progress on this project heretofore.

The time integration is typically first order accurate. In the important area of numerical transport, these terms involving

spatial derivatives are treated so as to be usually second order accurate. More specifically, the transport terms in the hydrodynamic equations (IV123, 124, 127, 128) are given mixed first order (Donor cell) --second order interpolative differencing. A weight is chosen to make the scheme generally second order accurate in the smooth regions of the flow with transition to first order transport in regions that are forming shocks. The evolution equations for the gravitational field are handled in the same way though the transport terms in this case will nearly always be second order since these quantities show no tendency to steepen into "shock-like" structures.

We use conservative differencing for the hydrodynamic equations. In the case of the continuity equation (IV123), this allows the total baryon number computed by (IV130) to remain constant throughout the numerical evolution to within computer roundoff. The same technique is used where possible for the evolution of the gravitational field variables, though it is less clear in this case what physical object one is conserving. General techniques for numerical topics such as conservative differencing, numerical transport, artificial viscosity, and the solution of elliptic equations are given by Roache[1] (see also the text by Ames[2]). However in most cases the discussion in such texts is limited to *model* partial differential equations. Hence, in a number of instances, these numerical techniques have required modification for use in our code.

A number of the aspects of our numerical method are the same as those reported by Dykema.[3] This is particularly true of the finite

difference treatment of the hydrodynamic equations and, by extension, the evolution equations for our dynamical gravitational field variables, λ and ℓnT. There have been significant recent refinements for treating explicit Eulerian numerical transport.[4,5] Though the exact techniques vary, these methods are generally called *monotone* transport, or *monotonicity* (see Hawley, Smarr and Wilson[4] for comparisons). Since these new techniques will soon be used in our numerical algorithm and because the older method of numerical transport has worked well and has not been changed, we do not review this topic here. The reader is referred instead to the complete and up-to-date discussion by Dykema[3] on our approach to numerical transport, conservative differencing, and artificial viscosity (see also Crowley[6] and Leith[7]).

Just as we have emphasized in the previous chapters areas where our analytic method has undergone significant refinement, we concentrate here on those aspects of our numerical treatment which have recently changed. These numerical refinements include the identification of a *numerical regularization* technique to allow proper finite differencing of coupled elliptic systems near the singular points of the coordinate system ($r = 0$ and $\theta = 0$ in our case, though the technique appears applicable to other curvilinear coordinate systems). This scheme has allowed the elimination of the anomalous behavior in the gravitational field quantities near these singular points, that has plagued a number of past multi-dimensional numerical relativity efforts[8,9] including our own.[3,10] We have also found a method to

produce convergence to solutions of the nonlinear Hamiltonian constraint equation (IV63) even in situations (once a black hole has formed) where the solution is in a very nonlinear regime. Finally we will also describe an improved adaptive mesh positioning criterion which has allowed fairly zone-efficient calculations to be made of the dynamics of collapse, whether to a hydrodynamic bounce or to the formation of a black hole, as well as following the radiation field out into the wave zone.

a) Adaptive Mesh, Centering, and Boundary Conditions

From the symmetry assumptions discussed in Chapter IV and with the symmetry boundary conditions given there, our finite difference mesh need only extend over one quadrant of the (r,θ) plane. The mesh is taken to be characterized by a discrete set of coordinate locations (r_j,θ_k) in the plane. It will be taken as a general convention here that a j subscript refers to a radial position, while k subscripts give angular positions. The number of zones in either direction is specifiable; we take j to run over

$$1 \leq j < JM \quad , \tag{1}$$

and k between

$$1 \leq k < KM \quad . \tag{2}$$

The nodal positions given by (r_j,θ_k) will be referred to as the A-mesh. These positions are defined as follows. Define angular zone widths $\Delta\theta_{k+\frac{1}{2}}$ to give

$$\theta_{k+1} = \theta_k + \Delta\theta_{k+\frac{1}{2}} , \qquad k = 1,\cdots,KM - 1 \quad . \tag{3}$$

The zone widths $\Delta\theta_{k+\frac{1}{2}}$ are to be considered centered between θ_{k+1} and θ_k. We take as the edges of the quadrant

$$\theta_2 = 0 , \qquad \theta_{KM} = \frac{\pi}{2} \quad . \tag{4}$$

The zone widths are taken to always be positive and must be consistent with the boundary locations (4). A dummy location exists at the negative angle

$$\theta_1 = - \Delta\theta_{3/2} \quad . \tag{5}$$

Dummy zones are placed outside the computational quadrant to facilitate the application of Neumann type boundary conditions. We will see more of these momentarily.

Equations (3) and (4) above define the A-mesh angular positions. We take the second set of angular positions

$$\theta_{k+\frac{1}{2}} = \theta_k + \frac{1}{2}\,\Delta\theta_{k+\frac{1}{2}} , \qquad k = 1,\cdots,KM \quad , \tag{6}$$

defined using the zone widths $\Delta\theta_{k+\frac{1}{2}}$ to be the B-mesh angular locations. Notice that $\theta_{k+\frac{1}{2}}$ will always be exactly centered between θ_{k+1}

and θ_k. Notice also that $\theta_{3/2}$ is a negative location, or dummy zone, next to the symmetry axis and that $\theta_{KM+\frac{1}{2}}$ lies at an angle greater than $\frac{\pi}{2}$ and so is a dummy zone for the equatorial plane. Once $\theta_{k+\frac{1}{2}}$ are defined (6), the second set of zone widths

$$\Delta\theta_k = \theta_{k+\frac{1}{2}} - \theta_{k-\frac{1}{2}} , \qquad k = 2,\cdots,KM \quad , \tag{7}$$

can be given. These are considered to be A-mesh quantities and are nearly, though not necessarily exactly, centered on the locations θ_k.

We treat the radial direction in like fashion. The A-mesh positions, r_j, satisfy

$$r_{j+1} = r_j + \Delta r_{j+\frac{1}{2}} , \qquad j = 1,\cdots,JM - 1 \quad , \tag{8}$$

and the widths $r_{j+\frac{1}{2}}$ are considered B-mesh quantities centered (exactly) between r_{j+1} and r_j. The boundary locations are defined to be

$$r_2 = 0 , \qquad r_{JM} = r_m \quad , \tag{9}$$

where r_m has been used in Chapter IV in defining asymptotic boundary conditions. There is a dummy A-mesh radial location:

$$r_1 = - \Delta r_{3/2} \quad . \tag{10}$$

The B-mesh locations are defined by

$$r_{j+\frac{1}{2}} = r_j + \frac{1}{2}\,\Delta r_{j+\frac{1}{2}} , \qquad j = 1,\cdots,JM \quad , \tag{11}$$

and the corresponding (A-mesh) zone widths Δr_j by

$$\Delta r_j = r_{j+\frac{1}{2}} - r_{j-\frac{1}{2}} , \qquad j = 2,\cdots,JM \quad . \tag{12}$$

As before, Δr_j and $\Delta r_{j+\frac{1}{2}}$ are required to be positive. B-mesh dummy zones reside at $r_{3/2}$ below the origin and $r_{JM+\frac{1}{2}}$ beyond r_{JM} (for certain B-mesh centered quantities, $r_{JM+\frac{1}{2}}$ will assume the role of r_m).

Nowhere in this discussion was it assumed that $\Delta\theta_k$, $\Delta\theta_{k+\frac{1}{2}}$, Δr_j and $\Delta r_{j+\frac{1}{2}}$ were to be independent of k and j, respectively. In fact great computational advantages derive from taking these to be functions of the (discrete) angular and radial coordinates, respectively. Such a graded mesh allows more zones to be put where they are needed and increases the ratio of physical length scales that can be covered with a fixed number of zones. We have thus far made great use of grading the mesh in the radial direction. We have not as yet employed a grading in the angular direction, though we will likely do so in our calculations in the near future. We typically use a uniformly graded mesh defined by

$$\Delta r_{j+\frac{1}{2}} = \sigma \Delta r_{j-\frac{1}{2}} \quad , \tag{13}$$

where σ is a constant. The constant σ is determined by specifying the outer radial location, r_{JM}, the size of the innermost radial zone, r_3, and the number of radial zones, JM, employed. We find σ by an iterative technique. With uniform spacing in the angular direction, the zone widths are

$$\Delta\theta_{k+\frac{1}{2}} = \Delta\theta_k = \frac{\pi}{2} (KM - 2)^{-1} \quad . \tag{14}$$

If the mesh is graded, the value of σ can change in time. This is necessary if for example we choose to change the size of the innermost radial zone, r_3, or if the outer radius, r_{JM}, is changed. We typically keep r_{JM} constant and r_3 is allowed to change to follow the collapse of the material in matter-filled applications. Associated with gradual changes, or redefinitions, of the mesh is a *grid velocity*, $V_j^{(g)}$, defined by

$$r_j^{n+1} = r_j^n + V_j^{(g)} \Delta t \quad , \tag{15}$$

where Δt is the coordinate time increment and the superscripts on the zone locations refer to the time levels. In fact, equation (15) is used in reverse to derive the grid velocity. Hence, our nodal points are moving with respect to the spatial coordinates. The evolution equations that have been derived in Chapter IV, however, give the time rate of change of a quantity at a fixed spatial coordinate location. Since we want the new values of any given quantity, on a new time slice, at the nodal positions, i.e. at a given (r_j,θ_k), the grid velocity must be used to compute a convective derivative for the nodal locations:

$$\frac{D}{Dt} \psi_{k,j} = \partial_t \psi_{k,j} + \vec{V}^{(g)} \cdot \vec{\nabla} \psi_{k,j} \tag{16}$$

where $\psi_{k,j}$ represents the discrete values of any evolved quantity.

This just represents a continuous interpolation process. The grid velocity then modifies velocities and fluxes in the transport terms of the evolution equations.[3]

We remark here that it has been extremely important to use the radial grid velocity judiciously so that our gravitational core collapse calculations are followed with sufficient resolution. This is particularly true of collapse calculations which result in a black hole. Because we wish to measure gravitational radiation from these models, the mesh is required to extend out into the wave zone, where the outermost radius will typically be on the order of hundreds of M. Then the mesh must also become refined in size near the center to keep the collapsing star well resolved. An example of a mesh satisfying these purposes is shown in Figure 1. The choice of a grid velocity which appears to work well is to redefine r_3 on each time slice so that the radial grid velocity at this innermost zone equals the radial material velocity, V_j^r. The mesh in the innermost zones therefore moves so that the flow is locally nearly Lagrangian with respect to the nodal points. We call this a *quasi-Lagrangian* grid velocity. If the collapse of the core is nearly homologous, then this choice for the grid velocity keeps roughly the initial number of radial zones within the core. The remarkable feature of this choice, given our maximal time slicing, quasi-isotropic gauge, is that even when a black hole forms the collapsed core and the vacuum throat region that forms remain well zoned. (For a discussion of this throat region and a demonstration of

Figure 1a,b. The property of a radially graded mesh allowing both the asymptotic regions (Figure 1a) and the interior of the core (Figure 1b) to remain well zoned as reflected by the numerical construction of the lapse function.

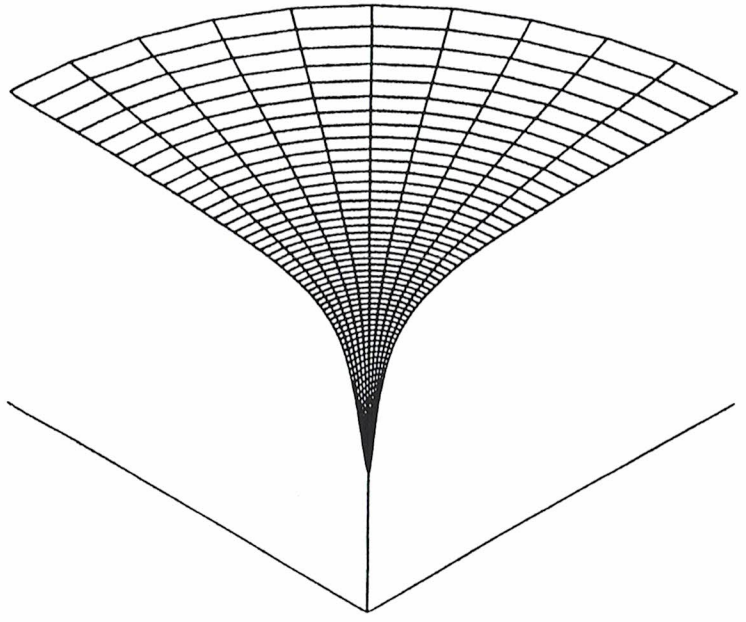

Figure 1a

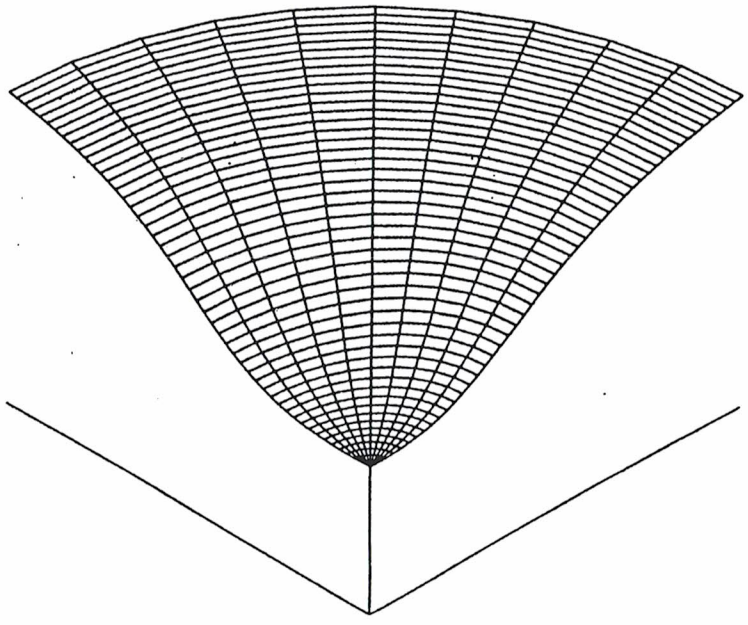

Figure 1b

the geometry resulting from a black hole collapse calculation see Chapter VI.) These calculations only break down once the grid stretch, defined as the quantity σ, becomes so large that the finite differencing ceases to be accurate.

In the preceding discussion we had set up two separate meshes. The reason this is done is so that different state variables can be centered in ways that make the implementation of finite differences and averages most natural. Most quantities are zone-centered (with respect to the A-mesh) at locations $(\theta_{k+\frac{1}{2}},r_{j+\frac{1}{2}})$. The exceptions are velocity-like quantities, V^i, $V^{(g)i}$, β^i, S_i (with radial components centered at the radial faces $(\theta_{k+\frac{1}{2}},r_j)$, angular components centered at the angular faces $(\theta_k,r_{j+\frac{1}{2}})$), and $K^r{}_\theta$ (which is corner-centered, i.e. at (θ_k,r_j)). These definitions in particular make the differences produced by the elliptic systems most natural.

The angular components of velocity-like variables, as well as $K^r{}_\theta$, are properly centered to directly apply their angular boundary conditions:

$$\beta^\theta(2,j) = \beta^\theta(KM,j) = 0 \quad , \tag{17a}$$

$$W^\theta(2,j) = W^\theta(KM,j) = 0 \quad , \tag{17b}$$

$$S_\theta(2,j) = S_\theta(KM,j) = 0 \quad , \tag{17c}$$

$$K^r{}_\theta(2,j) = K^r{}_\theta(KM,j) = 0 \quad , \tag{17d}$$

where here parenthesis are used to avoid confusion with tensor indices.

Radial components of velocity-like variables and zone-centered quantities are correctly angular centered to apply their vanishing Neumann conditions at $\theta = 0$ and $\theta = \frac{\pi}{2}$:

$$A(1,j) = A(2,j) \quad , \quad A(KM,j) = A(KM-1,j) \quad , \tag{18a}$$

$$B(1,j) = B(2,j) \quad , \quad B(KM,j) = B(KM-1,j) \quad , \tag{18b}$$

$$D(1,j) = D(2,j) \quad , \quad D(KM,j) = D(KM-1,j) \quad , \tag{18c}$$

$$E(1,j) = E(2,j) \quad , \quad E(KM,j) = E(KM-1,j) \quad , \tag{18d}$$

$$\alpha(1,j) = \alpha(2,j) \quad , \quad \alpha(KM,j) = \alpha(KM-1,j) \quad , \tag{18e}$$

$$K^r{}_r(1,j) = K^r{}_r(2,j) \quad , \quad K^r{}_r(KM,j) = K^r{}_r(KM-1,j) \quad , \tag{18f}$$

$$K^\phi{}_\phi(1,j) = K^\phi{}_\phi(2,j) \quad , \quad K^\phi{}_\phi(KM,j) = K^\phi{}_\phi(KM-1,j) \quad , \tag{18g}$$

$$U(1,j) = U(2,j) \quad , \quad U(KM,j) = U(KM-1,j) \quad , \tag{18h}$$

$$\beta^r(1,j) = \beta^r(2,j) \quad , \quad \beta^r(KM,j) = \beta^r(KM-1,j) \quad , \tag{18i}$$

$$W^r(1,j) = W^r(2,j) \quad , \quad W^r(KM,j) = W^r(KM-1,j) \quad , \tag{18j}$$

$$S_r(1,j) = S_r(2,j) \quad , \quad S_r(KM,j) = S_r(KM-1,j) \quad . \tag{18k}$$

The requirement that λ and ℓnT vanish on the symmetry axis is not naturally produced by our centering assumptions; we typically take them to satisfy instead

$$\lambda(2,j) = \ell nT(2,j) = 0 \quad , \tag{19}$$

and their boundary conditions at $\theta = \frac{\pi}{2}$ are as in (18a-k).

The symmetry boundary conditions at the origin are in most cases naturally applied. The exceptions are the Neumann conditions (given in Chapter IV) for β^r/r, W^r/r, and $K^r{}_\theta/r$. These are solved for in the above forms for numerical regularity purposes (to be discussed below). Nonetheless, we are usually less concerned with the radial centering problems of these Neumann conditions because the radial resolution is usually high.

b) Elliptic Systems and Numerical Regularization

Solution of our elliptic systems can be discussed in the context of the simple Poisson equation

$$\Delta\phi = \rho \quad , \tag{20}$$

where ρ is to be considered constant with respect to ϕ. Iterative techniques to solve (20) generally can be represented by associating with (20) the parabolic equation

$$\partial_m\phi = \eta(\Delta\phi - \rho) \quad . \tag{21}$$

Given $\eta > 0$, the diffusion equation (21) has the steady-state solution to (20). The label m is a "time" which indicates the iteration number. Let us consider the finite difference form of (20) in cartesian coordinates in two dimensions. If ϕ is considered corner-centered

then

$$\phi^{m+1}_{k,j} = \phi^m_{k,j} + \Delta m\cdot\eta\cdot\left\{\frac{1}{\Delta x^2}\left(\phi^m_{k,j+1} - 2\phi^m_{k,j} + \phi^{m+1}_{k,j-1}\right)\right.$$

$$\left. + \frac{1}{\Delta y^2}\left(\phi^m_{k+1,j} - 2\phi^m_{k,j} + \phi^{m+1}_{k-1,j}\right) - \rho_{k,j}\right\} \quad . \tag{22}$$

Notice that when updated values are available (i.e. $\phi_{k,j-1}$ and $\phi_{k-1,j}$ because these nodal points have already been passed) they are immediately used. This enhances the rate of convergence.[1,2]

We can extend these arguments for solutions to (20) to more general equations than (22). A general scalar elliptic equation of the form (20) will have an iterative finite difference representation of

$$\phi^{m+1}_{k,j} = \phi^m_{k,j} + \omega\left\{A_{k,j}\phi^m_{k,j+1} + B_{k,j}\phi^{m+1}_{k,j-1}\right.$$

$$\left. + C_{k,j}\phi^m_{k+1,j} + D_{k,j}\phi^{m+1}_{k-1,j} + E_{k,j} - \phi^m_{k,j}\right\} \quad . \tag{23}$$

Notice in (23) that the factor ω, called the relaxation factor, is defined by requiring unit coefficient for $\phi_{k,j}$, the last term within the parentheses on the right-hand-side. This factor must lie in the range

$$1 \leq \omega \leq 2 \quad , \tag{24}$$

for (23) to converge. When ω is taken to be $\omega > 1$, the iteration method is called *successive over relaxation* (SOR). SOR produces very

rapid convergence for optimal values of ω.[1] For the Poisson equation in cartesian coordinates with Dirichlet boundary conditions, this optimal value is known to be 1.73. For other coordinate topologies and boundary conditions it can be expected to differ from this value. Nonetheless, our experimentation with SOR in our code with spherical coordinates has indicated values in the range $1.7 < \omega < 1.75$, quite close to the optimum Poisson value.

Faster methods are known for solving these systems than the SOR method. We may soon convert the code to a faster matrix solver. However, to date the lapse equation (IV116), with Neumann conditions at the origin, symmetry axis and equatorial plane and with a Dirichlet condition at large radius, is solved straightforwardly using SOR in the form (23) with $\omega = 1.73$.

The Hamiltonian constraint (IV63), used to obtain the metric variable $\psi = B^{1/2}$, is nonlinear. To find its solution, we use a best available guess for ψ to evaluate the source (the right-hand-side). Then the linear operator is solved by SOR to obtain a temporary function $\bar{\psi}$. The next approximation to the solution is formed by taking a weighted linear combination of $\bar{\psi}$ and the last guess. This is a modified Picard (outer) iteration. Writing equation (IV63) as $\Delta\psi = N(\psi)$, where where Δ is the 3-dimensional scalar Laplacian, the algorithm becomes,

$$\Delta\bar{\psi}^{n+1} = N(\psi^n) \quad , \tag{25a}$$

$$\psi^{n+1} = \psi^n + \tilde{\omega}(\bar{\psi}^{n+1} - \psi^n) \quad . \tag{25b}$$

During the early stages of collapse, before a black hole forms, the value of this weight is largely unimportant and can be taken as unity. Once a black hole forms, the solutions for the conformal factor are in a very nonlinear regime and the use of a correct weight is crucial to finding a solution. The optimal weight appears to be $\tilde{\omega} = 0.22$ once a black hole forms and values $\tilde{\omega} > 0.5$ appear to be divergent.

The evolution equation (IV36) for $B = \psi^2$ can be used to provide a good first approximation for the elliptic solver. The boundary conditions for on axis, equator, and origin are similar to those for the lapse and are straightforwardly applied. The Robin condition (IV66) at the outer boundary is given by

$$\psi_{JM+\frac{1}{2}} = \left[\psi_{JM-\frac{1}{2}}\left(1 - \frac{\Delta r_{JM}}{2r_{JM}}\right) + \frac{\Delta r_{JM}}{r_{JM}}\right]\left(1 + \frac{\Delta r_{JM}}{2r_{JM}}\right)^{-1} \quad . \tag{26}$$

The shift potential equations (IV89a,b) are decoupled with the definitions (IV87a,b) for the potentials χ and Φ. Furthermore, the appearance of the two-dimensional Laplacian allows these equations to be Fourier decomposed and replaced by a set of ordinary differential equations (ODE). This avoids the use of iterative or relaxation solution methods and significantly speeds the solution of these equations on the computer.

A finite Fourier transform of χ, Φ, $P = \alpha(2K^r{}_r + K^\phi{}_\phi)$, and $Q = 2\alpha(K^r{}_\theta/r)$ gives:

$$\chi_{k+\frac{1}{2}} = a_0 + 2 \sum_{m=1}^{KM-3} a_m \cos 2m\theta_{k+\frac{1}{2}} \quad ,$$

$$\Phi_k = 2 \sum_{m=1}^{KM-3} b_m \sin 2m\theta_k \quad ,$$

$$P_{k+\frac{1}{2}} = p_0 + 2 \sum_{m=1}^{KM-3} p_m \cos 2m\theta_{k+\frac{1}{2}} \quad ,$$

$$Q_k = 2 \sum_{m=1}^{KM-3} q_m \sin 2m\theta_k \quad , \qquad (27)$$

consistent with the parities of the functions under axisymmetry and equatorial plane symmetry. The inverse transforms are

$$p_m = \left(\frac{1}{KM-2}\right) \sum_{k=2}^{KM-1} P_{k+\frac{1}{2}} \cos 2m\theta_{k+\frac{1}{2}} \quad ,$$

$$q_m = \left(\frac{1}{KM-2}\right) \sum_{k=3}^{KM-1} Q_k \sin 2m\theta_k \quad , \qquad (28)$$

with identical expressions for amplitudes a_m and b_m. In the above expressions the radial index is suppressed; all amplitudes are implicitly functions of r.

The amplitudes a_0 and p_0 are handled separately. The expected dependence of β^i near r = 0 (see (IV46)) implies a singular dependence, $a_0 \sim$ constant $\times$ ℓnr, for χ. The angle average of $\frac{\beta^r}{r}$, $\langle \frac{\beta^r}{r} \rangle = \left(\frac{1}{KM-2}\right) \sum_{k=2}^{KM-1} \left(\frac{\beta^r}{r}\right)_{k+\frac{1}{2}}$, is calculated directly from equation (IV9):

$$\left\langle \frac{\beta^r}{r} \right\rangle = -\int_r^{r_m} \frac{P_0}{r}\, dr + \frac{1}{r_m^3}\left(\frac{1}{2} D_0 - \frac{3}{16} D_2\right) - \frac{1}{2r} \langle \ell nT \rangle_{r=r_m} \quad , \qquad (29)$$

where $\langle \ell nT \rangle = \left(\frac{1}{KM-2}\right) \sum_{k=2}^{KM-1} (\ell nT)_{k+\frac{1}{2}}$. The last two terms giving $\langle \frac{\beta^r}{r} \rangle$ at $r = r_m$ are, respectively, the longitudinal (IVA15a) and the transverse, or wave, (Evans, 1984) contributions. The amplitude a_0 is never explicitly calculated.

Equations (IV89a,b) are transformed giving,

$$r\partial_r(r\partial_r a_m) - 4m^2 a_m = p_m \quad , \qquad (30)$$

$$r\partial_r(r\partial_r b_m) - 4m^2 b_m = q_m \quad , \qquad (31)$$

a set of uncoupled ODE's for m = 1,$\cdots$,KM - 3. These are solved using the tridiagonal algorithm.[1] The inner boundary conditions are $\partial_r a_m = \partial_r b_m = 0$ at r = 0. The conditions on the outer boundary are given by the Fourier transform of the transverse, weak field conditions $\partial_r \chi = \frac{1}{2r^2} \ell nT$ and $\Phi \approx 0$ ($b_m = 0$) for m = 2,$\cdots$,KM - 3. For m = 1 there is a longitudinal contribution (only the lowest order, r^{-3}, moments are calculated) in addition to the above wave condition to the boundary condition on a_1 ($b_1(r_m) = 0$). This longitudinal contribution is $a_1^{(L)} = \frac{3}{32} D_2 \frac{1}{r_m^3}$, a Dirichlet condition, while the transverse part implies a Neumann condition

$$\partial_r a_1^{(T)} = -\frac{1}{2r_m^2(KM-2)} \sum_{k=2}^{KM-1} (\ell nT)_{k+\frac{1}{2}} \cos 2\theta_{k+\frac{1}{2}} \Big|_{r=r_m} \quad . \qquad (32)$$

Finally we close with a discussion of the numerical problems encountered with the accuracy of finite differencing coupled elliptic systems near the singular points of curvilinear coordinate systems and the techniques we have used to circumvent these numerical irregularities. We employ spherical coordinates in our calculations and hence problems in the finite difference approximation appear at the origin, $r = 0$, and to a lesser extent on the symmetry axis, $\theta = 0$. Similar numerical regularity problems also occurred in an earlier version of this code which employed topological cylindrical coordinates.[10] In that case the irregularities showed up along the entire (coordinate singular) symmetry axis. Similar numerical irregularities have long been a source of problems in using 2-dimensional numerical relativity codes. We have developed techniques for eliminating this aberrant behavior in our spherical coordinate numerical relativity code. The general method however appears immediately applicable to other coordinate topologies. We have identified two causes of these numerical irregularities near symmetry points. The first is due to the loss of finite difference accuracy and increase of truncation errors near these regions in curvilinear coordinate systems. The second is related to the appearance of nontrivial, local homogeneous solutions to coupled elliptic systems.

The usual arguments on the formal size of truncation errors in finite difference approximations are based on the use of a Taylor expansion. For a problem in cartesian-like coordinates with zone

increments Δx, centered spatial differences will produce truncation errors with respect to the corresponding derivatives they replace of order $(\Delta x/\ell)^2$, where ℓ is the characteristic physical length. These errors can be arbitrarily reduced with increase in the resolution (i.e. $\Delta x \to 0$). The problem with finite differencing in curvilinear coordinates, near the special points or regions of the coordinate system, is that Taylor series do not in general exist there. One encounters in spherical coordinates differential operators of the form $\frac{1}{r}\,\partial_r$, for example (similarly one has $\frac{1}{\rho}\,\partial_\rho$ in cylindrical coordinates). With this explicit appearance of the radial coordinate, attempts to produce centered finite differences of such operators will produce truncation errors that are *the maximum* of $(\Delta r/\ell)^2$ or $(\Delta r/r)^2$, where ℓ is again the characteristic physical length. Far from the origin of coordinates these errors can be made sufficiently small. However in the vicinity of $r = 0$, the errors associated with most finite difference representations will be of order unity (or worse).

We can illustrate this problem and its solution with a specific example. Consider the radial second order operator

$$\frac{1}{r^2}\,\partial_r(r^2\,\partial_r\psi) \quad , \tag{33}$$

associated with the flat space three-dimensional Laplacian (IV63). Let us consider that this operator produces zone centered values, i.e. located at positions $r_{j+\frac{1}{2}}$ and that ψ is zone centered as well: $\psi_{j+\frac{1}{2}}$. Using our mesh definitions, one can straightforwardly

difference (33):

$$\frac{1}{r^2_{j+\frac{1}{2}}} \frac{1}{\Delta r_{j+\frac{1}{2}}} \left[r^2_{j+1} \frac{1}{\Delta r_{j+1}} (\psi_{j+\frac{3}{2}} - \psi_{j+\frac{1}{2}}) \right.$$

$$\left. - r_j^2 \frac{1}{\Delta r_j} (\psi_{j+\frac{1}{2}} - \psi_{j-\frac{1}{2}}) \right] \quad . \tag{34}$$

Let us also assume that ψ has the local radial dependence

$$\psi(r) = c_0 + c_1 r^2 + \mathcal{O}(r^4) \quad , \tag{35}$$

just as we anticipate for the conformal factor. Applying (33) to (35) gives the analytic value $6c_1$. If on the other hand we take from (35)

$$\psi_{j+\frac{1}{2}} = c_0 + c_1 r^2_{j+\frac{1}{2}} \quad , \tag{36}$$

and use (34), we obtain

$$c_1 \frac{1}{r^2_{j+\frac{1}{2}}} \frac{1}{\Delta r_{j+\frac{1}{2}}} \left[r^2_{j+1} (r_{j+\frac{3}{2}} + r_{j+\frac{1}{2}}) \right.$$

$$\left. - r_j^2 (r_{j+\frac{1}{2}} + r_{j-\frac{1}{2}}) \right] \quad . \tag{37}$$

Evaluating this at the first three radial locations, $j = 2,3,4$, yields the values $8.0\ c_1$, $6.22\ c_1$, $6.08\ c_1$, respectively. Hence, it can be seen that the errors near the origin in such a straightforward finite differencing (34) of (33) are of order unity.

The solutions to these problems is to choose the specific finite difference representation for the operator in question which

reproduces the expected analytic result under the assumption that the general local dependence of the function is known. This altered finite difference operator for (33) for example will differ from the straightforward one (34) away from the origin only at the level of second order, which is already conceded to the approximation as a whole. For (33), we would use instead

$$\frac{3}{r^3_{j+1} - r^3_j} \left[\frac{2r^3_{j+1}}{r_{j+\frac{3}{2}} + r_{j+\frac{1}{2}}} \frac{1}{\Delta r_{j+1}} (\psi_{j+\frac{3}{2}} - \psi_{j+\frac{1}{2}}) \right.$$

$$\left. - \frac{2r^3_j}{r_{j+\frac{1}{2}} + r_{j-\frac{1}{2}}} \frac{1}{\Delta r_j} (\psi_{j+\frac{1}{2}} - \psi_{j-\frac{1}{2}}) \right] \quad , \tag{38}$$

which, assuming (36) as the expected form for ψ, reproduces the analytic value.

A second problem which will be typically encountered in solving coupled elliptic systems is local homogeneous solutions. We can illustrate why this is *not* normally a problem by considering the scalar Poisson equation

$$\Delta\phi = 4\pi\rho \quad . \tag{39}$$

The homogeneous solution for this equation is just a constant, say c_0. Assuming our symmetry conditions, the local dependence of ϕ near $r = 0$ would be $\phi = c_0 + r^2(c_1 + c_2 \sin^2\theta) + \theta(r^4)$, in spherical coordinates. Regardless of whether this equation (39) is written in cartesian coordinates or spherical coordinates prior to finite differencing,

the difference representations of the partial derivatives in the Laplacian will identically cancel off the constant c_0. The finite differencing of (39) can then concentrate on reproducing the expected next order behavior in ϕ. The value c_0 is of course only determined by the global solution of (39) once suitable boundary values have been prescribed.

The situation changes drastically when one considers vector or tensor (or in general multi-component coupled) elliptic systems. Consider a 2-tensor $K^i{}_j$ which exhibits our assumed symmetries including a tracefree condition (i.e. like the extrinsic curvature tensor). The cartesian components in the limit $r \to 0$ have the form (IV49)

$$\lim_{r \to 0} K^i{}_j = \text{diag}[g_1, g_1, -2g_1] \quad , \tag{40}$$

where g_1 is a constant. If a tensor-like Laplace operator, like the "tensor Laplacian" (IV79a,b), in *cartesian coordinates* operates on (40), this "constant" or homogeneous solution will be annihilated. The same is true of a finite difference representation. However, if the tensor (40) is transformed to spherical coordinates, this local homogeneous solution will be of the form (IV55,58) which has angular dependence! If the finite difference operator is to produce accurate results, these terms must still be identically annihilated.

To do this requires that the differential equations for the coupled elliptic systems be written in a form first which allows the

subsequent finite difference equations to identically annihilate the local homogeneous solutions. The vector and tensor Laplacian equations, (IV67a,b) and (IV79a,b) can easily be manipulated into this form (see Evans, Smarr and Wilson[11]). When this is done the results are dramatic. Figure 2a shows the local behavior near $r = 0$ in the extrinsic curvature component $K^{\phi}{}_{\phi}$. A large numerical anomaly is evident within the first 5 to 10 radial zones. Figure 2b indicates the greatly improved local behavior in the finite difference calculation after the technique has been regularized.

igures 2a,b. The local behavior near r = 0 in the extrinsic curv-
:ure component K^{ϕ}_{ϕ}. An anomalous numerical "spike" is evident at
ıe origin affecting the first 5-10 zones in Figure 2a. The symmetry
‹is is to the right and the equatorial plane to the left. In Figure
) the same component plotted after the finite differencing has been
'egularized." Note that the vertical scales in the two figures are
ifferent, with Figure 2a being dominated by the numerical error.
:nce, there is great improvement in Figure 2b.

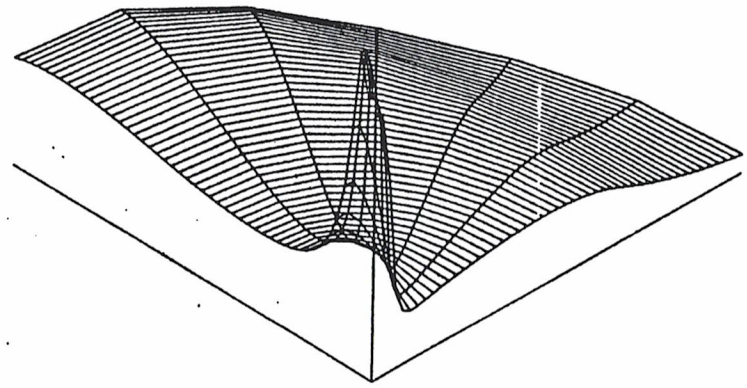

Figure 2a

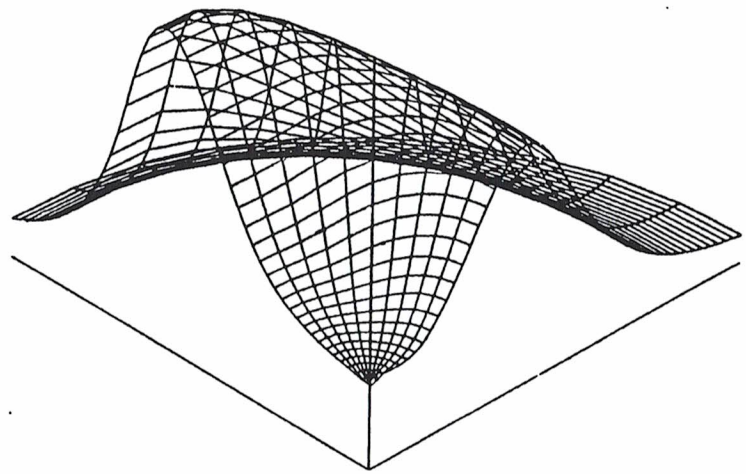

Figure 2b

Chapter V References

1. Roache (1976).
2. Ames (1977).
3. Dykema (1980).
4. Hawley, Smarr, and Wilson (1984); and references therein.
5. Barton (1984).
6. Crowley (1975).
7. Leith (1965).
8. Smarr (1979).
9. Nakamura (1981).
10. Wilson (1979).
11. Evans, Smarr and Wilson (1984).

CHAPTER VI

We present here a number of preliminary results from calculations made with the computer code that has been developed by implementing the analytic and numerical techniques described in the preceding chapters. Several test results from calculating vacuum (Brill wave) spacetimes and matter-containing models that form black holes will be shown. More significantly, we have produced a set of model oblate core collapse and bounce calculations. These allow a comparison of the relativistic hydrodynamic motion and gravitational radiation production along a sequence of successively higher maximum bounce densities. Some of the generic features and specific results from these models will be discussed below.

Several consistency checks made during these core collapse calculations indicate significant accuracy. These internal checks strongly suggest that our calculation of the total emitted energy in gravitational radiation from these collapses is fairly accurate. We have an even higher degree of confidence in the calculation of the *longitudinal* and kinematical parts of the gravitational field (ϕ, W^i, α, β^i), that in our frame dominate the gravitational effects on the fluid, and in the relativistic hydrodynamic calculation itself. This allows us to accurately find the *quadrupole moment* and its time derivative for the configuration, though of course this is a completely

gauge specific result. Nonetheless, this point will lead to an important quantitative result on the efficacy of the quadrupole moment formula for gravitational radiation from stellar core collapse.

We have less confidence, at present, in our ability to make detailed predictions on the gravitational radiation *waveforms*, $h_+^{TT}(t - r)$, resulting from these aspherical core collapse calculations. This is because of an as yet unresolved problem in an asymptotic boundary condition. It appears that gauge effects that occur at the outer edge of the computational mesh simultaneously with the violent near-zone dynamics (due to elliptic gauge conditions) generate small, but noticeable amounts of spurious incoming radiation at the edge of our mesh. From the size of these effects in the gravitational radiation *flux* indicators, we believe the total integrated energy loss is still fairly accurate (within 10-15%). However, because the flux responds to sharp gradients in the waveforms, there appear to be significant late time (and early time) deviations in the waveforms that only minimally affect the radiation flux.

Finding the problem with the asymptotic boundary conditions will no doubt be aided by the enhanced understanding of the asymptotic structure of the gravitational field in our gauge, as worked out and presented in Chapters III and IV. In any case, we do not believe this will stand as a significant impediment to progress. We expect a resolution of issues of accuracy to come shortly, once the boundary problem is eliminated, after a series of code tests are performed.

Several tests relating to wave propagation will likely be more directly implemented using some of the analytic calculations derived during the writing of this thesis (specifically the asymptotic form of a weak gravitational wave in our gauge given in Chapter IV Appendix B).

a) Confidence Tests

We use the term confidence tests here because we do not mean to imply that results from a systematic code testing program are available. We have indicated that such a program will be conducted soon. Rather, our intention is to present several quantitatively accurate results which have come out of our computer calculations, but in an unsystematic way. As such they do not nearly span the conceivable range of numerical issues that should receive adequate scrutiny.

At the same time, it should not be assumed that the code can be tested in all physical regimes. If this were the case, there would hardly be reason to undertake a numerical approach in the first place. A rigorous testing program can only nip at the edges of the nonlinear regime that is of interest, by using exact solutions available in different perturbative regimes and comparing these with code generated results. However, after any such rigorous testing program, there will still be required a leap of faith in declaring any new physical results accurate. Code testing is necessary but not sufficient. We believe that the ultimate test of a numerical physics

calculation, and in this regard it is similar to experimental physics, is for several researchers or groups, working along independent lines (with different gauges for example), to produce consistent answers.

The first confidence test to be discussed emerges from a vacuum Brill wave calculation. Brill waves, or axisymmetric gravitational waves, were considered analytically long ago (1959) by Brill.[1] He demonstrated, under the restrictions of axisymmetry and time symmetric data, that localized configurations of such waves as initial data have positive mass-energy at infinity (using (IIIA7)) and that the only such spacetimes with vanishing mass are flat. Only quite recently has the Positive Energy theorem been proven for general asymptotically flat configurations.[2,3] Several numerical Brill spacetime evolutions have been reported previously.[4,5]

Brill initial data consists of setting to zero all hydrodynamic quantities, taking $K^i{}_j = 0$ (for time symmetry; though we note that time asymmetric data can be used also[5]), and specifying some functional dependence in T or ℓnT. From the considerations of Chapter II, the initial data is required to satisfy only the Hamiltonian constraint (II74), which for these systems is

$$R = 0 \quad . \tag{1}$$

Writing (1) in our gauge yields

$$\frac{1}{r^2}\partial_r(r^2\partial_2\psi) + \frac{1}{r^2\sin\theta}(\sin\theta\partial_\theta\psi)$$

$$= -\frac{1}{4}\psi\left[\frac{1}{r}\partial_r(r\partial_r\,\ell nT) + \frac{1}{r^2}\partial_\theta\partial_\theta\,\ell nT\right] \quad , \tag{2}$$

from (IV63). By either assuming a larger amplitude for ℓnT or a shorter characteristic length, the strength of the gravitational field is increased, as measured by ψ. Weak Brill waves can be considered to be those in which linearized theory (Chapter IV Appendix B) is sufficient to describe the subsequent evolution. For a sufficiently strong Brill wave, an horizon may lie on the initial surface or in the near future development. Such a strong, localized initial "wave" will then suffer gravitational collapse to a black hole with only a fraction of the energy escaping to infinity. These systems are of considerable interest in and of themselves and we will no doubt seek to explore those configurations with our code.

What we wish to use here is the simple observation, that for any Brill spacetimes which do not undergo gravitational collapse, the total initial mass-energy will radiate through any finite radius edit two-surface. Hence the total time-integrated gravitational radiation flux should equal the initially computed mass if the numerical simulation is accurate.

We time integrate the Bondi-Sachs flux (IV154) to obtain the total mass loss. To monitor the mass of the configuration, we use the *Brill mass* indicator.[1,4,5] This can be derived by taking the

ADM mass (IIIA7) in the equivalent form

$$M_{ADM} = -4 \lim_{r \to \infty} \int d^2S^k \, D_k^{(f)} \, \ell n\psi \quad , \tag{3}$$

where we have used flat space derivatives, $D_k^{(f)}$, and surface element and have replaced ϕ with $\ell n\psi$. This has the same effect in the limit $r \to \infty$. Gauss' theorem allows us to replace (3) (on an R^3 manifold) with

$$M = -4 \int d^3x \, \Delta_3^{(f)} \, \ell n\psi \quad . \tag{4}$$

Then using the identity

$$\Delta_3^{(f)} \, \ell n\psi = \frac{1}{\psi} \Delta_3^{(f)} \psi - (\partial_r \, \ell n\psi)^2 - \frac{1}{r^2} (\partial_\theta \, \ell n\psi)^2 \quad , \tag{5}$$

and (2) plus the fact[1]

$$\lim_{r \to \infty} \int_r d^3x \, \Delta_2^{(f)} \, \ell nT = 0 \quad , \tag{6}$$

gives the expression for the Brill mass in vacuum:

$$M_B = 4 \int dr \, d\theta \, d\phi \, r^2 \sin\theta \left[(\partial_r \, \ell n\psi)^2 + \frac{1}{r^2} (\partial_\theta \, \ell n\psi)^2 \right] \quad . \tag{7}$$

The result is obviously positive definite. We use this mass indicator in vacuum calculations because it is produced from volume integration instead of a surface integral. The surface integral formulations of mass depend for their validity on being calculated at radii beyond all gravitational radiation wavefronts, in order to pick off the

static monopole part of the field. Consequently, the ADM mass (IIIA7) and Hawking mass (IIIA11) are much less well behaved as the wave passes the finite radius edit two-surface than is the Brill mass (7).

A plot of the Brill mass and integrated Bondi-Sachs flux versus time is shown in Figure 1 for a typical Brill wave calculation. The initial mass and total integrated mass loss agree to within 1%. For this balance to have been accurately achieved indicates that several different aspects of the numerical technique are performing well during the evolution. The Hamiltonian constraint (IV63) must produce an accurate conformal factor, or ψ, to be read as an indication of the system mass in (7). The propagation of the gravitational wave must proceed without spurious numerical diminution or enhancement of the wave strength. And the Bondi-Sachs indicator must accurately read the radiated flux.

We next show a result indicating the ability of our code to track a solution deep into the nonlinear regime characterizing a black hole. To simplify the analysis, we will examine this property in spherical symmetry. In spherical symmetry, the momentum constraints (IV26a,b) reduce to

$$\frac{1}{r^3} \partial_r (r^3 A^3 K^\phi_{\ \phi}) = -\frac{1}{2} A^3 \, S_r \quad , \tag{8}$$

since $A = B = \phi^2$. This can be integrated,

$$K^\phi_{\ \phi} = -\frac{1}{2(Ar)^3} \int_0^r dr(Ar)^3 \, S_r \quad . \tag{9}$$

igure 1. The Brill mass computed for a Brill spacetime (curve A) and he total radiated mass-energy measured by the Bondi-Sachs integral curve B) are shown plotted versus time. The vertical scale is ormalized to the initial mass. The expected balance between the wo measures is evident and the agreement is within 1%.

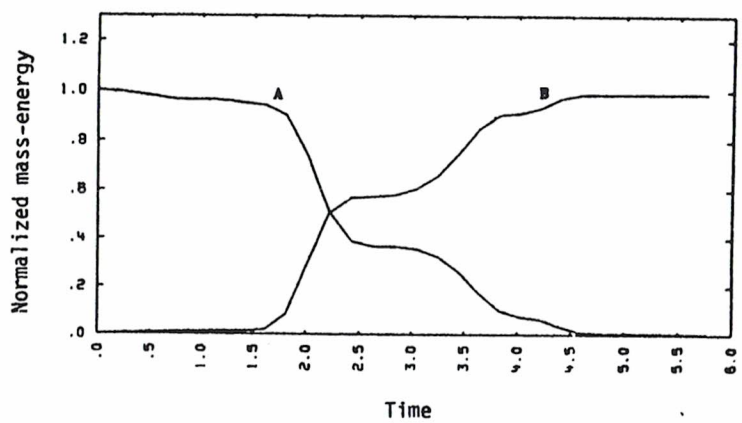

Figure 1

We assume the spherical configuration is collapsing, $S_r < 0$, and that S_r has compact support (i.e. that there is a vacuum region outside the object). Then the integral in (9) can be given by a constant

$$C_0^2 = -\frac{1}{2}\sqrt{3}\int_0^{r_0} dr(Ar)^3 S_r \quad , \tag{10}$$

and the extrinsic curvature component satisfies

$$K^{\phi}{}_{\phi} = \frac{3^{-1/2}}{(Ar)^3} C_0^2 \quad , \tag{11}$$

in the vacuum exterior.

Next, we consider the spherically symmetric, vacuum Hamiltonian constraint found from (IV63) with (11):

$$\frac{1}{r^2}\partial_r(r^2\partial_r A^{1/2}) = -\frac{1}{4} C_0^4 r^{-6} A^{-7/2} \quad . \tag{12}$$

This produces a solution for A which also holds in the vacuum exterior. We seek a particular solution to (12) of the form

$$A^{1/2} = kr^n \quad . \tag{13}$$

Substituting (13) in (12) yields a solution for $n = -\frac{1}{2}$ and $k = C_0^{1/2}$, or

$$Ar = C_0 \quad . \tag{14}$$

This solution represents the vacuum *throat* region of a dynamic

(collapsing) black hole in our gauge. For the dependence (14) to be obtained, A must be significantly larger than its asymptotic value of unity. Hence the association with a black hole.

Finally we use the result of Shapiro and Teukolsky[6,5]

$$\left[1 + \frac{r}{A}\partial_r A\right]^2 = 1 - \frac{2M}{Ar} + (Ar)^2 K^{\phi}{}_{\phi}{}^2 \quad , \tag{15}$$

which is a first integral describing exterior Schwarzschild geometry in our dynamic gauge. Using (14) in (15) gives

$$C_0 = \frac{3}{2} M \quad , \tag{16}$$

and one can see that, after a black hole forms, the integral (10) over the momentum density is directly related to the mass of the hole. For the behavior of the solution, (14) and (16), to be maintained in a numerical calculation, we believe represents a significant test of the code. Equation (16) predicts the dependence

$$Ar = \frac{3}{2} M \tag{17}$$

from (14) in the throat. In addition, these results give a constant extrinsic curvature in the throat, with

$$K^{\phi}{}_{\phi} = \frac{2}{3\sqrt{3}\, M} \quad . \tag{18}$$

We can produce an imbedding diagram by plotting Ar, or an angle average if used for aspherical collapse, versus coordinate radius

r. The "coordinate" Ar is an areal radius (the Schwarzschild radial coordinate), as can be seen by inspection of the line element (IV6) in spherical symmetry. At large radii r and Ar are nearly equal. Figures 2a-e show this imbedding diagram at various stages of collapse of a spherical core. Similar calculations have been made for aspherical collapse, but the diagrams then are more ambiguous, and we do not present them here. Figure 2a shows the configuration with nearly flat geometry at the start of the evolution. Figures 2b-e are snapshots at subsequent times in the collapse. The development of the throat is evident. Notice that even at very late times (Figure 2e) the value of the areal radius in the throat is holding at $\frac{3}{2}$ M.

Finally, we present a consistency check for a non-spherical core collapse and bounce calculation. The mass of a configuration computed during a *numerical* evolution is not constrained to remain constant. Thus we regard as an important test of the accuracy of a numerical relativistic simulation, the degree to which the correct value of the mass is held during a calculation. This has been a guiding consideration in the development of these codes.[4,5,7] Figure 3a displays, on an absolute scale, the variation of the Hawking mass versus time for a deep hydrodynamic core bounce calculation. We will present details of this calculation later; here we wish only to point out that the variations in M_H are under ±0.5% throughout the calculation. Figure 3b shows for comparison the variation of the central value of the lapse during the simulation. Notice that the bounce occurs in a highly relativistic regime from the depth of the lapse.

Figures 2a-e. These figures show an imbedding diagram representing stages in the development of a throat as a black hole forms. The initial geometry in Figure 2a is nearly flat. Even at late times, the analytic value Ar = $\frac{3}{2}$ M is maintained.

Figure 2a

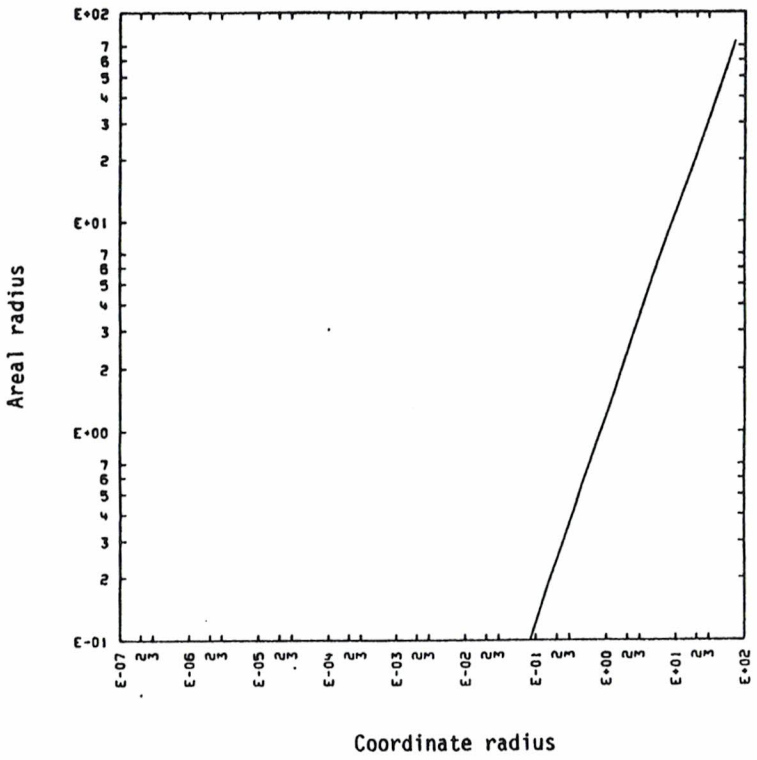

Figure 2b

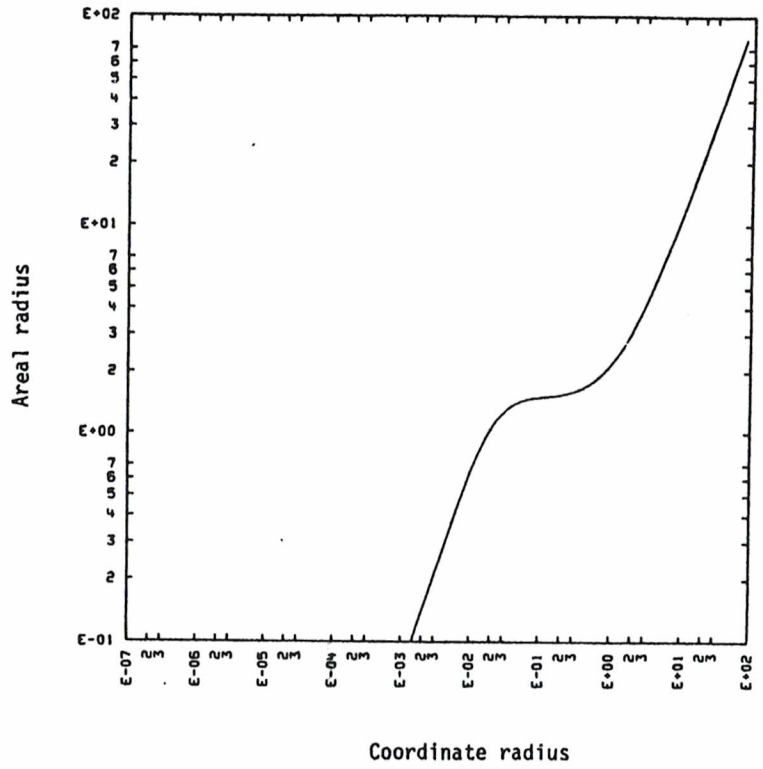

Figure 2c

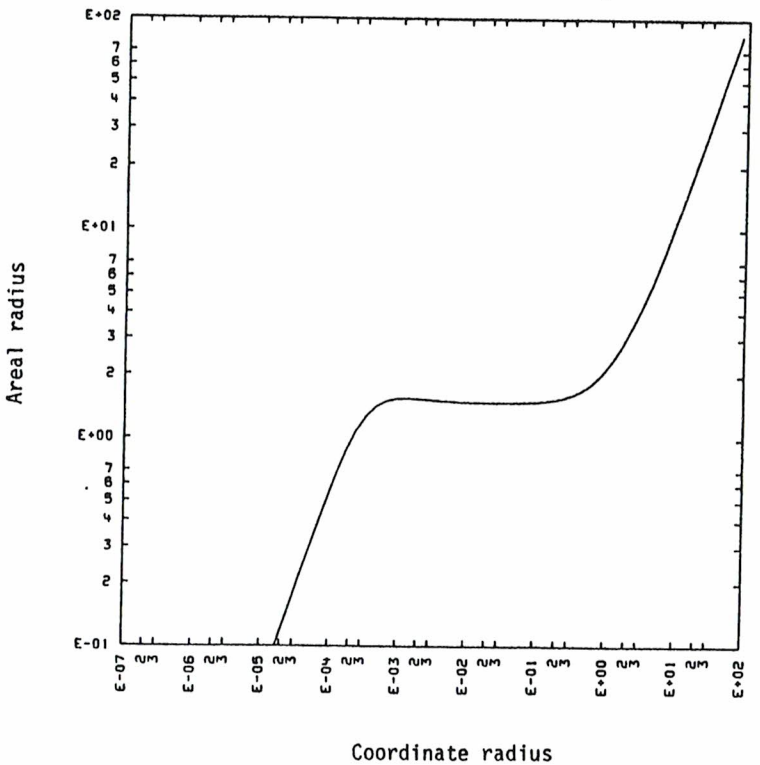

Figure 2d

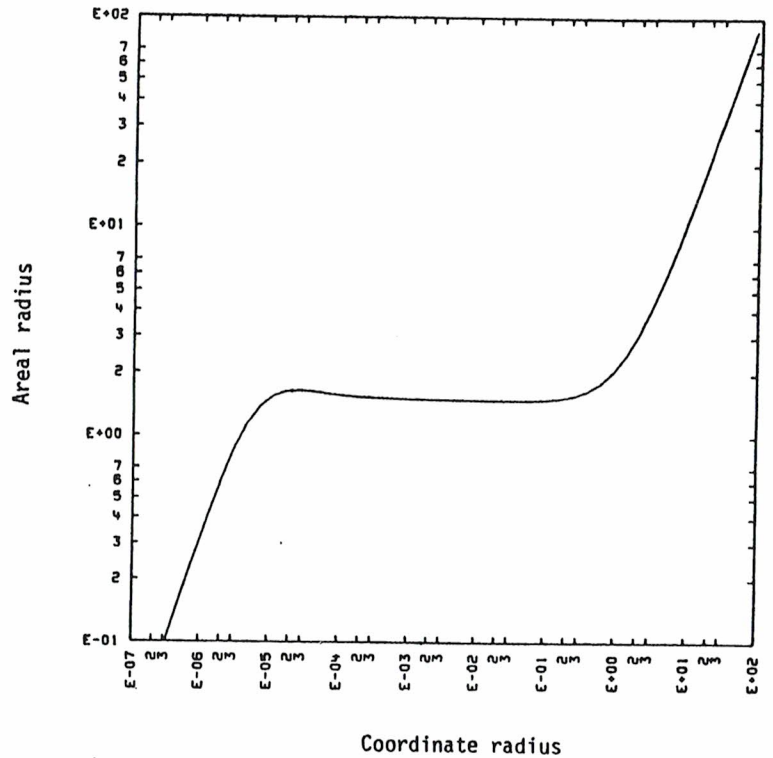

Figure 2e

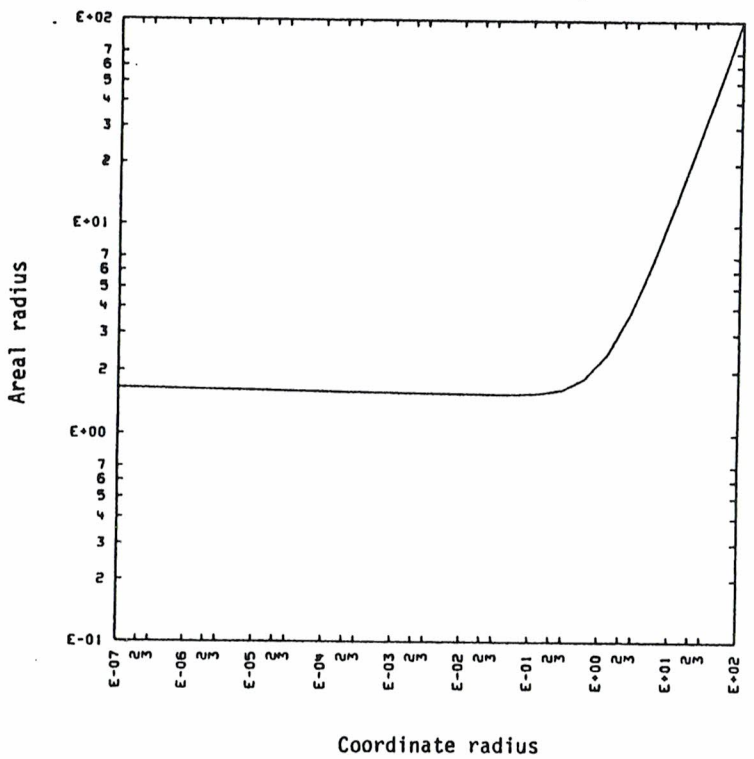

Figures 3a,b. Figure 3a displays the accurate control of the Hawking mass throughout a numerical evolution of nonspherical core collapse. The mass-energy is plotted on an absolute scale. For comparison, the highly relativistic nature of this collapse is indicated in Figure 3b by the central value of the lapse function.

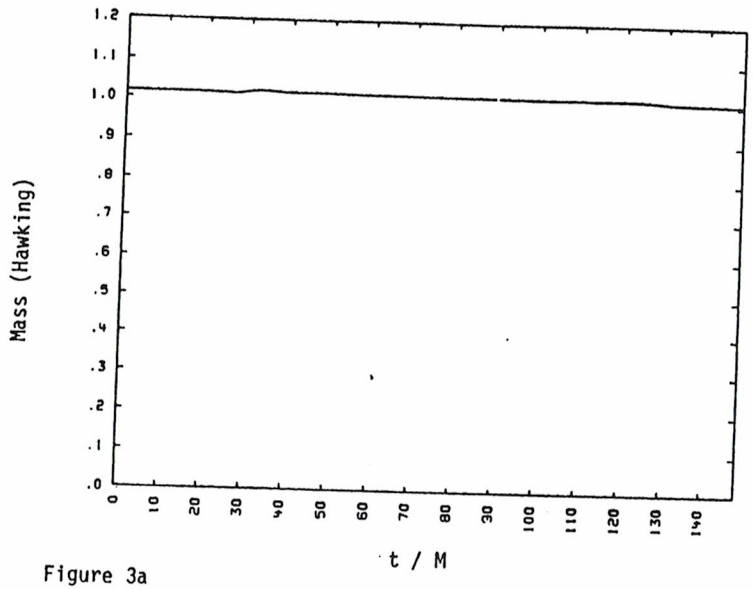

Figure 3a

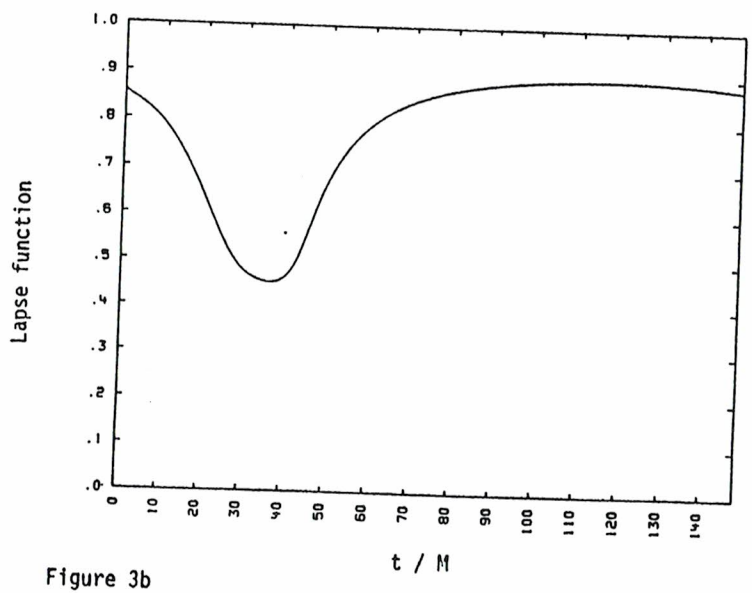

Figure 3b

b) Oblate Core Collapse

We next present some preliminary results from simulations of highly oblate core collapse and hydrodynamic bounce. Earlier relativistic two-dimensional hydrodynamic core bounce calculations have been produced by Wilson[7] and Smarr. A small one parameter survey has been conducted in which the cores were given initial data which produced successively deeper and more relativistic collapses. We will describe variations in a number of the features, e.g. gravitational radiation efficiency, lapse depth, maximum densities, quadrupole moments, mass-energy changes, etc., across this sequence.

First however, we describe the generic collapse model. In all these models, an adiabatic equation of state (II105) was used with $\Gamma = 2$ to model a stiff fluid (see Chapter II Appendix for restrictions on Γ in relativistic regimes). The starting point for setting up a collapsing oblate star is to produce an equilibrium spherical star, in this case an $n = 1$ ($\Gamma = 2$) polytrope, which is then altered. The initial models are constructed assuming Newtonian gravity. (These objects will start out fairly nonrelativistic typically, but in any case, once the constraints (IV63, 67a,b) are solved, the data will represent a proper relativistic configuration. Though these cores will no longer be in equilibrium, in due course the energy balance is even more drastically altered, so this is a somewhat minor concern.) The density profile of the $n = 1$ polytrope is

$$\rho = \rho_c \frac{\sin\xi}{\xi}, \qquad \xi = \frac{\pi r}{R_0} \tag{19}$$

where R_0 is the radius of the star. In assigning initial data, we typically depart from the dependence (19) by beginning to taper the density profile exponentially just prior to the first zero of (19). This ensures that the code always has some amount of fluid to push around. The central value, ρ_c, is determined by integrating ρ and units are chosen by setting the baryonic mass to unity. From (III21), this will be preserved even after transforming with ϕ to obtain proper relativistic data. However, as we describe momentarily, to this unit baryonic mass is added kinetic energy, internal energy (pressure), and, once the solution of the Hamiltonian constraint for the conformal factor ϕ has been obtained, a negative contribution of gravitational energy. In short, the total mass-energy of the system implicit in the asymptotic gravitational field will typically differ from unity, indicating some amount of binding energy (positive or negative). Before solving the constraints, however, we must conclude the specification of the free data.

We specify the internal energy density, or equivalently the pressure, by taking

$$p(r) = p_c \rho_c^{-2} \cdot \rho(r)^2 , \tag{20}$$

which from (III07) is consistent with $\Gamma = 2$. The value of p_c can be chosen, based on the radius R_0, to produce equilibrium. Instead, to

produce nonequilibrium configurations, this amount of pressure is multiplied globally by a set factor $f < 1$; for the models to be described we took $f = 0.62$. The densities are then ellipsoidally deformed to give the core some large initial oblateness; for the models described here, we took 1.5 :1 as the ratio of the equatorial to polar radii.

Considering the energy again, an equilibrium polytrope has a positive binding energy after the solution of the Hamiltonian constraint for ϕ as would have been expected from the Newtonian analog. The reduction in the pressure further increases the binding energy. We would like, however, to model as closely as possible, under the current circumstances, the collapse dynamics of a *stellar* core. The collapse of a degenerate iron core is initiated, typically by electron captures, at a radius on the order of a thousand times larger than the bounce radius. Hence, barring significant dissipative processes, the binding energy of the core will be nearly zero throughout the collapse with the remaining energy residing in the form of kinetic energy acquired during the infall.

Starting our calculation at such large radii would be prohibitively expensive because our Courant condition is determined by the light speed, not the hydrodynamic velocity. We therefore add to our collapse model an initial velocity field and start the calculation much closer to bounce. The magnitude of the velocity is taken to be proportional to ellipsoidal distance over the region of significant density. Outside the bulk of the core (typically beyond the 1% density contour), the velocity is tapered exponentially back toward

zero. This velocity field therefore gives the star an initial, nearly homologous motion. The proportionality constant between $|v|$ and ellipsoidal distance is chosen so that the integrated kinetic energy (in the Newtonian set up) is sufficient to give a nearly vanishing binding energy.

The hydrodynamic data is then determined merely by the specification of the initial core radius. The sequence of runs to be described is characterized by variations in the initial radius of the star, which then leads to variations in the density at the hydrodynamic bounce. The free gravitational field quantities, ℓnT and $\hat{K}_T^{ij}$, must also be specified. In these models we have simply taken

$$\ell nT = 0 \ , \qquad \hat{K}_T^{ij} = 0 \quad , \tag{21}$$

initially. This represents a fairly good choice to minimize the amount of initial gravitational radiation in the problem. However, we have essentially reached the point in these simulations where it is necessary to model, in the initial data, the small amount of gravitational radiation which would be present from the infall phase that occurs prior to the start of our integration. This is an area we will likely actively research soon. Finally, the constraints are solved producing proper initial data.

We are now in a position to describe a typical collapse calculation. Five runs have been produced along this sequence, which we label here as Run A through Run E in descending order of maximum

central density. The run to be described first is Run B. This object bounced at a central density of roughly 1.6×10^{15} g cm^{-3}, which is about six times higher than *nuclear density*[8]:

$$\rho_n = 2.5 \times 10^{14} \text{ g cm}^{-3} \quad . \tag{22}$$

Typical supernova calculations indicate bounce densities of 1.5 - 2.0 ρ_n,[8,9] so this run produces a much more relativistic object. The starting radius for this object is roughly 12 M. Figures 4a-f show the hydrodynamic state, density contours and velocity field vectors, at several stages during the collapse. Figure 4a depicts the start of the calculation and indicates the infall phase of the collapse. The small circular arc is a fiducial marker at a radius of 2 M indicative of the horizon size if the entire core forms a black hole. It therefore suggests the relative importance of relativistic effects. Notice that the linear scale of the figures changes during the collapse in order to keep the details of the core dynamics visible.

Figure 4b catches the formation of the primary recoil shock from the oblate bounce. The velocity vectors are exaggerated in length and most of the core remains unshocked. Hence the bounce is primarily adiabatic. (This is largely due to the stiff EOS.) This is also roughly the point of maximum oblateness. Figure 4c show the shock erupting from the core. The star continues to compress though re-expansion is occurring along the symmetry axis. In Figure 4d, the (incomplete) primary shock front is moving out through the more

Figures 4a-f. Rest energy density contours and velocity field vectors are plotted for one quadrant of the r, θ plane for the core. The vertical axis is the symmetry axis and the horizontal axis represents the equatorial plane. The rest of the core is inferred by symmetry. The fiducial circular arc indicates a radius r = 2M. Hydrodynamic milestones are described in the text.

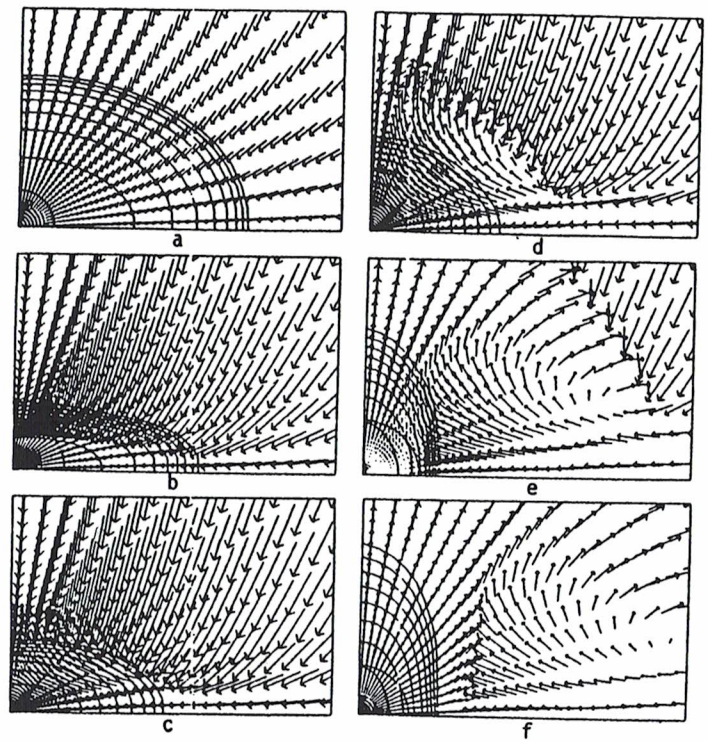

Figure 4

tenuous material surrounding the core. The star is passing roughly through the point of vanishing quadrupole moment and is close to maximum compression and the minimum central value of the lapse. The velocities in the core at this point are on the order of 0.3 -0.4 c. The fiducial arc, though difficult to see in Figure 4d, indicates the core radius is close to 4 M at this point. These facts reinforce the point that a collapse in this regime is not treatable by slow-motion or weak-field approximations.

In Figure 4e, a vortex is evident in the wake of the primary shock. In addition, prolate bounce is occurring and a secondary shock front is forming. Finally, in Figure 4f, the re-expansion phase has begun and the secondary shock is propagating outward.

In Figure 5a-h, we show a similar set of snapshots of the Bondi-Sachs flux (IV.64) integrand

$$r^2 AB\left[\frac{1}{A}\, a_r\, \ell nT - \lambda\right]^2 \quad . \tag{23}$$

Notice that the factor r^2 has been included, which produces in (23) an invariant amplitude for the pulse in the wave zone. The longitudinal part of the field dominates (23) in Figure 5a due to the rapid, nonspherical motion of the core. In Figure 5b, the longitudinal dependence is giving way to the nascent radiation pulse. The wave continues to grow in amplitude in Figures 5c-e as it proceeds through the induction zone: $r \lesssim \lambda_{WAVE}$. The wave has reached its invariant amplitude in Figures 5f and 5g. The inner edge of the wave zone

Figures 5a-h. The Bondi-Sachs flux integrand showing the formation and propagation of the gravitational wave pulse is plotted over one quadrant of the r, θ plane. The equatorial plane is on the left and the symmetry axis is to the right. Note the $\sin^4\theta$ radiation pattern.

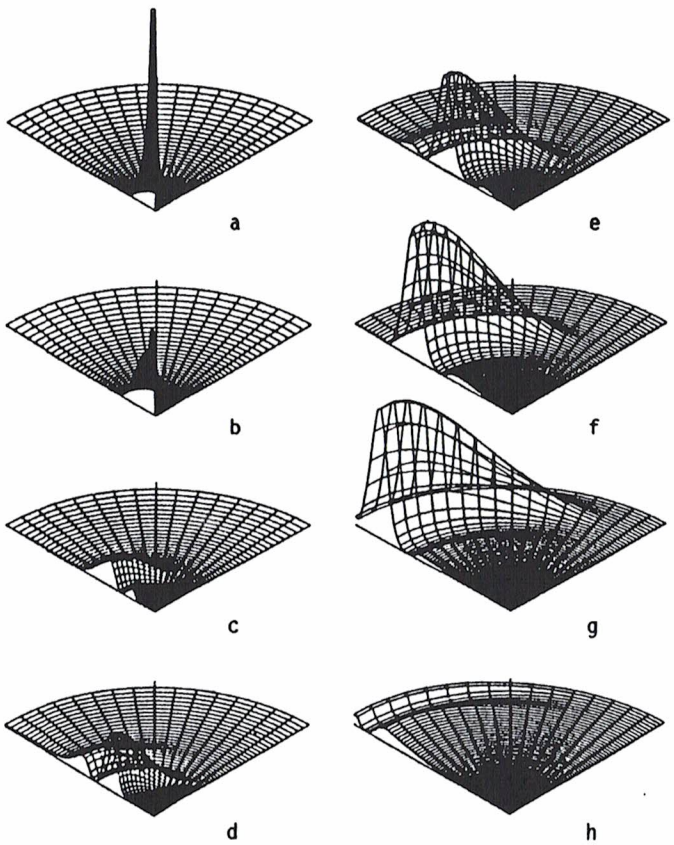

Figure 5

appears from our simulations to be at just about one λ_{WAVE}. The main pulse has clearly propagated off the mesh in Figure 5h. It is also important to notice the dominant quadrupolar nature of the radiation emission as evidenced by the obvious $\sin^4\theta$ radiation pattern.

We conclude this description of Run B by displaying the lapse function as an indication of the strength of the gravitational field. Asymptotically, or in weak field, the gravitational potential Φ is related to the lapse by

$$\Phi \cong 1 - \alpha \quad . \tag{24}$$

Typical values are $\Phi \approx 10^{-6}$ on the solar surface and $\Phi \approx 10^{-3}$ on a white dwarf. In Figures 6a, b, the lapse function is shown at the beginning of the simulation and near the point of maximum compression. The extreme relativistic nature of the object is evident, with $1 - \alpha \approx 0.45$ in Figure 6b.

Before leaving our discussion of generic features from these calculations, mention must be made of the gravitational waveforms that we calculate and are of so much interest to us. We have already indicated that we do not as yet place a high degree of confidence in our calculated waveforms. The waveform resulting from Run D is displayed in Figure 7a. This run is of great interest because the maximum density that occurred during the bounce was $\rho_c \approx 5.0 \times 10^{14}$ g cm^{-3}, or roughly twice nuclear density (22) and therefore close to values indicative of realistic supernova models. In Figure 7b, this waveform

Figures 6a,b. The lapse function plotted over one quadrant of the r, θ plane. Axes are as in Figure 5a-h. Figure 6a depicts the lapse at the start of the calculation. Figure 6b represents roughly the point of maximum compression.

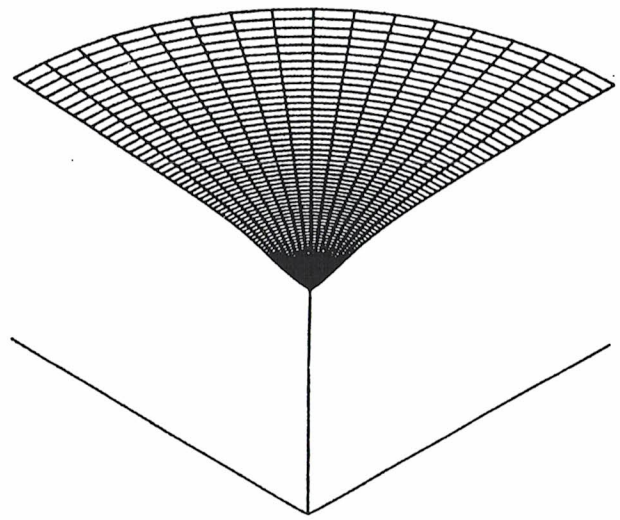

Figure 6a

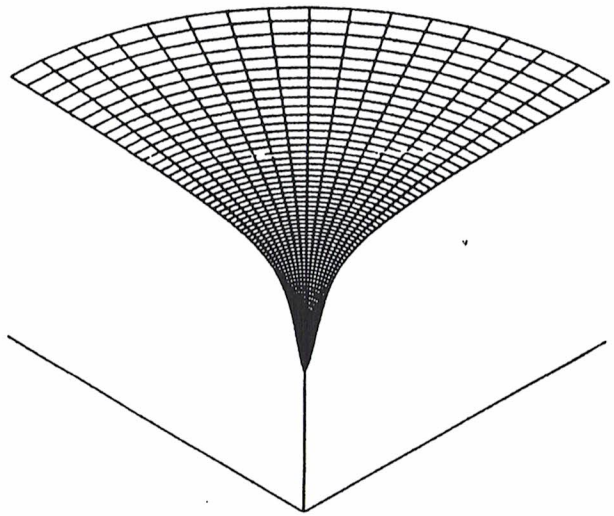

Figure 6b

Figures 7a,b. Figure 7a depicts the gravitational waveform generated by the collapse as calculated with our code. Figure 7b shows both the above waveform and the quadrupole formalism predicted waveform.

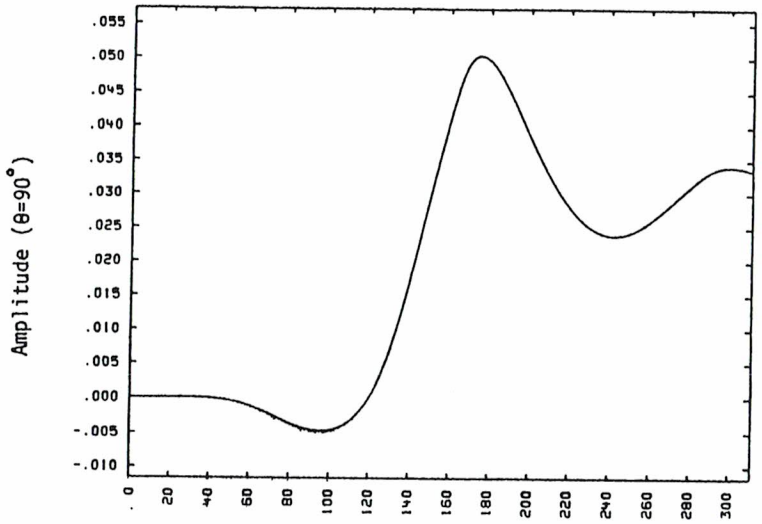

Figure 7a

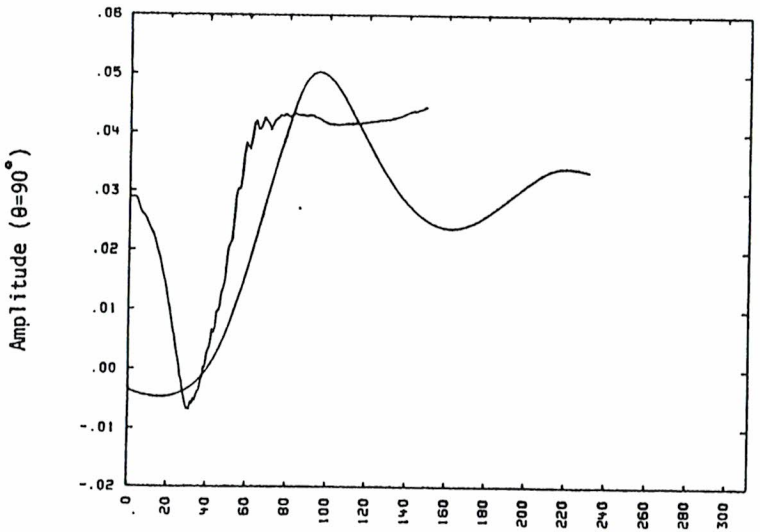

Figure 7b

is compared to the quadrupole formalism predicted waveform given by

$$h_+^{\,I} = \frac{3}{2r}\,\ddot{I}_{ZZ}\cdot\sin^2\theta \quad , \tag{25}$$

in axisymmetry. Here I_{ZZ} is given by

$$I_{ZZ} = \int d^3x \left(Z^2 - \frac{1}{3}r^2\right)\rho = 2\pi \int dr\, d\theta\, r^4 \sin\theta \left(\cos^2\theta - \frac{1}{3}\right)\rho \quad , \tag{26}$$

and this is a gauge dependent result. Hence, we only expect agreement between the self-consistently calculated waveform produced by the code and (25) in the limit of weak-field and slow-motion sources. For Run D we do not in fact find agreement, and we will discuss this discrepancy below. Nonetheless, Figure 7b indicates several concerns about the self-consistent waveform. First, our assumption of the initial data given in (21) apparently depresses the early behavior of our waveform. The late ringing behavior is also suspect, relating to the gauge problems at the outer boundary discussed earlier in this chapter. What the calculation is probably getting right and what is most important for calculating the gravitational radiation efficiency (i.e. the fractional loss of system mass-energy to the gravitational waves), is the rapid rise of the waveform near t = 150 M (in Figure 7a). This is because the flux is dependent on the time rate of change of h_+.

Having described some details from individual collapse calculations, we conclude our discussion by relating results from the sequence of runs. We have said that the models on this sequence are characterized by the initial assumed radius. The specification of

the thermodynamic state of these objects is such that different initial radii lead to varying bounce densities. So while it is not known ahead of time, the maximum density at bounce can also be used to characterize the calculation. These densities are given in Table 1 in units of nuclear density (22) for the sequence of runs. Also given there is the minimum central value of the lapse function that occurred during the calculation, indicating the relative strength of relativistic effects. The total time-integrated Bondi-Sachs energy loss is tabulated as a gravitational radiation efficiency (fraction of M radiated).

The quadrupole moment formalism predicts an angle integrated gravitational radiation flux of

$$\frac{dE^{(quad)}}{dt} = \frac{3}{10} \dddot{I}_{ZZ}^{\,2} \quad , \tag{27}$$

from (25). This is a gauge specific result, but how inaccurate is it? It is sometimes off-handedly stated that for a supernova core bounce, the general relativistic effects are only 15%, so general relativistic corrections are not needed to compute the gravitational radiation to this level of accuracy. One simply calculates a Newtonian collapse model and uses the quadrupole formula.

However, the term 15% effects usually refers to the gravitational potential at the *surface* of the core. The "potential" in the interior can be on the order of 40%. If this is regarded as the size of deviations in the metric components from flat space, then it is

TABLE 1

Run	ρ_c^{max}/ρ_n	α_c^{min}	$\Delta E^{code}/M$	$\Delta E^{quad_1}/M$	$\Delta E^{quad_2}/M$
A	11.2	0.46	0.0072	0.017	0.13
B	6.4	0.55	0.0023	0.014	0.046
C	4.0	0.62	0.0047	0.015	0.023
D	2.0	0.71	0.0058	0.012	0.0063
E	0.2	0.88	0.0030	0.0021	0.0011

also the size of relative changes in tensors under gauge transformations. This level of uncertainty would be significant by itself. However, inspection of (25) - (27) reveals that the quadrupole flux depends upon high powers of the coordinate radius {10} and time coordinate {6}. Hence, 40% effects due to gauge changes in the spatial and time coordinates will tend to make (27) uncertain to factors of 2 to 5.

We have calculated (27) after making an approximate spatial gauge change. This is done within the context of the existing collapse calculation by computing the quadrupole moment (26) with a new radial coordinate defined by

$$\bar{r} = Ar \quad . \tag{28}$$

This gives an altered quadrupole moment of

$$I_{ZZ} = 2\pi \int d(Ar)d\theta(Ar)^4 \sin\theta\left(\cos^2\theta - \frac{1}{3}\right)\rho \quad . \tag{29}$$

This roughly mocks the quadrupole moment which would be calculated in the radial gauge[10] (though still computing (27) with maximal time slicing). In any case, it gives the quadrupole formula in α different gauge.

The results of computing the quadrupole flux with these two different expressions is shown in the last two columns. The first is the result from our gauge; the second from (29). There is significant disagreement between the two, and with the code calculated energy loss, even for Run D the supernova density bounce. We regard the

difference between the two quadrupole results as evidence of inappropriateness for gravitational collapse to these densities. Notice that the second quadrupole formula predicts in Run A 13% mass loss to gravitational radiation!

The quadrupole formula is suspect on yet another ground. It depends for its validity on the slow-motion approximation. Yet even for the Run D collapse, the velocities in the core during the bounce are of order 0.3 c. This gives *phase shifts* across the core of roughly 60°. Hence a significant amount of destructive interference is likely to occur.

In connection with these comments on the quadrupole formula, we show the two quadrupole waveforms (25) at $\theta = \frac{\pi}{2}$ for these runs in Figures 8a-e. Notice the convergence in the results in progressing toward Run E. We also show in Figures 9-13 the time variation of the Hawking mass and the time-integrated Bondi-Sachs flux, as a function of time, for these five runs. Notice the consistent agreement between the final drop in the Hawking mass and the radiated energy. We see for the first time in these calculations, due to improved accuracy in the technique, the effect of the radiation reaction on the mass of the system. The variations in the Hawking mass, prior to the arrival of the radiation pulse at the edge of the mesh, are on the order of 1%. Since the lowest order gauge effects are not present in M_H at finite r (IV152), the origin of this variation is not known. It may however be related to the previously described boundary condition error in the

Figures 8a-e. These show the equatorial restriction of the quadrupole waveforms in our gauge (Curves A) and in the transformed, nearly radial gauge (Curves B) for Runs A through E, respectively. Note the convergence of the waveforms toward Run E.

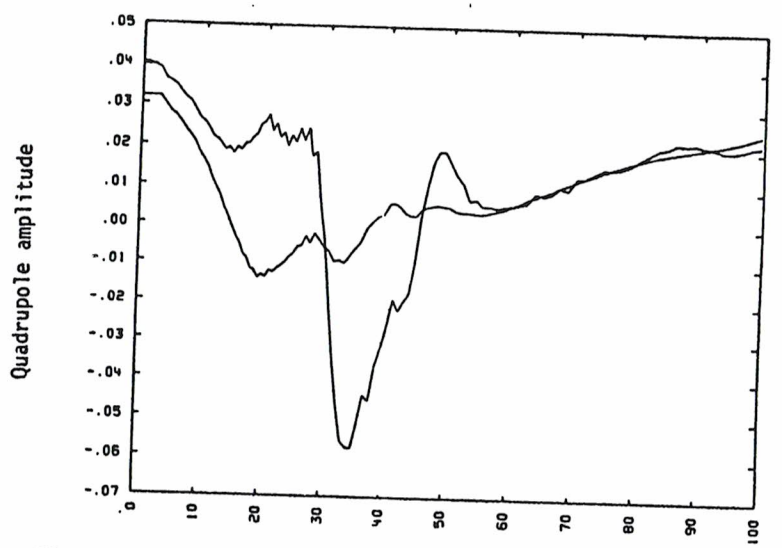

Figure 8a

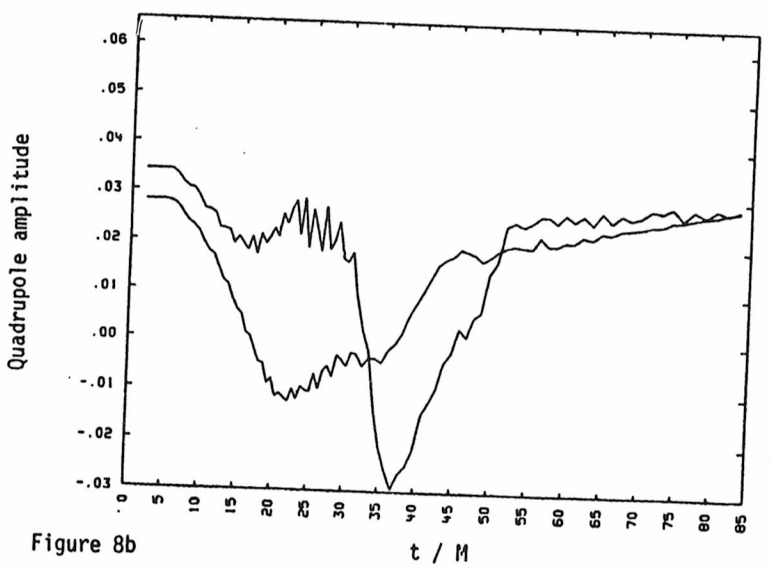

Figure 8b

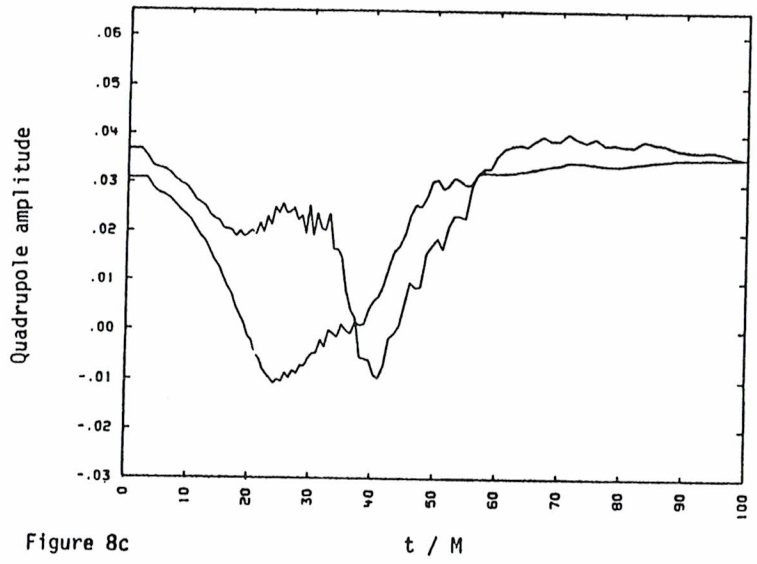

Figure 8c

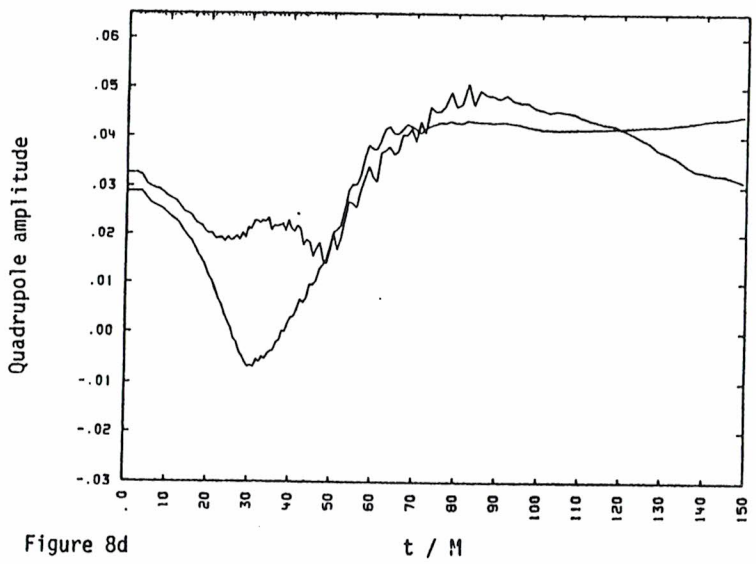

Figure 8d

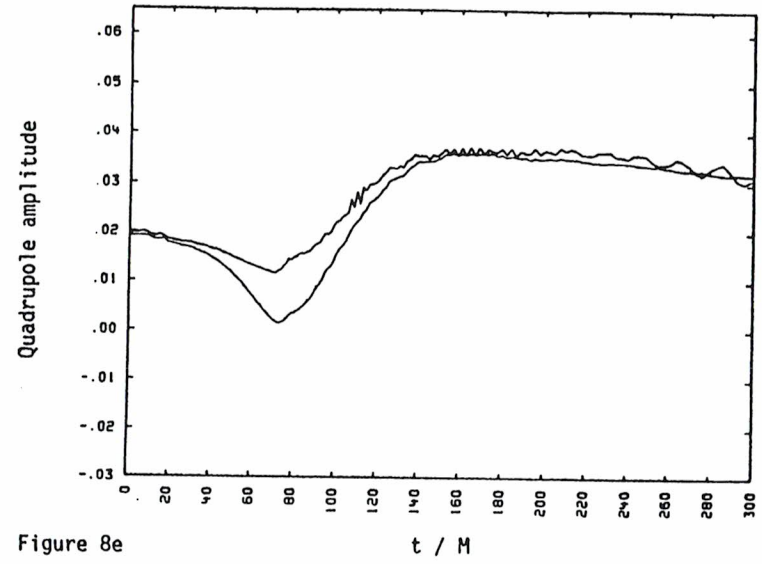

Figure 8e

Figures 9-13. In the (a) plots are given the time variation of the Hawking mass and the time-integrated Bondi-Sachs flux. Notice that when the gravitational wave pulse reaches the edge of the mesh a consistent drop in the Hawking mass occurs. The radiation reaction on the mass of the source is thus visible in our calculations. The (b) plots show the variation of the lapse on the same time scale. Notice the correlation between the variations of the Hawking mass in the early phase with the violence of the core.

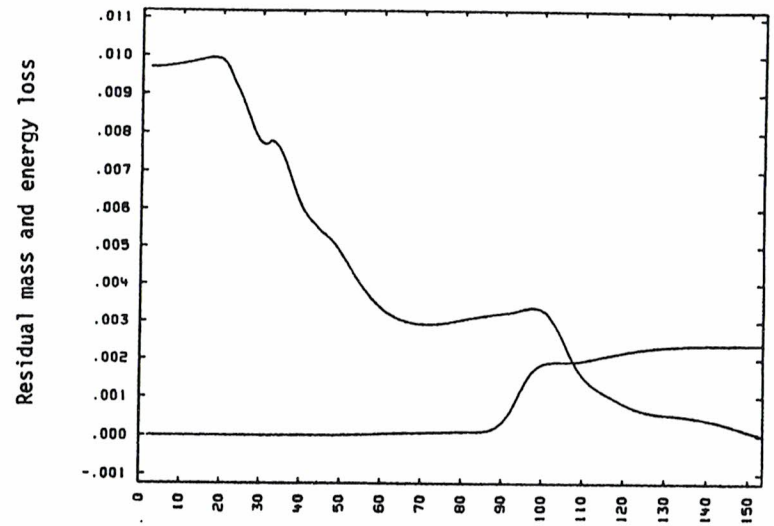

Figure 9a

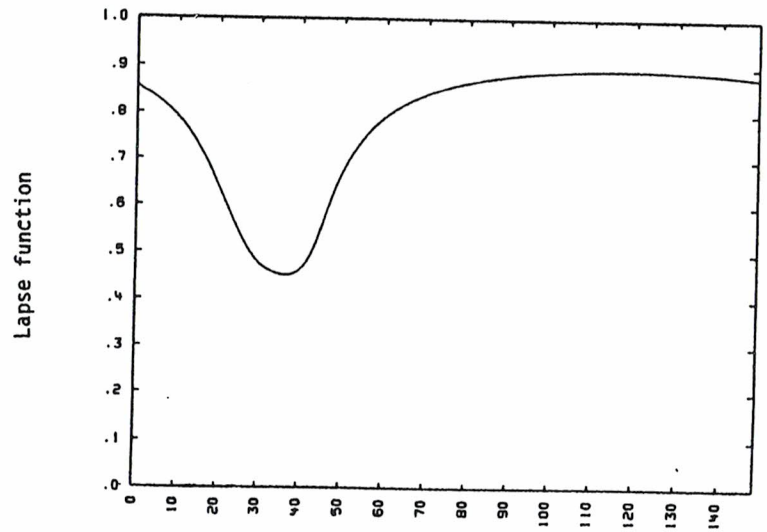

Figure 9b

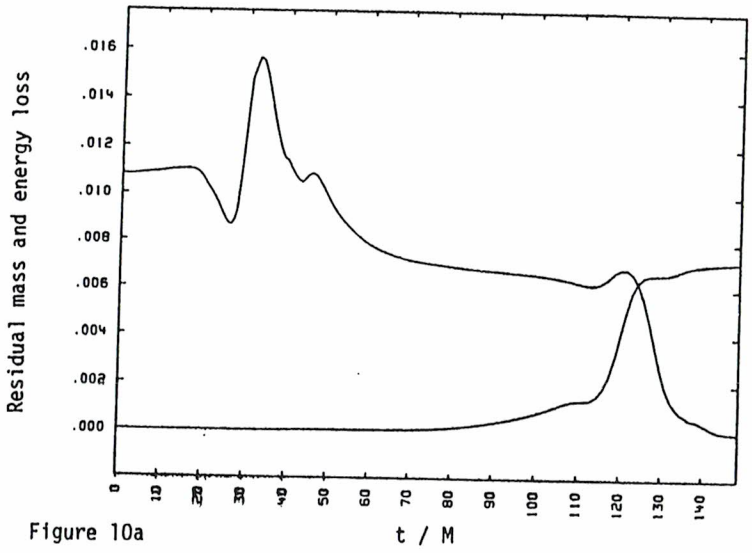

Figure 10a

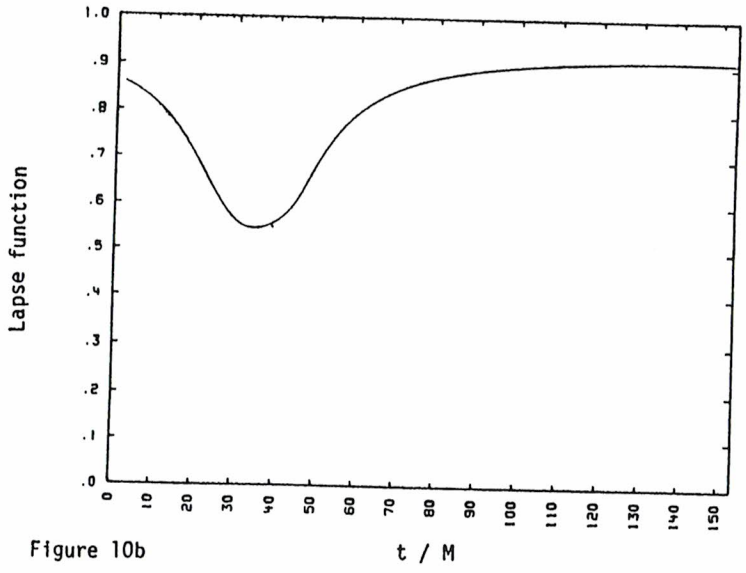

Figure 10b

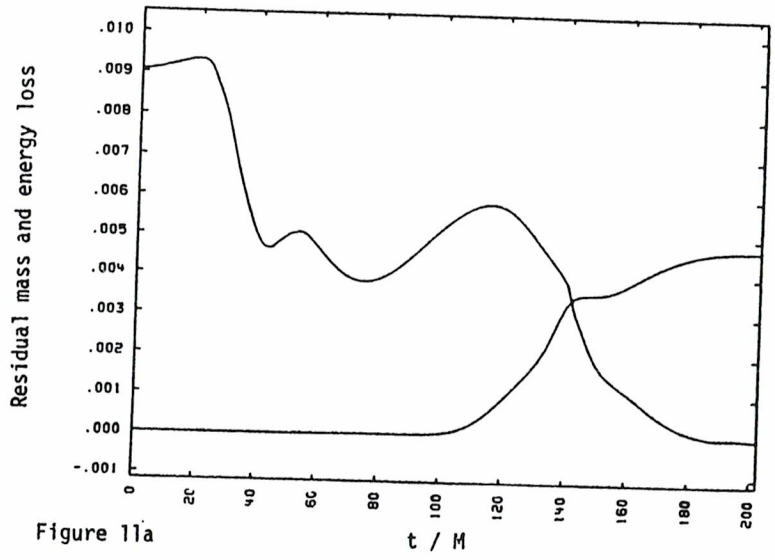

Figure 11a

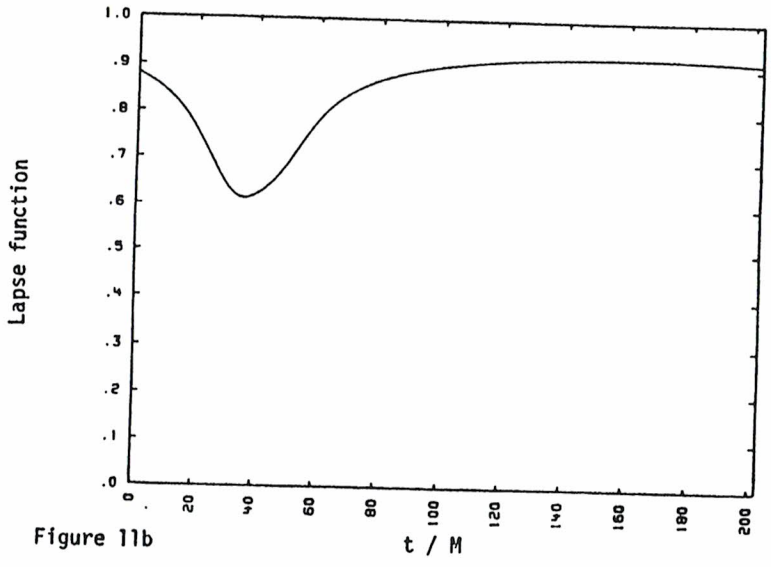

Figure 11b

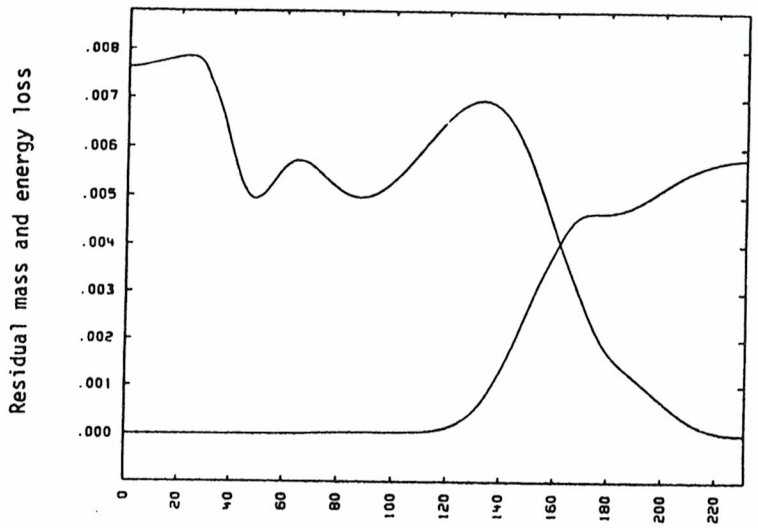

Figure 12a

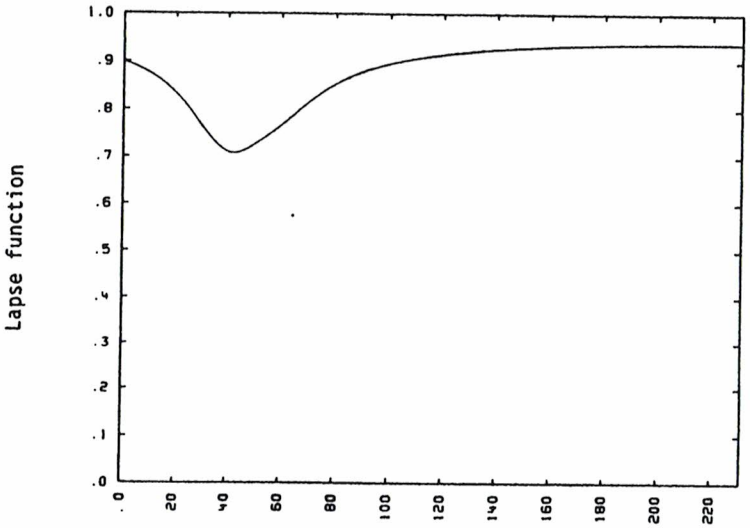

Figure 12b

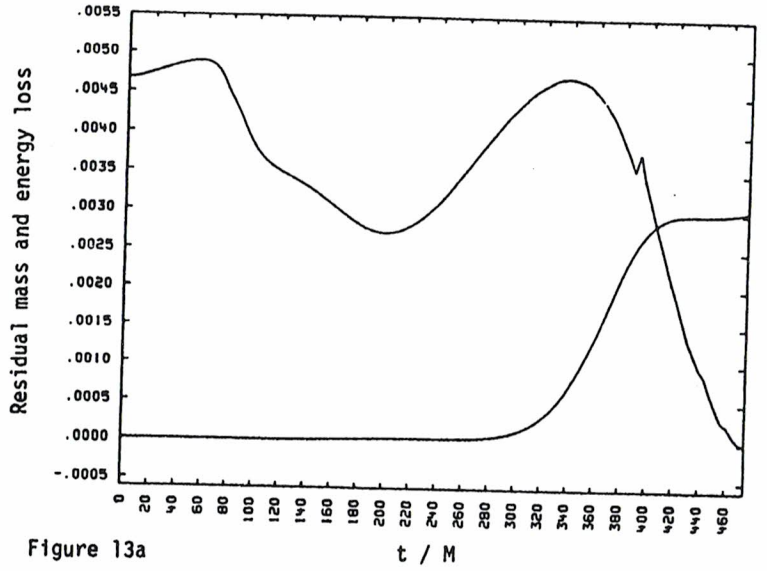

Figure 13a

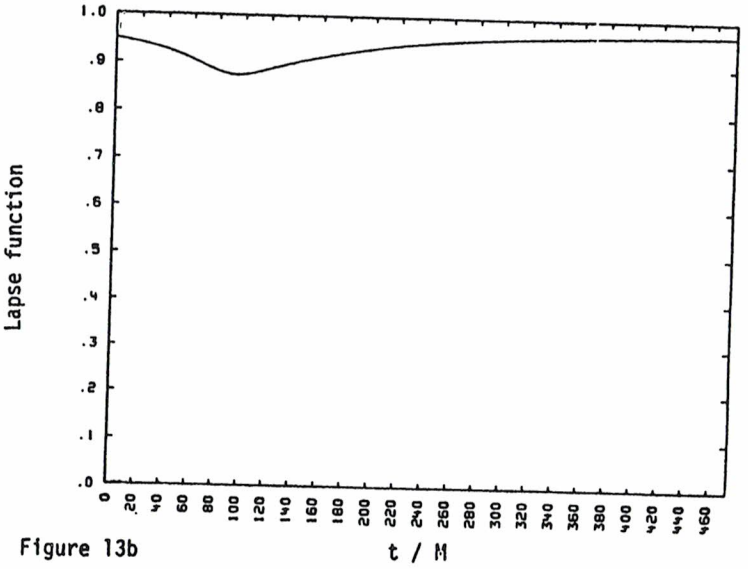

Figure 13b

wave quantities. If true and this problem is corrected, then the static $\mathcal{O}\left(\frac{M}{r}\right)$ correction to $M_H(r)$ can be accounted for and measurments of the mass at finite radius may be extended to accuracy on the order of 1 part in 10^4.

Chapter VI References

1. Brill (1959).
2. Schoen and Yau (1979).
3. Witten (1981).
4. Eppley (1977).
5. Dykema (1980).
6. Shapiro and Teukolsky (1980).
7. Wilson (1979).
8. Bowers and Wilson (1982).
9. Wilson, private communication.
10. Bardeen and Piran (1983).

CHAPTER VII

CONCLUSIONS

We have presented a fully constrained approach within the ADM formalism to solving the Einstein equations of general relativity and the relativistic hydrodynamic equations. Utilizing the maximal time slicing condition and a simplifying spatial gauge (quasi-isotropic coordinates), this method was shown reduced down to the final differential equations that are required to simulate axisymmetric nonrotating asymptotically flat spacetimes. The method is therefore aimed toward applications of studying issues relevant to gravitational collapse of stellar cores and collapse of supermassive stars. Numerical techniques and a computer code have been developed to implement this analytic approach.

We have been able to surmount several problems that have plagued previous efforts on this project. The York approach to identifying a constrained part of the extrinsic curvature has been used to produce much improved initial data substantially free of spurious pre-existing gravitational radiation. A numerical regularization technique has been developed to allow accurate finite differencing of coupled elliptic systems near the singular points of the coordinate system. A new adaptive mesh zoning criterion has been used which is successful in maintaining good resolution of both the wave zone and the core during gravitational collapse.

Results from runs with our code indicate substantial accuracy. For the first time we are able to hold the various quasi-local mass indicators constant throughout the collapse to within 1% typically. Also, for the first time we are able to see directly the radiation reaction effect on the mass (loss) of the system. We anticipate conducting a rigorous series of code tests in the near future and then producing a survey of collapse models to study gravitational collapse issues. We believe that sufficient understanding has been developed during the course of this work to now allow the construction of a code to simulate rotating collapse with magnetic fields and a realistic nuclear equation of state. Then realistic stellar collapse models, including general relativity self-consistently calculated, can be produced on the computer to obtain astrophysically possible gravitational radiation waveforms and energy loss efficiencies.

BIBLIOGRAPHY

Ames, W. F., Numerical Methods for Partial Differential Equations, 2nd Ed., Academic Press, New York, 1977.

Arnowitt, R. Deser, S., Misner, C. W., "The Dynamics of General Relativity," Gravitation: An Introduction to Current Research, ed. L. Witten, John Wiley, New York, 1962.

Bardeen, J. M., "Gauge and Radiation Conditions in Numerical Relativity," Gravitational Radiation, eds. N. Deruelle and T. Piran, North-Holland, Amsterdam, 1983.

Bardeen, J. M. and Piran, T., "General Relativistic Axisymmetric Rotating Systems: Coordinates and Equations," Phys. Reports 96, 206 (1983).

Barton, R., personal communication, 1984.

Berger, M. and Ebin, D., "Some Decompositions of the Space of Symmetric Tensors," J. Diff. Geom. 3, 379 (1969).

Bondi, H., "Spherically Symmetric Models in General Relativity," Mon. Not. Roy. Astron. Soc. 107, 410 (1947).

Bondi, H., Van der Burg, M. G. J., and Metzner, A. W. K., "Gravitational Waves in General Relativity VII. Waves from Axi-Symmetric Isolated Systems," Proc. Roy. Soc. A269, 21 (1962).

Bowen, J. M., "Initial Value Problems on Non-euclidean Topologies," Ph.D. Dissertation, University of North Carolina at Chapel Hill, 1979.

Bowen, J. M. and York, J. W., "Time Asymmetric Initial Data for Black Holes and Black Hole Collisions," Phys. Rev. D21, 2047 (1980).

Bowers, R. L. and Wilson, J. R., "A Numerical Model for Stellar Core Collapse Calculations," Astrophys. J. Supp. 50, 115 (1982).

Brill, D. R., "On the Positive Definite Mass of the Bondi-Weber-Wheeler Time-Symmetric Gravitational Waves," Ann. Phys. 7, 466 (1959).

Callen, H. B., Thermodynamics, Wiley, New York, 1960.

Cantor, M., "Spaces of Functions with Asymptotic Conditions," Indiana Univ. Math. J. 24, 897 (1974).

Cantor, M., "A Necessary and Sufficient Condition for York Data to Specify an Asymptotically Flat Spacetime," J. Math. Phys. 20, 1741 (1979a).

Cantor, M., "Some Problems of Global Analysis on Asymptotically Simple Manifolds," Compositio Math. 38, 3 (1979b).

Cantor, M. and Piran, T., "Conformally Connected Universes," Gen. Rel. and Grav., (to appear), (1982).

Centrella, J. M., "Plane-Symmetric Cosmologies: A Study of Inhomogeneities in the Universe using Numerical Relativity," Ph.D. Dissertation, University of Cambridge, England, 1979.

Centrella, J. and Matzner, R. A., "Plane Symmetric Cosmologies," Astrophys. J. 230, 311 (1979).

Centrella, J. and Wilson, J. R., "Planar Numerical Cosmology I. The Differential Equations," Astrophys. J. 273, 428 (1983).

Chaljub-Simon, A. and Choquet-Bruhat, Y., "Global Solutions of the Lichnerowicz Equation in General Relativity on an Asymptotically Euclidean Complete Manifold," Gen. Rel. and Grav. 12, 175 (1980).

Choquet-Bruhat, Y., "The Cauchy Problem," Gravitation: An Introduction to Current Research, ed. L. Witten, John Wiley, New York, 1962.

Choquet-Bruhat, Y., DeWitt-Morette, C., and Dillard-Bleick, M., Analysis, Manifolds and Physics, North-Holland, Amsterdam, 1977.

Chrzanowski, P., Talk at the Yale Workshop on the Dynamical Construction of Spacetime, (unpublished), (1977); see Smarr (1979).

Crowley, W. P., Numerical Methods in Fluid Dynamics, Lawrence Livermore Laboratory, UCRL-51824, 1975.

Davis, M., Ruffini, R., Press, W. H., and Price, R. H., "Gravitational Radiation from a Particle Falling Radially into a Schwarzschild Black Hole," Phys. Rev. Lett. 27, 1466 (1971).

Deser, S., "Covariant Decompositions of Symmetric Tensors and the Gravitational Cauchy Problem," Ann. Inst. Henri Poincaré 7, 149 (1967).

Dykema, P. G., "Numerical Simulation of Axisymmetric Gravitational Collapse," Ph.D. Dissertation, The University of Texas at Austin, 1980.

Eardley, D., "Global Problems in Numerical Relativity," Sources of Gravitational Radiation, ed. L. Smarr, Cambridge University Press, Cambridge, 1979.

Eardley, D., unpublished results, 1983.

Eardley, D. M. and Smarr, L., "Time Functions in Numerical Relativity: Marginally Bound Dust Collapse," Phys. Rev. D19, 2239 (1979).

Eckart, C., "The Thermodynamics of Irreversible Processes, III: Relativistic Theory of the Simple Fluid," Phys. Rev. 58, 919 (1940).

Eppley, K. R., "The Numerical Evolution of the Collision of Two Black Holes," Ph.D. Dissertation, Princeton University, 1975.

Eppley, K. R., "Evolution of Time-symmetric Gravitational Waves: Initial Data and Apparent Horizons," Phys. Rev. D16, 1609 (1977).

Estabrook, F., Wahlquist, H., Christensen, S., DeWitt, B., Smarr, L., and Tsiang, E., "Maximally Slicing a Black Hole," Phys. Rev. D7, 2814 (1973).

Evans, C. R., "A Method for Numerical Simulation of Gravitational Collapse and Gravitational Radiation Generation," Numerical Astrophysics: A Meeting in Honor of James Wilson, eds. J. Centrella, R. Bowers, J. LeBlanc, and M. LeBlanc, Jones and Bartlet, San Francisco, 1984.

Evans, C. R., Smarr, L. L., and Wilson, J. R., "Numerical Relativistic Gravitational Collapse with Spatial Time Slices," Radiation Hydrodynamics, Reidel, Dordrecht, 1984.

Goddard, A. J., "A Generalization of the Concept of Constant Mean Curvature and Canonical Time," Gen. Rel. and Grav. 8, 525 (1977).

Hahn, S. G. and Lindquist, R. W., "The Two Body Problem in Geometrodynamics," Ann. Phys. 29, 304 (1964).

Hawking, S. W., "Gravitational Radiation in an Expanding Universe," J. Math. Phys. 9, 598 (1968).

Hawking, S. W. and Ellis, G. F. R., The Large Scale Structure of Space-Time, Cambridge University Press, Cambridge, 1973.

Hawley, J. F., Smarr, L. L., and Wilson, J. R., "A Numerical Study of Nonspherical Black Hole Accretion. I. Equations and Test Problems," Astrophys. J. Supp. 55, 211 (1984).

Hellwig, G., Differential Operators of Mathematical Physics, Addison-Wesley, Reading, Mass., 1967.

Isaacson, R. A., Welling, J. S., and Winicour, J., "Null Cone Computation of Gravitational Radiation," J. Math. Phys. 24, 1824 (1983).

Landau, L. D. and Lifshitz, E. M., Fluid Mechanics, Pergamon Press, London, 1959.

Leith, C. E., "Numerical Simulation of the Earth's Atmosphere," Methods in Computational Physics 4, 1 (1965).

Lichnerowicz, A., "L'Integration des Équations de la Gravitation Relativiste et le Problème des n Corps," J. Math. Pures et Appl. 23, 37 (1944).

Lichnerowicz, A., Théories Relativistes de la Gravitation et de L'Electromagnetisme, Masson and Cie, Paris, 1955.

Lichnerowicz, A., Relativistic Hydrodynamics and Magnetohydrodynamics, Benjamin, New York, 1967.

Mathews, J., "Gravitational Multipole Radiation," J. Soc. Indust. Appl. Math. 10, 768 (1962).

May, M. M. and White, R. H., "Hydrodynamic Calculations of General-Relativistic Collapse," Phys. Rev. 141, 1232 (1966).

May, M. M. and White, R. H., "Stellar Dynamics and Gravitational Collapse," Methods in Computational Physics, Vol. 7, Academic Press, New York, 1967.

Misner, C. W. and Sharp, D. H., "Relativistic Equations for Adiabatic, Spherically Symmetric Gravitational Collapse," Phys. Rev. 136, B571 (1964).

Misner, C. W., Thorne, K. S., and Wheeler, J. A., Gravitation, W. H. Freeman, San Francisco, 1973.

Moncrief, V., "Decomposition of Gravitational Perturbations," J. Math. Phys. 16, 493 (1975).

Morse, P. M., Feshbach, H., Methods of Theoretical Physics, 2 pt., McGraw-Hill, New York, 1953.

Nakamura, T. K., "General Relativistic Collapse of Axially Symmetric Stars Leading to the Formation of Black Holes," Prog. Theo. Phys. 65, 1876 (1981).

Newman, E. and Penrose, R., "An Approach to Gravitational Radiation by a Method of Spin Coefficients," J. Math. Phys. 3, 566 (1962).

Newman, E. and Penrose, R., "Errata: An Approach to Gravitational Radiation by a Method of Spin Coefficients," J. Math. Phys. 4, 998 (1963).

Ó Murchadha, N. and York, J. W., "Existence and Uniqueness of Solutions of the Hamiltonian Constraint of General Relativity on Compact Manifolds," J. Math. Phys. 14, 1551 (1973).

Ó Murchadha, N. and York, J. W., "Initial-Value Problem of General Relativity. I. General Formulation and Physical Interpretation," Phys. Rev. D10, 428 (1974).

Oppenheimer, J. R. and Snyder, H., "On Continued Gravitational Contraction," Phys. Rev. 56, 455 (1939).

Piran, T., "Numerical Codes for Cylindrical General Relativistic Systems," J. Comp. Phys. 35, 254 (1980).

Piran, T., "Coordinate Conditions for Numerical Relativity," preprint of lecture at the Third Marcel Grossmann Meeting, Shanghai, China, 1982.

Piran, T., "Methods of Numerical Relativity," Gravitational Radiation, eds. N. Deruelle and T. Piran, North-Holland, Amsterdam, 1983.

Reinhart, B. L., "Maximal Foliations of Extended Schwarzschild Space," J. Math. Phys. 14, 719 (1973).

Roache, R. J., Computational Fluid Dynamics, Hermosa Publishers, Albuquerque, 1976.

Sachs, R. K., "Gravitational Waves in General Relativity VIII. Waves in Asymptotically Flat Spacetime," Proc. Roy. Soc. A270, 103 (1962).

Schoen, P. and Yau, S. T., "On the Proof of the Positive Mass Conjecture in General Relativity," Commun. Math. Phys. 65, 45 (1979).

Shapiro, S. L. and Teukolsky, S. A., "Gravitational Collapse to Neutron Stars and Black Holes: Computer Generation of Spherical Spacetimes," Astrophys. J. 235, 199 (1980).

Smarr, L. L., "The Structure of General Relativity with a Numerical Illustration: The Collision of Two Black Holes," Ph.D. Dissertation, The University of Texas at Austin, 1975.

Smarr, L., "Gauge Conditions, Radiation Formulae and the Two Black Hole Collision," Sources of Gravitational Radiation, ed. L. Smarr, Cambridge University Press, Cambridge, 1979.

Smarr, L., Čadež, A., DeWitt, B., and Eppley, K., "Collision of Two Black Holes: Theoretical Framework," Phys. Rev. D14, 2443 (1976).

Smarr, L., Taubes, C., and Wilson, J. R., "General Relativistic Hydrodynamics: The Comoving, Eulerian, and Velocity Potential Formalisms," Essays in General Relativity, ed. F. J. Tipler, Academic Press, New York, 1980.

Smarr, L. and York, J. W., "Radiation Gauge in General Relativity," Phys. Rev. D17, 1945 (1978a).

Smarr, L. and York, J. W., "Kinematical Conditions in the Construction of Spacetime," Phys. Rev. D17, 2529 (1978b).

Stark, R. and Piran, T., preprint, 1984.

Synge, T. L., "Relativistic Hydrodynamics," Proc. Lond. Math. Soc., Ser. II 43, 376 (1937).

Taub, A. H., "On Circulation in Relativistic Hydrodynamics," Arch. Ration. Mech. Anal. 3, 312 (1959).

Taub, A. H., "Relativistic Fluid Mechanics," Ann. Rev. Fluid Mech. 10, 301 (1978).

Teukolsky, S. A., "Linearized Quadrupole Waves in General Relativity and the Motion of Test Particles," Phys. Rev. D26, 745 (1982).

Thorne, K. S., "Gravitational-wave Research: Current Status and Future Prospects," Rev. Mod. Phys. 52, 285 (1980a).

Thorne, K. S., "Multipole Expansions of Gravitational Radiation," Rev. Mod. Phys. 52, 299 (1980b).

Tolman, R. C., "Effect of Inhomogeneity on Cosmological Models," Proc. Nat. Acad. Sci. 20, 169 (1934).

von Neumann, J. and Richtmyer, R. D., "A Method for the Numerical Calculation of Hydrodynamic Shocks," J. Appl. Phys. 21, 232 (1950).

Weinberg, S., Gravitation and Cosmology: Principles and Applications of the General Theory of Relativity, John Wiley & Sons, New York, 1972.

Welling, J. S., "Numerical Calculations in the Characteristic Initial Value Problem in General Relativity," Ph.D. Dissertation, University of Pittsburgh, 1983.

Wilson, J. R., "A Numerical Method for Relativistic Hydrodynamics," Sources of Gravitational Radiation, ed. L. Smarr, Cambridge University Press, Cambridge, 1979.

Witten, E., "A New Proof of the Positive Energy Theorem," Commun. Math. Phys. 80, 381 (1981).

York, J. W., "Gravitational Degrees of Freedom and the Initial-Value Problem," Phys. Rev. Lett. 26, 1656 (1971).

York, J. W., "Role of Conformal Three Geometry in the Dynamics of Gravitation," Phys. Rev. Lett. 28, 1082 (1972).

York, J. W., "Conformally Invariant Orthogonal Decomposition of Symmetric Tensors on Riemannian Manifolds and the Initial-Value Problem of General Relativity," J. Math. Phys. 14, 456 (1973).

York, J. W., "Kinematics and Dynamics of General Relativity," Sources of Gravitational Radiation, ed. L. Smarr, Cambridge University Press, Cambridge, 1979.

York, J. W., "Energy and Momentum of the Gravitational Field," Essays in General Relativity, ed. F. J. Tipler, Academic Press, New York, 1980.

York, J. W., "The Initial Value Problem and Dynamics," Gravitational Radiation, eds. N. Deruelle and T. Piran, North-Holland, Amsterdam, 1983.

York, J. W. and Piran, T., "The Initial Value Problem and Beyond," Spacetime and Geometry, eds. R. Matzner and L. Shepley, University of Texas Press, Austin, 1982.

Zerilli, F. J., "Tensor Harmonics in Canonical Form for Gravitational Radiation and Other Applications," J. Math. Phys. 11, 2203 (1970).